IN SILICO IDENTIFICATION, PRODUCTION AND CHARACTERIZATION OF NOVEL BIOACTIVE PEPTIDES WITH ANTIMICROBIAL, ANTI-BIOFILM AND ANTI-INFLAMMATORY ACTIVITY

Antonio Masino

Dottorato in Biotecnologie – 34° ciclo

Università di Napoli Federico II

Dottorato in Biotecnologie – 34° ciclo

Università di Napoli Federico II

IN SILICO IDENTIFICATION, PRODUCTION AND CHARACTERIZATION OF NOVEL BIOACTIVE PEPTIDES WITH ANTIMICROBIAL, ANTI-BIOFILM AND ANTI-INFLAMMATORY ACTIVITY

Antonio Masino

Dottorando:	Antonio Masino
Relatore:	Eugenio Notomista
Coordinatore:	Prof. Marco Moracci
Settore Scientifico Disciplinare:	Biochimica (BIO/10)

Ai miei genitori,
a mia sorella,
a Rosa,
per esserci, sempre.

INDEX

RIASSUNTO

Lo sviluppo e l'impiego degli antibiotici ha rivoluzionato l'approccio al trattamento e alla prevenzione delle malattie infettive; tuttavia, il loro abuso in medicina e in veterinaria, l'uso in zootecnia e in agricoltura ha favorito lo sviluppo dell'antibiotico-resistenza. A destare maggiore preoccupazione è la comparsa di patogeni resistenti a numerosi antibiotici (MDR, MultiDrug-Resistant) che riducono ulteriormente la possibilità di un trattamento efficace. Data la situazione è chiaro che per combattere il fenomeno dell'antibiotico-resistenza sono necessarie nuove classi di agenti antimicrobici in grado di garantire un'efficacia duratura nel tempo.
A tal proposito una classe molto interessante di molecole sono i peptidi antimicrobici (AMP), molecole presenti in molte forme di vita, spesso definiti anche "peptidi per la difesa dell'ospite" (HDP, Host Defence Peptides) per sottolineare il ruolo fisiologico che rivestono nei meccanismi dell'immunità innata. Tra i peptidi antimicrobici, una classe molto diffusa e ben caratterizzata sono i cosiddetti peptidi antimicrobici cationici (CAMP), che sebbene eterogenei in termini di lunghezza e struttura, condividono caratteristiche chimico-fisiche, come carica netta positiva (generalmente > +2) ed elevato contenuto di residui idrofobici (tipicamente il 50%). Tali caratteristiche sono alla base del loro meccanismo d'azione, infatti, a differenza degli antibiotici convenzionali il cui bersaglio è generalmente una molecola intracellulare del batterio, i peptidi antimicrobici interagiscono con le membrane batteriche ricche in fosfolipidi anionici. Dopo una prima interazione tra peptide e membrana, esso adotta una conformazione anfipatica che gli consente di inserirsi in membrana con conseguente alterazione della fluidità e morte del batterio. Considerando il loro particolare meccanismo d'azione è improbabile che i batteri possano sviluppare una completa resistenza, infatti, ciò richiederebbe un cambiamento sostanziale nella composizione della membrana con costi metabolici molto elevati per i batteri. Nonostante ciò, alcuni ceppi batterici hanno acquisito una resistenza ai CAMP attraverso la secrezione di proteasi capaci di idrolizzare gli stessi CAMP, ma un numero sempre maggiore di evidenze sperimentali dimostra che tagli proteolitici di proteine dotate di attività biologiche da parte di proteasi batteriche possono dare origine a peptidi bioattivi "nascosti" nella sequenza e con attività spesso totalmente diverse da quelle della proteina dalla quale derivano. Tali proteine sono state chiamate

CAMP-RP (CAMP-Releasing Proteins) perché l'azione di tagli proteolitici permette il rilascio di regioni che, una volta libere da vincoli conformazionali della proteina nativa, diventerebbero dei veri e propri CAMP. Dunque, tali peptidi possono anche essere definiti "CAMP criptici". Esempi di CAMP-RP sono: emoglobina, trombina, lattoferrina, lisozima, istoni, ribonucleasi e apolipoproteine.
Le attività del presente lavoro di tesi si collocano all'interno di una vasta linea di ricerca il cui obiettivo principale è lo sviluppo di nuovi agenti antimicrobici basati su CAMP criptici umani.
Per raggiungere tale scopo è stata sviluppata una piattaforma computazionale/sperimentale per l'identificazione, la produzione in forma ricombinate, scalabile ed economica, e la caratterizzazione dei CAMP criptici.
In particolare, il presente lavoro di tesi ha avuto come obiettivi sia la validazione di elementi preesistenti della piattaforma che l'implementazione di nuovi strumenti per rendere la piattaforma più efficiente. Più in dettaglio, gli obiettivi del presente lavoro di tesi possono essere riassunti nei seguenti punti fondamentali:

i) Analisi *in silico* del secretoma umano per la preparazione di una lista di potenziali peptidi criptici umani.
ii) Caratterizzazione preliminare dei peptidi generati dal sistema bioinformatico e prodotti per sintesi chimica.
iii) Produzione ricombinante e caratterizzazione completa dei più interessanti fra i peptidi identificati al punto (ii).
iv) Sviluppo di una strategia di marcatura fluorescente dei peptidi bioattivi per agevolarne la caratterizzazione molecolare in particolare lo studio delle interazioni con membrane, endotossine (LPS, LTA ecc.) e cellule batteriche ed eucariotiche.

i) Analisi in silico del secretoma umano.

Al fine di ricercare, con un approccio più razionale, i peptidi "criptici" presenti nel secretoma umano, è stato utilizzato un "tool *in silico*" che ha consentito di localizzare regioni antimicrobiche in precursori proteici e di fornire una predizione quantitativa dell'attività antimicrobica associata ad esse. In particolare, il tool è basato sulla constatazione che il potenziale antimicrobico di un dato peptide è linearmente correlato ad un punteggio definito A.S. (Absolute Score) che dipende da carica, idrofobicità, lunghezza del peptide e due coefficienti, specifici di ciascun ceppo batterico, che definiscono

l'importanza relativa di carica e idrofobicità. Usando questo approccio sono state analizzate circa 2000 sequenze di proteine umane secrete per ottenere una lista di potenziali CAMP-RP contenenti almeno un peptide con A.S. elevato. La lista è stata analizzata manualmente allo scopo di selezionare i più interessanti candidati sulla base dei seguenti criteri:

- Il ruolo fisiologico e l'abbondanza della proteina preferendo quelle coinvolte in processi come difesa immunitaria e coagulazione.
- La posizione del peptide all'interno della struttura primaria della proteina preferendo quelli in corrispondenza o in prossimità dei terminali della proteina.
- L'assenza di lunghi tratti di residui idrofobici che potrebbero compromettere la solubilità del peptide.
- Un numero di residui di cisteina preferibilmente ≤ 2.

Questa analisi ha portato a selezionare 17 CAMP-RP contenenti 34 potenziali peptidi antimicrobici che sono stati prodotti mediante sintesi chimica dal gruppo di ricerca del dott. Cesar de la Fuente-Nuñez (Università della Pennsylvania, USA) per poterne verificare l'attività biologica.

ii) Caratterizzazione preliminare dei peptidi selezionati.

I peptidi selezionati sono stati preliminarmente caratterizzati per la loro attività antimicrobica attraverso saggi di Minima Concentrazione Inibente (MIC), conducendo le analisi su 10 ceppi di batteri patogeni clinicamente rilevanti, sia Gram negativi che Gram positivi. Va sottolineato che tutti i 34 peptidi selezionati hanno mostrano attività antimicrobica contro tutti i ceppi batterici utilizzati, in molti casi comparabile a quella del ben caratterizzato peptide antimicrobico (P)GKY20, utilizzato come controllo positivo. Complessivamente questi risultati ci hanno, da un lato, permesso di validare il sistema di screening basato sul tool bioinformatico, ma hanno al tempo stesso fornito un ampio pannello di nuovi CAMP potenzialmente utilizzabili per applicazioni biomediche e biotecnologiche. Incoraggiati da questi risultati si è deciso di selezionare un più piccolo gruppo di peptidi particolarmente interessanti per una più approfondita caratterizzazione. La scelta è caduta sui peptidi ospitati nelle proteine coinvolte nella coagulazione del sangue e/o secreti dalle piastrine: le subunità Aα, Bβ e γ del fibrinogeno; le proteine SCUB1 e 3 secrete dalle piastrine; il fattore di von Willebrand. Questa scelta è stata motivata dal fatto che le proteine coinvolte

nella coagulazione del sangue, da un certo punto di vista, possono essere considerate parte del sistema di difesa dell'ospite, inoltre, è già stato dimostrato che molte di queste proteine ospitano CAMP, come già riportato per il C-terminale della trombina umana e la stessa subunità Bβ del fibrinogeno.

L'attenzione del nostro gruppo di ricerca si è concentrata in particolare sui peptidi ospitati dalle subunità del fibrinogeno (descritti in questo lavoro di tesi) e sul fattore di von Willebrand (che sarà oggetto di future ricerche nel laboratorio dove questa tesi è stata preparata), mentre il Prof. de la Fuente-Nuñez e i suoi collaboratori hanno deciso di lavorare sui peptidi derivati dalle proteine SCUB che si sono mostrati molto attivi non solo *in vitro* su numerosi ceppi Gram negativi e Gram positivi ma anche *in vivo* in un modello murino di infezione cutanea. Pertanto si può ipotizzare che i CAMP presenti al C-terminale delle proteine SCUB possano trovare applicazioni mediche come agenti antimicrobici.

iii) Produzione ricombinante dei peptidi derivanti dal fibrinogeno.

Un'accurata caratterizzazione delle proprietà dei peptidi bioattivi richiede un metodo efficace per la loro produzione in quantità adeguate. Per tale motivo, parte del lavoro di tesi è stato dedicato alla produzione in forma ricombinante su larga scala dei peptidi derivanti dal fibrinogeno e dalla trombina (GKY20), utilizzando una strategia per l'espressione in *E. coli,* precedentemente sviluppata nell'ambito della citata piattaforma. Brevemente, la strategia prevede la preparazione di peptidi fusi al C-terminale di un carrier, chiamato onconasi (ONC), da cui i peptidi vengono rilasciati mediante idrolisi chimica acida e successivamente purificati sfruttando le diverse proprietà di solubilità del peptide/carrier. Va notato che tale strategia permette di preparare peptidi dotati di una prolina o di una cisteina all'estremità N-terminale, essenziale per la marcatura descritta al punto (iv). Tali peptidi sono stati poi caratterizzati per quanto riguarda le loro proprietà antimicrobiche, antibiofilm e per il loro effetto tossico su cellule eucariotiche. I risultati ottenuti hanno mostrato che tutti i peptidi hanno attività antimicrobica su tutti i ceppi saggiati con valori di MIC compresi tra 1.5 e 12.5 μM. In particolare il peptide derivante dalla subunità γ del fibrinogeno, (P)FIBy-TWK25, ha mostrato valori di MIC molto simili a quelli del noto peptide di riferimento (P)GKY20, indicandolo come promettente peptide antimicrobico. È stato valutato inoltre l'effetto

sinergico dei CAMP derivati dal fibrinogeno in combinazione tra di loro, con GKY20 o con antibiotici. Tutte le combinazioni di peptidi hanno dato interazione sinergica con indice FIC < 1. In particolare nel caso della coppia (P)FIBγ-GII30/(P)GKY20 si è osservato un indice FIC < 0.5 che indica un'interazione particolarmente favorevole. I peptidi del fibrinogeno hanno mostrato sinergia quando usati in combinazione con la colistina con valori di FIC compresi tra 0.18-0.31. Oltre l'attività contro batteri in fase planctonica, alcuni dei CAMP selezionati hanno mostrato attività nell'eradicare il biofilm preformato di PAO1, oltre che ridurre la vitalità dei batteri all'interno del biofilm. In particolare, il peptide (P)FIBα-GVV27 usato ad una concentrazione pari a 30 μM ha indotto una riduzione al 60% circa della vitalità cellulare residua. Ugualmente, una concentrazione compresa tra 20 e 30 μM del peptide (P)FIBβ-GVV28 ha ridotto la vitalità delle cellule nel biofilm fino al 70% circa. Infine, sebbene tutti i peptidi abbiano mostrato attività antimicrobiche, non è stata osservata invece una significativa citotossicità su linee cellulari di monociti (THP-1) e cheratinociti (HaCaT) umani.

iv) Sviluppo di una strategia di marcatura dei peptidi.

Allo scopo di potenziare ulteriormente la piattaforma sperimentale precedentemente descritta è stato sviluppato un nuovo strumento per la caratterizzazione in particolare dei CAMP ma, più in generale, di qualsiasi peptide bioattivo. Questo strumento sfrutta la fluorescenza sensibile all'ambiente della luciferina e dell'aminoluciferina, due molecole note soprattutto come substrati della Luciferasi. Questi fluorofori rispondono a variazioni anche minime nel loro microambiente locale, agendo pertanto come reporter sia di cambiamenti conformazionali che di eventi di *binding* delle macromolecole a cui sono legati. Le due sonde fluorescenti hanno permesso di studiare l'interazione di vari peptidi con membrane modello, micelle di SDS, micelle di LPS e cellule intere di *E. coli*. Inoltre, utilizzando la nuova strategia di marcatura fluorescente, è stata studiata quantitativamente l'interazione con l'LPS di alcuni CAMP, incluso (P)FIBγ-TWK25 uno dei CAMP derivati dal fibrinogeno appena identificati. L'elevata affinità di questo peptide per l'LPS sia in forma micellare che non micellare suggerisce che esso possa funzionare anche come LPS-scavenger, una proprietà estremamente importante dal punto di vista farmacologico.

SUMMARY

The rapid increase in drug-resistant infections emphasizes the urgent need to develop new antimicrobials. Promising candidates are antimicrobial peptides (AMPs), also known as host defense peptides (HDPs), essential components of innate immunity in eukaryotes. Among them, cationic AMPs (CAMPs) are particularly intriguing: due to a peculiar amino acidic composition, they damage selectively bacterial membranes rich in anionic lipids bypassing bacterial resistance. The activities of this PhD thesis were framed in the context of a wider project whose goal is the development and validation of a computational/experimental platform for the identification, preparation and characterization of CAMPs with the final aim to develop biotechnological and biomedical CAMP-based applications. Using a previously developed *in silico* tool, human secretome was screened to identify “cryptic” CAMPs hidden inside human proteins. 34 new promising CAMPs from 17 proteins were selected, synthesized and characterized thus allowing both to confirm the validity of the tool and to obtain a panel of new potential antimicrobials. Six peptides derived from the three subunits of fibrinogen were selected for a deeper characterization and prepared in the recombinant form using another tool of the platform for the scalable, cheap production of CAMPs in *E. coli*. These peptides proved to be wide spectrum bactericidal antimicrobials with synergic activity when combined with each other, with a thrombin-derived CAMP – thus suggesting that cryptic CAMPs from the same district can cooperate – and with the antibiotics colistin and tobramycin. Some of the peptides also showed a significant antibiofilm activity. In parallel, a new tool for the characterization of CAMPs and, more in general, of any bioactive peptide has been developed exploiting the environment-dependent fluorescence of luciferin and aminoluciferin. These fluorophores allow the monitoring of even small variations in the local microenvironment, acting as reporters of conformational changes and binding events. The two probes allowed to study the interaction of the peptides with model membranes, SDS, LPS and *E. coli* cells. Using the new labelling strategy, the interaction with LPS of some CAMPs, including one of the newly identified fibrinogen-derived CAMPs, has been studied quantitatively. The high affinity of this peptide for micellar and non-micellar LPS suggests that it might work also as an LPS-scavenger, a property very intriguing from the pharmacological point of view.

Chapter 1 - INTRODUCTION

1.1 Antibiotic resistance and "multidrug resistant bacteria" (MDR)

For many years, the use of antibiotics has proved extremely important to fight infections caused by bacteria.
In recent decades, however, their abuse in human healthcare has led to the fast emergence and spread of antibiotic resistance (Yu Z et al., 2020).
In addition to the excessive antibiotics usage in human healthcare, also those used in veterinary and the waste generated by pharma-industries, hospitals and livestock producers has stimulated the development of the drug resistance phenotype in the environment, thus increasing the prospective resistome-spill over to humans and animals (Oyekale et al., 2017).
As a result, many pathogenic strains have become "multidrug resistant" (MDR) i.e. resistant to three or more antibacterial drug classes (Fischbach et al., 2009).
Looking at the speed of drug resistance emergence and its serious threat to the global health, development of new drugs to treat such infections is a top priority for the World Health Organization (WHO) (The Lancet Infectious Diseases, 2017).

1.2 Bacterial mechanisms of antibiotic resistance

Understanding the molecular detail of resistance mechanisms is of great interest allowing the rational development of novel therapeutic approaches to evade or block resistance (Wilson et al.,2020).
To date, several self-defence mechanisms have been identified in MDR microbial pathogens (Khare et al., 2021). The most effective are:

- Modification or destruction of antibiotics.
  Bacteria can produce enzymes that modify antibiotics via addition of chemical groups preventing the interaction between the antibiotics and their targets in bacteria.
  Frequently observed modifications include phosphorylation (chloramphenicol, aminoglycosides), adenylation (lincosamides, aminoglycosides) and acetylation (streptogramins, chloramphenicol, aminoglycosides) of the antibiotics. Other enzymes may also be capable of destroying

antibiotics (e.g. β-lactamases). These enzymes are often present on mobile genetic elements (Tooke et al., 2019).

- Modification of cell permeability.
  To limit the entry of antibiotics inside the cells, bacteria can modulate cellular permeability. This is usually obtained through the regulated expression/reduction of porins, outer membrane protein channels used by the antibiotics to cross the outer membrane (Vergalli et al., 2019).
  Other resistant strains reduce the antibiotic concentration inside the cell through efflux pumps, which transport the antibiotic molecules out of the cell, usually in non-specific manner (Shriram et al., 2018).

- Modification of the antibiotic targets.
  Through this strategy bacteria prevent the optimal interaction between antibiotics and targets (Munita et al., 2016). Target modifications include: enzymatic modification of the binding sites on the targets; replacement of the original targets and (point) mutation in the target-coding genes.

- Horizontal gene-transfer.
  Bacteria can share genetic components with other bacteria and transfer the resistant DNA through horizontal gene transfer. Bacteria, usually, acquire external genetic material mainly through three processes: transformation, transduction and conjugation (Johnston et al., 2014; Dubnau et al., 2019). (Wozniak et al., 2010; Dib et al., 2015; Delavat et al., 2017).

Another important phenomenon that increases resistance to antibiotics is the development of the so-called “biofilm”.
Biofilms are clusters of single or multiple species of bacteria enveloped in a matrix composed by polysaccharides, proteins, and DNA that protect the bacteria from environmental pressures (Haney et al., 2018). They are clinically relevant, as they are responsible for up to two-thirds of hospital-acquired infections and contribute to chronic infections growing attached to human tissues and medical devices (Haney et al., 2018).

1.3 Host defense peptides (HDPs) as a new class of antimicrobials

A class of very interesting molecules that could help solve the bacterial resistance problem are antimicrobial peptides (AMPs). AMPs are multifunctional molecules discovered in various organisms from animals, plants, fungi, and even single-cell microorganisms (Hancock et al., 2001; Shah et al., 2016).
In addition to a broad range direct antimicrobial activity, they also show several others biological activities like endotoxin neutralization, angiogenesis (Koczulla et al., 2003), wound healing activity (Hilchie et al., 2013; Mangoni et al., 2016) and immunomodulatory and adjuvant functions by acting as chemotactic for immune cells and inducing cytokines and chemokines secretion (Pachón-Ibáñez et al., 2017).
For this reason, AMPs are also termed "Host Defence Peptides" (HDPs) to describe their role in the innate immune response (Boparai et al., 2020).
AMPs are very heterogeneous in structure, length and aminoacidic composition. In terms of net charge, AMPs can be divided into non-cationic and cationic (Cardoso et al., 2021). While non-cationic AMPs are less common (Harris et al., 2009), cationic AMPs (CAMPs) are widespread and hundreds of them have been characterized (Maróti et al., 2011).
Even if heterogeneous in length (10-60 amino acids) and structure, CAMPs share a consensus amino acids composition, with a net positive charge (usually > +2) and a substantial proportion (typically 50%) of hydrophobic residues mediating their interaction with bacterial membranes (Hancock et al., 2006; Yeaman et al., 2003; Pasupuleti et al., 2012; Pizzo et al., 2018).
As for the secondary structures, most AMPs show four architectures: (i) α-helical peptides (for example LL-37), (ii) peptides containing β-sheet elements (generally stabilized by disulfides), (iii) peptides combining both α and β structures (for example β defensins) and (iv) peptides unusually rich in particular aminoacids such as proline, arginine, tryptophan or histidine (Fig.1) (Zhang G et al., 2014).

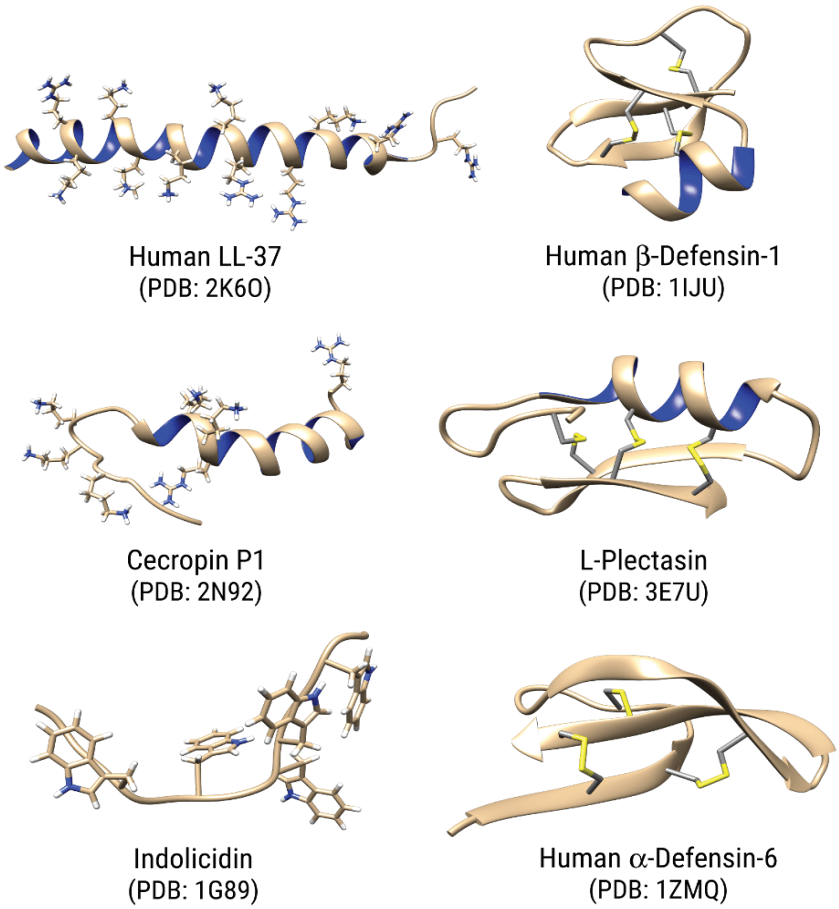

Figure 1: Representative models of common antimicrobial peptides (AMPs) showing alpha-helical, beta-sheet, amphiphilic structural motifs that relate form and function. Molecular graphics images were produced using the Chimera package from the Computer Graphics Laboratory, University of California, San Francisco.

1.4 Mechanism of action

Antimicrobial peptides have atypical mechanisms of action, different from those of most conventional antibiotics.

For example, many CAMPs directly target bacterial membranes. CAMPs not stabilized by disulfides are generally unfolded in aqueous solutions, after the initial electrostatic and hydrophobic interactions with bacterial surface rich in anionic phospholipids, they fold into amphipathic conformations (Malmsten, 2016) which allow their insertion into the membrane.

Various models have been used to describe how CAMPs damage membrane structure and functions (Fig.2). These models can be classified under two broad categories: transmembrane pore and non-pore models (Fig.2).

The transmembrane pore models are the “barrel-stave pore” and “toroidal pore models”:

- In the “barrel stave model”, the CAMPs are initially oriented parallel to the membrane but eventually insert perpendicularly in the lipid bilayer promoting lateral peptide-peptide interactions, in a manner similar to that of membrane protein ion channels (Shabir et al., 2017). Peptide amphipathic structure is essential for pore formation mechanism as the hydrophobic regions interact with the membrane lipids and hydrophilic residues form the lumen of the channels (Fig.2) (Brogden, 2005).
- In the “toroidal pore model”, the peptides insert perpendicularly in the lipid bilayer inducing a local curvature of the lipid bilayer with the pores partly formed by peptides and partly by the phospholipid head group. Several CAMPs such as magainin 2 (Lee TH et al., 2016), lacticin Q (Lee TH et al., 2016) and melittin (Lee TH et al., 2016; Wimley, 2010) have been shown to form toroidal pores (Fig.2).

Both pore forming mechanisms lead to alteration of membrane fluidity, depolarization and cell death mediated by membrane disruption (Lee J et al., 2015).

CAMPs can also act without forming specific pores in the membrane like in the “carpet model” (Lee TH et al., 2016). In this case, the AMPs adsorb parallel to the lipid bilayer and reach a threshold concentration to cover the surface of the membrane, thereby forming a “carpet”. This leads to unfavorable interactions on the membrane surface. Consequently, the membrane integrity is lost, producing a detergent-like effect, which eventually disintegrates the membrane by forming micelles (Fig.2) (Lee TH et al., 2016). Examples of CAMPs acting by the carpet model are indolicidin and LL-37 (Shai, 2002).

However, membrane targeting is not the only mechanism of action, indeed some AMPs display intracellular mechanisms of action.

These AMPs cross lipid bilayers, without significantly affecting membrane stability, and target intracellular components like DNA, RNA, ribosomes and some proteins and enzymes thus blocking DNA duplication, proteins synthesis and other metabolic functions (Fig.2) (Falanga et al., 2017; Savini et al., 2018).

Examples of antimicrobial peptides that translocate across cell membranes and target intracellular components (Lohner, 2017) are: buforin II (Perez et al., 2015), dermaseptin (Belmadani et al., 2018), HNP-1 (Beadell et al., 2017), pleurocidin (Zhang M et al., 2016) and indolicidin (Tsai et al., 2018).

Selectivity toward bacterial cells of all these peptides is granted by the differences between the bacterial membranes and the membrane of eukaryotic cells (Guilhelmelli et al., 2013; Zasloff et al., 2002).
Bacterial membranes contain high percentages of lipids with negatively charged head groups, such as phosphatidylglycerol (PG) and cardiolipin (Zhang G et al., 2014) whereas the membrane of eukaryotic cells is asymmetric: the outer leaflet is composed by zwitterionic phospholipids such as phosphatidylcholine (PC), sphingomyelin and other neutral components such as cholesterol, whereas most of the lipids with negatively charged head groups are in the inner leaflet. Thus, the positively charged CAMPs have a strong electrostatic interaction with the negatively charged phospholipids on the outer leaflet of the bacterial membrane but a weak interaction with the outer leaflet of the eukaryotic membrane (Fig.3).
As CAMPs directly target bacterial membrane, it is reasonable to hypothesize that, in contrast to conventional antibiotics, the development of CAMPs resistance is very unlikely. Bacteria could acquire resistance only modifying the composition of their membrane (Zasloff, 2002). Such a change not only would require several mutations but could also be detrimental to bacterial cells as membrane bears essential metabolic functions (Baltzer et al., 2011). The fact that many CAMPs have multiple intracellular targets further decreases the probability that pathogens easily develop a resistant phenotype.

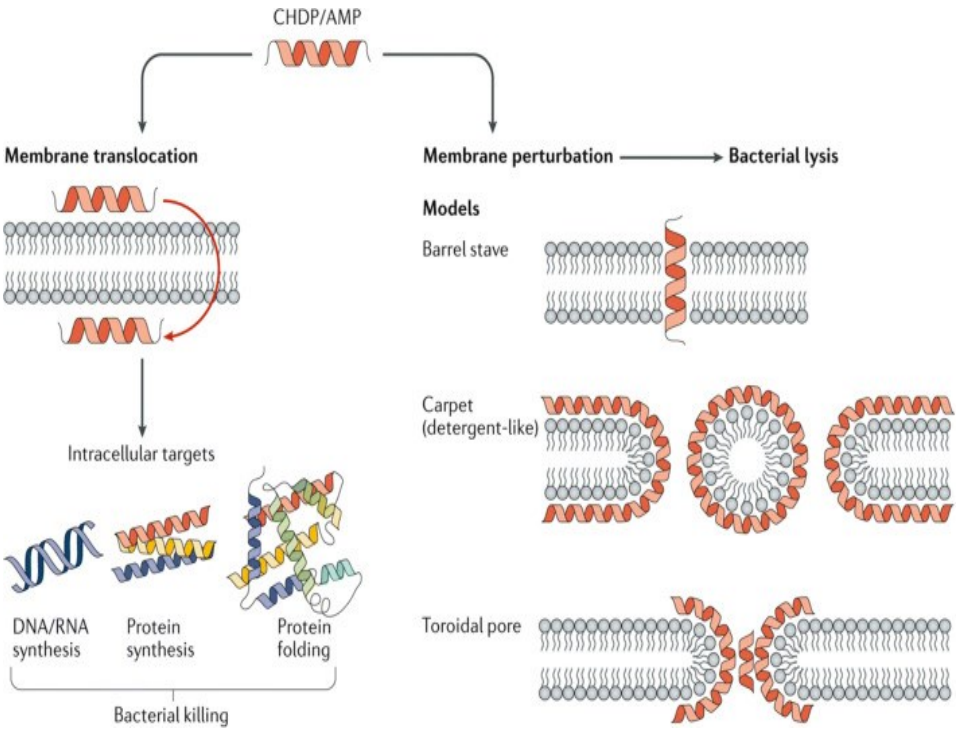

Figure 2: Mechanism of action of the CAMPs. The left part of the scheme shows the mechanism based on the existence of intracellular targets. The right part shows three models describing how CAMPs could damage membranes, from top to bottom: the barrel stave pore, the carpet model and the toroidal pore (from Mookherjee et al. 2020).

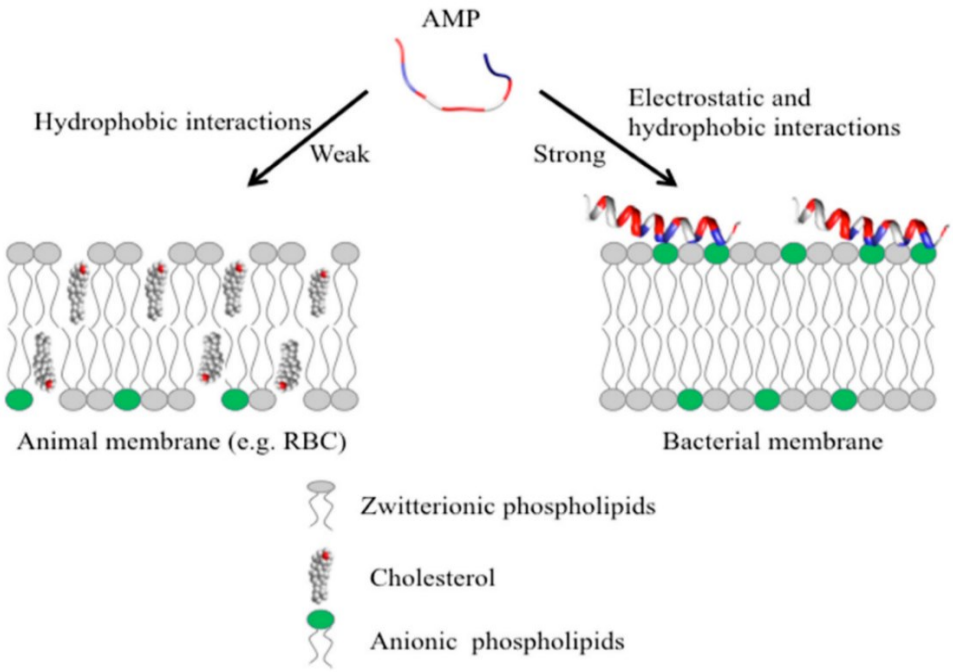

Figure 3: Molecular basis of the CAMP selectivity. Animal membranes (left) are asymmetric containing only zwitterionic phospholipids the outer layer; in addition they are rich in cholesterol. Bacterial membranes (right) are rich in anionic phospholipids and do not contain cholesterol. CAMPs selectively and strongly interact with bacterial membranes through electrostatic and hydrophobic interactions made possible by peptide folding. RBC: red blood cell. (From Suzana K. Straus, 2018).

1.5 Beyond the direct antimicrobial activity

1.5.1 Immunomodulatory activities

As mentioned above, in addition to their direct antimicrobial activity, many AMPs often possess immunomodulatory activities. More specifically some AMPs can induce a variety of immune responses: activation, attraction and differentiation of white blood cells, stimulation of angiogenesis, wound healing activity, reduction of inflammation by lowering the expression of proinflammatory chemokines and controlling the expression of chemokines and reactive oxygen/nitrogen species (Scheenstra et al., 2020; Hilchie et al., 2013).

Studies on human and mouse cells have evidenced a variety of target cells stimulated by HDPs, including monocytes, macrophages, dendritic cells, epithelial cells, neutrophils, keratinocytes and others. The responses of these cells are often complex and dependent on the specific peptide, cell type, their activation state and the type of pathogen (Hilchie et al., 2013).
In this regards, well-studied peptides are defensins (which include the α, β and θ families) and cathelicidins like the well-known peptide LL-37 (Scheenstra et al., 2019; Cederlund et al., 2011; Bowdish et al., 2006).
Human α and β-defensins have been found to selectively chemoattract different subsets of T lymphocytes and immature dendritic cells, thus playing important roles as immune modulators in adaptive immunity as well (Bowdish et al., 2006; Hilchie et al., 2013).
As for LL-37, *in vivo* studies showed that it plays a central role in innate immune responses and inflammation, as it has been identified as a potent chemoattractant for mast cells (Niyonsaba et al., 2002).
Some other HDPs act as anti-inflammatory compounds during sepsis (Scheenstra et al., 2020; Martin et al., 2015), protecting the host from potentially lethal effects resulting from an excessive Toll-Like Receptor-mediated inflammatory response induced by bacterial endotoxins, such as lipopolysaccharide (LPS) and lipoteicoic acid (LTA) of Gram negative and Gram positive bacteria, respectively. HDPs act both directly by binding and sequestering LPS and indirectly by altering gene expression of various inflammatory cells (Bowdish et al., 2006).
The immunomodulatory activities of AMPs also include wound healing; very interestingly it has been demonstrated that cathelicidins can be used topically to stimulate wound healing in a diabetic mice model (Wu et al., 2010).

1.5.2 Antibiofilm activity

Besides their activity against planktonic bacteria, many AMPs also show antibiofilm activity (Di somma et al., 2020). This is particularly interesting because, usually, biofilm embedded bacteria are more resistant than planktonic bacteria to conventional antibiotics. Most

conventional antibiotics are active on biofilm only at concentrations 10-1000 times higher than the MIC.
However, the interaction of AMPs with the biofilm is very complex. AMPs can affect biofilm formation or degradation at different stages and with different mechanisms of action (Fig.4).
Some antibiofilm peptides block the initial attachment to a surface by inhibiting swimming, interfering with flagellar assembly or directly binding to the surface and preventing bacterial cell adhesion. Alternatively, antibiofilm peptides may inhibit biofilm development by degrading or preventing the production of important biofilm matrix components (Hancock et al., 2021) (Fig.4).
Other antibiofilm peptides act on developing or established biofilms causing biofilm erosion. This activity can be due to very different molecular mechanisms. Some antibiofilm peptides simply kill biofilm embedded cells through mechanisms similar to those active on palnktonic bacteria. These peptides usually are active on the biofilm at concentrations higher than those necessary to kill planktonic bacteria (*i.e.* for these peptides the minimum biofilm eradication concentration, MBEC, is generally larger than the MIC and the minimum bactericidal concentration, MBC).
Other peptides promote the dispersal of biofilm cells by stimulating twitching motility, this in turn makes the bacteria susceptible to the effects of antibiotics and of bactericidal AMPs (Hancock et al., 2021). These unusual peptides translocate into the cells where they target guanosine tetraphosphate (ppGpp) for degradation, disrupting the stringent-stress response required for biofilm formation. Generally, these peptides are active on biofilms at concentrations significantly lower that the MIC.

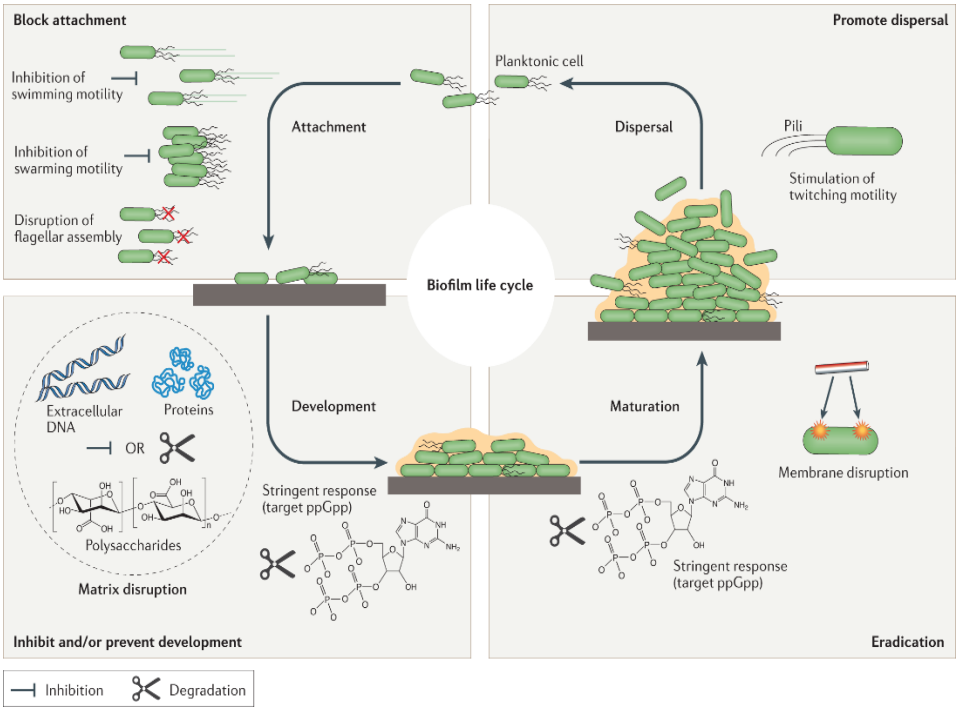

Figure 4: The biofilm life cycle provides several entry points for the antibiofilm effects of AMPs. Antimicrobial peptides are represented as amphipathic cylinders, with charged surfaces in red and hydrophobic surfaces in grey. (From Hancock et al., 2021).

Some of peptides with well characterized antibiofilm activity are nisin A, the human cathelicidin LL-37, hepcidin 20, human β-defensin 3 and the synthetic peptide DJK-5.

Nisin A is able to damage the membrane of biofilm-embedded cells of an MRSA strain of *S. aureus,* disturbing the membrane potential (Okuda et al., 2013). Human cathelicidin LL-37, one of the most studied antibiofilm peptides, can affect the bacterial cell signaling system. This peptide can inhibit *P. aeruginosa* biofilm formation at a concentration of 0.5 μg/mL by downregulating the genes related to the QS system, decreasing the attachment of bacterial cells on the surface and stimulating twitching motility mediated by type IV pili (Overhage et al., 2008; Mansour et al., 2014).

Hepcidin 20 can reduce the extracellular matrix mass of *Staphylococcus epidermidis* and alter its biofilm architecture by targeting the polysaccharide intercellular adhesin (PIA) (Brancatisano et al., 2014).

Human β-defensin 3 was shown to be able to reduce the expression of the icaA, IcaR, and icaD genes of *S. epidermidis* ATCC 35,984, which control the synthesis of the polysaccharide intracellular adhesin (PIA). This leads to a reduction of biofilm formation (Zhu et al., 2013).
Finally, broad-spectrum synergy between antibiofilm peptides, such as 1018 and DJK-5, and antibiotics, e.g. ceftazidime, tobramycin and ciprofloxacin, has been observed against biofilms *in vitro* (de la Fuente-Núñez et al., 2015; Reffuveille et al., 2014). This synergy has been observed also *in vivo* as recently demonstrated using a mouse abscess model (Pletzer et al., 2018). The molecular basis of synergy are not completely understood, although there are indications that some peptides increase cell permeability (Pletzer et al., 2018), potentially enhancing antibiotic uptake, whereas others increase biofilm dispersal, enabling antibiotic killing (Reffuveille et al., 2014).

1.6 Medical and biotechnological applications of CAMPs

The peculiar features of CAMPs allow their exploitation in several applications for which the use of conventional antibiotics is not permitted or not desirable.
For example, CAMPs find application in cosmetic and in food industry to prevent the development and spread of spoilage and pathogenic microorganisms. Nisin (Santos et al., 2018), and lactoferrin (Lönnerdal, 2014), are used as natural preservative for many food products. They are mainly used in dairy and meat products to inhibit the development of pathogenic food borne bacteria such as *Listeria monocytogenes* and many other Gram-positive food spoilage microorganisms (Gharsallaoui et al., 2016).
Enterocin AS-48 and enterocin CCM4231 are CAMPs used as preservatives for cider, fruit and vegetable juices and soy milk (Rai et al., 2016; Santos et al., 2018).
Moreover, CAMP-containing active packaging is a novel packaging method that has great potential in the food industry. For instance, ε-poly-L-lysine, used in conjunction with starch films, shows good inhibitory effects on *Aspergillus parasiticus* (aflatoxin producer) and *Penicillium expansum* (Luz et al., 2018).
CAMPs are also studied in agriculture as efficient weapons to fight plant-diseases by taking advantage of their specificity, low toxicity

and high biodegradability, that results in a low environmental impact with respect to chemical pesticides (Zeitler et al., 2013).
Obviously, application of antimicrobial peptides in the medical field is one of the most interesting perspective.
Some CAMPs are in clinical or pre-clinical trials as alternatives to antibiotics or as antibiotics adjuvants, by exploiting their synergistic interactions with antibiotics (Baltzer et al., 2011).
In medicine, CAMPs are also used to treat infections that occur after surgery, burns, accidental injury, skin disease, and chronic wound infections (Thapa et al., 2020).
For example, a peptide used for the treatment of skin infection is pexiganan (Pfalzgraff et al., 2018), a 22-amino acid synthetic analogue of the peptide magainin II (Gomes et al., 2020) which has antimicrobial activity against most clinical bacterial isolates cultured from infected diabetic foot ulcers (Gomes et al., 2020). When pexiganan and nisin are used in combination (dual-CAMP formulations) the concentration of pexiganan required to inhibit and eradicate both planktonic and biofilm-based bacterial cells of a co-cultures of *S. aureus* and *P. aeruginosa* is substantially reduced (Gomes et al., 2020).
Omiganan, a synthetic analogue of the natural CAMP indolicidin, is a topical agent that displays broad antifungal and antibacterial activity against all major pathogens responsible for local catheter site and catheter-associated bloodstream infections (Fritsche et al., 2008).
CAMPs can find application also in the treatment of human oral cavity diseases: dental caries, endodontic infections, candidiasis, and periodontal disease (Izadi et al., 2020). For instance, peptide ZXR-2 (FKIGGFIKKLWRSLLA) has shown high activity against pathogenic bacteria of dental caries, *Streptococcus mutans*, *Streptococcus sobrinus* and *Porphyromonas gingivalis* (Chen L et al., 2017).
Other fields of application of CAMPs are biomaterials industry and the manufacturing of advanced medical devices. The biomaterials used for the preparation of dental implants, contact lenses, bioresorbable prostheses and medical devices such as catheters, heart valves and fracture fixation devices are frequently the cause of bacterial infection (Vila et al., 2008). The most critical pathogenic event in the development of these implant-related infections is biofilm formation which originates from bacterial adhesion to the implant (Romanò et al., 2015). Therefore, there is a clear need for

broad-spectrum antimicrobials able to prevent colonization of biomaterials. For this purpose CAMPs have enormous potential as antimicrobial coatings of medical devices (Costa et al., 2011).
For example, a novel titanium coating has been developed preventing infection-related implant failures in dentistry and orthophedics. The coating incorporates an antimicrobial peptide, GL13K, derived from parotid secretory protein, which has been previously shown to be bactericidal and bacteriostatic in solution (Chen X et al., 2020). The robustness, antimicrobial activity and cytocompatibility of GL13K-biofunctionalized titanium make it a promising candidate for sustained inhibition of bacterial biofilm growth (Chen X et al., 2020).
CAMPs can also be used to develop biotechnological devices for disinfection of aqueous solutions, in fact they can be used to remove or to kill micro-organisms present in aqueous solutions thus allowing sanitizing of biomedical, pharmaceutical, and cosmetic formulations. As several CAMPs bind with high affinity bacterial endotoxins like lipopolysaccharides (LPS) and lipoteichoic acid (LTA), molecules with a high pro-inflammatory activity, CAMPS can also be used to remove endotoxins from pharmaceutical, and cosmetic formulations and, potentially, as dugs to prevent septic shock.

1.7 Cryptic CAMPs and their carriers

Many proteins with functions often apparently not involved in host defence can host CAMPs inside their sequences. These peptides can be defined antimicrobial “cryptides” or “cryptic” CAMPs since they are “hidden” in the sequence of proteins.
The existence of cryptic CAMPs can be explained through a very intriguing hypothesis: as some bacterial strains have acquired a limited resistance to CAMPs by secreting proteases, such as the “omptins” of enterobacteria (Haiko et al., 2009) or *Staphylococcus aureus*-derived proteinases (Sieprawska-Lupa et al., 2004), in response, to overcome this resistance, multicellular eukaryotes have developed a very interesting countermove, that is to secrete “CAMP-Releasing Proteins” (CAMP-RPs) which release active peptides only after a partial proteolytic processing operated by bacterial and/or host proteases. Thus, a bacterial strain that secretes proteases to protect from CAMPs would “suicide” by releasing these “cryptic” CAMPs from their precursors (Pizzo et al.,

2018; Pane et al., 2017). This mechanism has been demonstrated for Zf-3, a ribonuclease from *Danio rerio* (Zanfardino et al., 2010).
Examples of CAMP-RPs are lysozyme, lactoferrin, apolipoproteins, ribonucleases and many proteins involved in the coagulation cascade.
Lysozyme, widely distributed in saliva, tears, plasma and mucosal surfaces, can hydrolyze peptidoglycan thus damaging bacterial cell wall and causing bacterial lysis (Ragland et al., 2017) but, if inactivated by proteolysis, it releases CAMPs (Ibrahim et al., 2011) with anti-inflammatory and immunomodulating activity. These peptides are able to bind LPS and decrease expression of TNF-α, IL-6 and IL-1β, both in LPS- and IFN-γ-stimulated murine macrophages (Ibrahim et al., 2017).
Lactoferrin (LF), a secreted glycoprotein particularly abundant in milk but present in almost every other exocrine secretion, hosts several antimicrobial regions. For example, Lactoferricin B (LFcinB) is a 25-residue long peptide released by treating bovine LF with pepsin *in vitro* at acidic pH which has broad spectrum antibacterial activity, even superior to that of LF itself, and several biological activities (Sinha et al., 2013; Legrand, 2016).
Other examples of CAMP-RPs are Apolipoprotein B (ApoB) and Apolipoprotein E (ApoE), serum proteins that bind lipids to form lipoproteins (Dominiczak et al., 2011). In addition to their transport role, they host antimicrobial regions. In the receptor-binding region of ApoE, a cryptic CAMP named ApoE (133-150) has a significant antimicrobial activity on a broad spectrum of bacteria, including several clinical strains (Pizzo et al., 2018). Other two cryptic CAMPs have been identified in a human ApoB variant. Both cryptides, named $ApoB_L$ and $ApoB_S$, showed antimicrobial activity against both Gram positive and Gram negative strains, including pathogenic strains, while having negligible cytotoxic effects on a panel of human and murine cell lines (Gaglione et al., 2017). These peptides also show antibiofilm and LPS scavenging activity (Gaglione et al., 2017).
Very interestingly several proteins involved in blood clotting are CAMP-RPs. For example, it has been demonstrated that the C-terminus of humans thrombin hosts an antimicrobial domain which is an important source of bioactive cryptides generated during wounding and with therapeutic potential against infection and septic shock (Papareddy et al., 2010).

In particular, neutrophil elastase acts on sensitive regions in human thrombin, generating smaller fragments with antimicrobial activity (Papareddy et al., 2010). Moreover, proteolytic fragments from the C-terminus of thrombin were detected *in vivo*, where they are likely generated by the combined action of host and bacterial proteases like neutrophil elastase, cathepsin G and *P. aeruginosa* elastase (van der Plas et al., 2016; Petrlova et al., 2017). One of these fragments, corresponding to the last 25 residues of thrombin thus named GKY25, showed broad spectrum antibacterial activity with minimal inhibitory concentrations (MIC) in the range 2.5-20 μM depending on the strain. GKY25 showed protective activity also *in vivo* in mice infected with *P. aeruginosa* (Papareddy et al., 2010).
A shorter peptide named GKY20, obtained by progressive deletions of the termini of GKY25, showed antibacterial activity on three strains of *E. coli* and three of *S. aureus* with MIC values in the range 2.5-10 μM and 20-40 μM, respectively. This demonstrated that a minimum of 19-20 amino acids is required for good antimicrobial activity thus defining an “optimal” antimicrobial peptide with reduced toxicity and haemolytic activity (Kasetty et al., 2011).
In addition to its antimicrobial activity GKY25 also exerts potent anti-endotoxic and immunomodulatory effects. It interacts with lipid A, the endotoxic moiety of LPS, thus being able to act as an LPS scavenger (Singh et al., 2013). It also interacts directly with immune cells responsive to endotoxins, like monocytes and macrophages (Hansen et al., 2015). In particular it inhibits the dimerization of Toll-like receptor 4 (TLR4), one of the main receptors for the detection of endotoxins, thus reducing the activation of NF-kB and hence the production of inflammatory cytokines (Hansen et al., 2015).
Another key player in the blood coagulation process is human fibrinogen, a 340 kDa glycoprotein present at very high concentration in the human blood (about 3 mg/mL) that upon activation with thrombin is converted into fibrin, the most abundant component of blood clots (Kattula et al., 2017). Fibrinogen is composed by the polypeptide chains Aα, Bβ, and γ with the formal formula $(Aα, Bβ, γ)_2$ (Bellacchio et al., 2020).
It has been demonstrated that human fibrinogen, after incubation with thrombin, releases from its β chain a peptide with antimicrobial effects named GHR28 (GHRPLDKKREEAPSLRPAPPPISGGGYR) (Påhlman et al., 2013).

These few examples demonstrate that cryptic AMPs are with full rights host defense peptides with direct antimicrobial activity as well as several additional biological activities related to host defense. In particular, it has been hypothesized that the antimicrobial "cryptome" is, likely, an unexploited and potentially huge source of new bioactive peptides (Pizzo et al., 2018) with applications in human health and biotechnological industry.

1.8 State of the Art

The activities of the present PhD project have been framed in the context of a more complex research project whose general goal is the development of antimicrobial tools and antimicrobial formulations based on cryptic (human) CAMPs. A computational/experimental platform for the identification, purification and characterization of CAMPs has already been developed in the laboratory where this PhD thesis has been carried out. This platform includes: (i) an *in silico* tool for the identification of cryptic CAMPs hidden in the proteome of any desired organism; (ii) a tool for the scalable production of recombinant AMPs in *E. coli*, including a growth media optimized for the autoinduction expression in large scale fermenters; (iii) a tool for the production of recombinant AMPs with a cysteine residue at the N-terminus which find applications in labelling, immobilization and development of bioconjugates. The following sections describe in brief these three tools.

1.8.1 The in silico tool for cryptic CAMPs identification

Despite the large number of cryptic AMPs known, most of them are the result of occasional finding rather than of a rational approach.
The tool developed in the laboratory where this PhD thesis has been carried out allows not only to detect the presence of a potential cryptic CAMP inside a protein but it also provides an accurate localization of the cryptide position (Pane et al., 2017).
It is based on the finding that the antimicrobial potency (AP) of an HDP [defined as AP = Log(1000/MIC)] is linearly correlated to an "absolute score" ($AS = C^{m}H^{n}\ L/S_{max}$) which depends on charge (C), hydrophobicity (H) and length of the peptide (L), and on two bacterial strain specific coefficients (*m* and *n*) which determine the contribution of charge and hydrophobicity to the antimicrobial potency (Bosso et al., 2017). Using this approach, some very

promising human cryptic CAMPs have been already identified: GVF27 identified in the 11-hydroxysteroid dehydrogenase-1 β-like protein (Bosso et al., 2017), ApoE (133-150) in the sequence of human apolipoprotein E (Pane et al., 2016a), $ApoB_L$ and $ApoB_S$ in the sequence of human apolipoprotein B (Gaglione et al., 2017) and PAP-A3, the activation peptide of human pepsinogen A, isoform 3 (Pane et al., 2018a).

1.8.2 The tools for recombinant AMP production

After the identification of the CAMPs-RPs and their cryptic CAMPs, a crucial issue is their production.

In general, peptides can be obtained by solid phase peptide synthesis (SPPS), or by recombinant strategies. Solid phase peptide synthesis is very well suited to obtain small amounts of relatively short peptides (up to about 30-40 aa), but less suitable when longer peptides or large quantities of peptide are required. Moreover, “difficult sequences”, for example sequences rich in proline, valine and isoleucine, may complicate the synthesis causing very low yields of the desired peptide (Mueller et al., 2020).

Recombinant strategies appear a more suitable, less expensive approach for large-scale production of long peptides (Gaglione et al., 2019a). A very efficient strategy for the production of toxic peptide in *E. coli* has already been developed in the laboratory where this PhD thesis has been carried out (Pane et al., 2016b).

The strategy has been designed to overcome some of recombinant expression drawbacks as AMPs toxicity for the host, intracellular degradation by proteases and difficult purification of the peptide. To effectively circumvent these obstacles, the desired peptide is fused to the C-terminus of Onconase (ONC), a frog ribonuclease. ONC is a very well suited partner for several reasons: (i) it can be expressed at very high level as inclusion bodies (about 200 mg/L in terrific broth); (ii) no soluble ONC can be detected in the cultures thus minimizing the risk of toxic effects of the ONC-CAMP fusion proteins; (iii) it is a very small protein (104 aa) thus allowing higher yields of the peptides after the cleavage.

ONC sequence has been modified to improve its use as a carrier for toxic peptide expression. The optimized construct, named ONC-DCless-H6, contains a His tag sequence at the C-terminus suitable for easy purification, furthermore it does not contain Met, Cys and Asp, Asp-Pro and Asn-Gly dipeptides thus allowing the selective

cleavage of the CAMPs from the carrier using all the most common reagents for the chemical cleavage of polypeptides (CNBr, which cleaves at the C-side of Met; formic acid, which cleaves at the C-side of Asp in the Asp-Pro dipeptides; hydroxylamine, which cleaves at the C-side of Asn in the Asn-Gly dipeptides; 2- nitro-5-thiocyanatobenzoic acid, which cleaves at the N-side of Cys). As ONC is insoluble at pH 7, after the cleavage of the fusion protein, the CAMPs can be recovered in high purity by selectively precipitating the carrier (Pane et al., 2016b).
Given the limited length of CAMPs (generally less than 50 aa) the sequences coding for the desired peptides can be produced by chemical synthesis and cloned at the 3' of the ONC coding sequence. This offers the possibility to optimize the codon usage for the expression in *E. coli.*
Using this method several cryptic CAMPs have already been expressed with final yields ≥ 10 mg/L of culture and purity > 98%: a 20 aa CAMP derived from the C-terminus of human thrombin (GKY20) (Pane et al., 2016b); ApoE (133-150), the cryptic CAMP derived from apoliprotein E; ApoBL and ApoBS, the cryptic CAMP derived from apolipoprotein B (Gaglione et al., 2017); PAP-A3, the activation peptide of human pepsinogen A, isoform 3 and its two fragments IMY25 and FLK22 (Pane et al., 2018a).
More recently this method has been optimized for the large-scale industrial production by developing a growth media optimized for the autoinduction expression in fermenters (Gaglione et al., 2019a).

1.8.3 The tools for peptide labelling and immobilization

The method for recombinant AMP production has been modified to obtain peptides with a cysteine residue at the N-terminus (Pane et al., 2018b). This was made possible by the discovery that the Asp-Cys peptide bond can be selectively hydrolysed in mild acidic conditions thus releasing peptides with a N-terminal cysteine. Due to the very special reactivity of N-terminal cysteine residues these peptides can be used to immobilize peptides on surfaces, to label and/or functionalize peptides (Cui et al., 2015; Jeon et al., 2012), to prepare bioconjugates and even to ligate two peptide/proteins by the so-called native chemical ligation (Johnson et al 2007).

In particular the possibility to prepare peptides with an N-terminal cysteine provides the opportunity to develop new labelling strategies, based on environment sensitive fluorophores, that are very useful to characterize membrane binding peptides in general and AMPs in particular. Environment-sensitive fluorophores are peculiar as their excitation spectra, emission spectra and/or quantum yields (QY) depend on variables such as pH, solvent polarity, viscosity and even molecular crowding/aggregation state. These fluorophores are very valuable tools in the study of a wide variety of molecular and cellular processes (Klymchenko et al., 2017; Han et al., 2010). As protein and peptide labels, they find applications in the study of conformational variations of proteins, of protein/protein, protein/ligand and protein/membrane interactions but also in the design of biosensors (Klymchenko et al., 2017; Loving et al., 2010; Donadio et al., 2016). For these reasons, the search for new environment-sensitive fluorescent probes and, in particular, for protein and peptide labels, is a very active research field.

Firefly luciferin (Luc), the substrate of firefly luciferase, is the most popular bioluminescent compound (Li S et al., 2021). It is less known that Luc is also an environment-sensitive fluorophore with unusual properties, summarized in Figure 5. The hydroxyl group at position 6 of the benzothiazole moiety behaves as a weak acid with a $pK_a \approx 8.7$ (Fig. 5A) (Morton et al., 1969). Both the phenol and the phenolate forms are strongly fluorescent but with very different excitation and emission wavelengths (Fig. 5B) (Ando et al., 2010). However, as Luc is a “photoacid” (Ando et al., 2010; Kuchlyan et al., 2014), it undergoes a light-induced dissociation with a $pK_a < 1$ (Fig. 5B). Thus, in the presence of water or other proton acceptors, Luc fluorescence is exclusively the result of the magenta and green pathways shown in Figure 5B. Even in neutral and acidic aqueous media, only the emission of the phenolate at 530 nm is generally observed, regardless of the excitation wavelength. Only in anhydrous organic solvents, e.g., acetonitrile or DMSO, does Luc show the blue fluorescence emitted by the phenol form (blue pathway in Figure 5B) (Presiado et al., 2010; Kuchlyan et al., 2014). However, very low amounts of water cause the appearance of the green emission. For example, in acetonitrile containing 14% water, the intensity of the blue and green emissions is comparable (Presiado et al., 2010).

Two synthetic Luc analogues (Fig. 5B), methoxyluciferin (mLuc) and aminoluciferin (aLuc), bearing non-dissociable groups at position 6 of the benzothiazole moiety show a single emission peak, with emission maxima similar to those of Luc phenol and phenolate forms, respectively (Vieira et al., 2012; Kakiuchi et al., 2017). mLuc is a very weak fluorophore (Vieira et al., 2012), whereas aLuc is brighter than Luc itself; very interestingly, it is a strongly solvatochromic fluorophore with shifts up to 40 nm in the λ_{max} values (Kakiuchi et al., 2017).

In spite of these intriguing features, to our knowledge, no example of direct fluorescent labeling of proteins or peptides based on Luc exists. This is even more surprising, considering that a Luc moiety can be incorporated very easily at the N-terminus of proteins and peptides. The final step of biological synthesis of Luc is a spontaneous condensation between D-cysteine and 6-hydroxy-2-cyanobenzothiazole (Fig. 5C). This reaction is included among the so-called “click reactions” that are quantitative, irreversible and very fast in physiological conditions (phosphate buffer, pH 7–7.4, 25–37 °C) (Ren et al., 2009; Chen XT et al., 2018).

L-cysteine at the N-terminus of a peptide reacts with 2-cyanobenzothiazole (CBT) similarly to free cysteine, as the carboxyl group is not involved in the reaction (Fig. 5C). Moreover, the nature of the substituent at position 6 of CBT also has a limited impact on the reaction. Therefore, peptides with an N-terminal cysteine residue can be efficiently labeled by using any 6-substituted 2-cyanobenzothiazole (Fig. 5C) (Ren et al., 2009; Chen XT et al., 2018).

Starting from these premises, it is reasonable to hypothesize that the reaction of peptides with an N-terminal cysteine with 6-substituted CBTs would provide fluorescent peptides with intriguing properties, suited for conformational and binding studies.

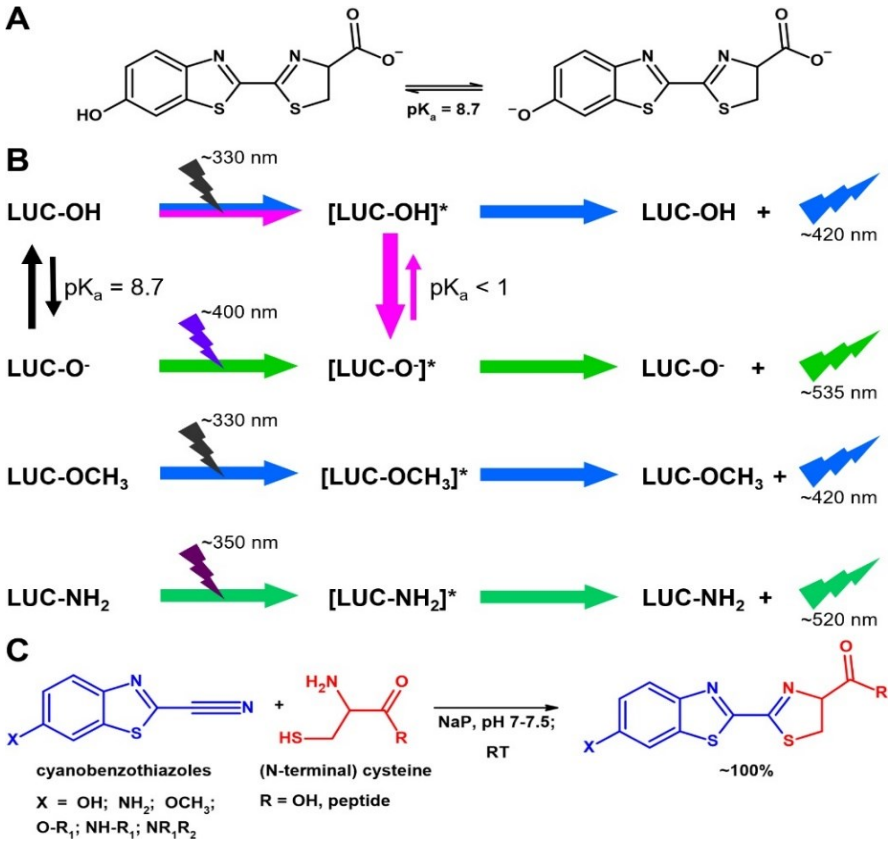

Figure 5. Structure, fluorescence and synthesis of luciferin and its analogues. **(A)** Structure of luciferin in phenol and phenolate forms. **(B)** Fluorescence of luciferin (Luc-OH), luciferin phenolate (Luc-O^-), methoxyluciferin (Luc-OCH3) and aminoluciferin (Luc-NH2). Excited states are indicated by an asterisk. **(C)** Condensation reaction between 6-substituted 2-cyanobenzothiazoles and cysteine (free or as N-terminal residue of a peptide). R_1 and R_2 can be a wide variety of alkyl and acyl groups. The nature of R_1 and R_2 has little or no impact on the reaction but can strongly influence fluorescence.

1.9 Aims

The main aims of this research work can be summarized as follows:

1) In silico analysis of human secretome to prepare a comprehensive list of new potential CAMP-RPs hosting high scoring CAMPs.
2) Preliminary characterization of a wide panel of newly identified CAMPs.
3) Recombinant production and thorough characterization of few selected particularly interesting CAMPs.
4) Development of luciferin-based labelling strategies to study the interaction of AMPs with liposomes, LPS and whole cells.

Chapter 2 - MATERIALS AND METHODS

2.1 Human proteome screening for cryptic peptides

The hypothetical CAMP-RPs and the corresponding cryptic CAMPs were identified using the *in silico* tool described by Pane et al. (Pane et al., 2017).
Each of about 2000 sequences of human secreted proteins obtained from the UniProt database (Torres et al., 2021) were analyzed and scored by the *in silico* tool. The method uses peptide length, charged residues and hydrophobic residues to create a score for the propensity of the peptide to present antimicrobial activity (Pane et al., 2017).

2.2 Materials

Expression host strain *E. coli* BL21(DE3) was purchased from Novagen (San Diego, CA, USA). To produce GKY20 peptide endowed with proline or cysteine residues at the N-terminal side, *pET22b(+)/ONC-DCless-H6-(P)GKY20* and *pET22b(+)/ONC-DCless-H6-(C)GKY20 vectors*, coding for the corresponding recombinant fusion proteins, were used. These plasmids, obtained as described in Pane et al. (Pane et al., 2016b; Pane et al., 2018b), were already available. All the other expression vectors named:

pET22b(+)/ONC-DCless-H6-(P)FIBα-GVV27,
pET22b(+)/ONC-DCless-H6-(P)FIBα-SFR22,
pET22b(+)/ONC-DCless-H6-(P)FIBβ-GVV28,
pET22b(+)/ONC-DCless-H6-(P)FIBβ-NWK23,
pET22b(+)/ONC-DCless-H6-(P)FIBγ-GII30,
pET22b(+)/ONC-DCless-H6-(P)FIBγ-TWK25,
pET22b(+)/ONC-DCless-H6-(C)FIBγ-TWK25,
coding for the corresponding recombinant fusion proteins, were purchased from GenScript (USA Inc., Piscataway, NJ, USA). Nucleotide and amino acid sequences of peptides were reported in figure 1. Codons were optimized for expression in *E. coli*.
Synthetic peptides identified by bioinformatic tool were provided by Dr. Caesar de la Fuente Nuñez (University of Pennsylvania, Philadelphia, Pennsylvania, USA).
LL-37 (LLGDFFRKSKEKIGKEFKRIVQRIKDFLRNLVPRTES) and (C)RGD (CGRGDSP) synthetic peptides were from CASLO ApS (Kongens Lyngby, Denmark).

Ni Sepharose™ 6 FastFlow was from GE Healthcare (Uppsala, Sweden). Nutrient broth (NB) was purchased from Difco (Detroit, Mich.). Tryptone and yeast extract were purchased from Condalab (Madrid, Spain). All other reagents were from Merck KGaA (Darmstadt, Germany).

A) **Nucleotide sequence of (P)FIBα- GVV27**
GATCCGGGAGTGGTCTGGGTTTCCTTTAGAGGGGCAGATTATTCCCTCAGGGCTGTTCGCATGAA
AATTAGGCCCCTTGTGACCCAA
Amino acid sequence
DPGVVWVSFRGADYSLRAVRMKIRPLVTQ

B) **Nucleotide sequence of (P)FIBα-SFR22**
GATCCGTCCTTTAGAGGGGCAGATTATTCCCTCAGGGCTGTTCGCATGAAAATTAGGCCCCTTGTG
ACCCAA
Amino acid sequence
DPSFRGADYSLRAVRMKIRPLVTQ

C) **Nucleotide sequence of (P)FIBβ-GVV28**
GATCCGGGTGTGGTGTGGATGAATTGGAAAGGCAGCTGGTATAGCATGCGTAAAATGAGCATG
AAAATTCGTCCGTTTTTTCCGCAGCAG
Aminoacid sequence
DPGVVWMNWKGSWYSMRKMSMKIRPFFPQQ

D) **Nucleotide sequence of (P)FIBβ-NWK23**
GATCCGAATTGGAAAGGCAGCTGGTATAGCATGCGTAAAATGAGCATGAAAATTCGTCCGTTTTT
TCCGCAGCAG
Aminoacid sequence
DPNWKGSWYSMRKMSMKIRPFFPQQ

E) **Nucleotide sequence of (P)FIBγ-GII30**
GATCCGGGTATTATTTGGGCGACCTGGAAAACCCGTTGGTATAGCATGAAAAAAACCACCATGA
AAATTATTCCGTTTAACCGTCTGACCATTGGC
Aminoacid sequence
DPGIIWATWKTRWYSMKKTTMKIIPFNRLTIG

F) **Nucleotide sequence of (P)FIBγ-TWK25**
GATCCGACCTGGAAAACCCGTTGGTATAGCATGAAAAAAACCACCATGAAAATTATTCCGTTTAA
CCGTCTGACCATTGGC
Aminoacid sequence
DPTWKTRWYSMKKTTMKIIPFNRLTIG

G) **Nucleotide sequence of (C)FIBγ-TWK25**
GATTGCACCTGGAAAACCCGTTGGTATAGCATGAAAAAAACCACCATGAAAATTATTCCGTTTAA
CCGTCTGACCATTGGC
Aminoacid sequence
DCTWKTRWYSMKKTTMKIIPFNRLTIG

Figure 1. Nucleotide and amino acid sequences of the recombinant peptides. Blue: peptide; red: DP or DC cleavage sites.

2.3 General procedures

Bacterial cultures were carried out according to Sambrook (Green et al., 2012). Sodium Dodecyl Sulphate PolyAcrylamide Gel Electrophoresis (SDS-PAGE) was carried out according to Laemmli (Laemmli, 1970). Gels were stained by Coomassie Blue staining solution containing 4 % (v/v) formaldehyde to cross-link proteins and polypeptides (Steck et al., 1980). Protein concentrations were determined using the Bradford Protein Assay (Merck KGaA, Darmstadt, Germany) with standard curves generated using bovine serum albumin (BSA). Concentrations of purified fusion proteins and peptides were determined by spectrophotometric analysis using the extinction coefficients calculated using the ProtParam tool (accessible to the address http://web.expasy.org/protparam/) (Gasteiger et al., 2005) (Extinction coefficients were listed in Table 1). Bicinchoninic acid protein assay kit (Thermo Scientific, Rockford, IL, USA) was used to quantify peptides without aromatic residues.

Recombinant proteins	ε_{280} $M^{-1}\ cm^{-1}$	$\varepsilon_{280}^{(0.1\%)}$ mg/mL
ONC-DCless-H6-(P)FIBα-GVV27	22,920	1.385
ONC-DCless-H6-(P)FIBα-SFR22	17,420	1.088
ONC-DCless-H6-(P)FIBβ-GVV28	33,920	2.001
ONC-DCless-H6-(P)FIBβ-NWK23	28,420	1.735
ONC-DCless-H6-(P)FIBγ-GII30	33,920	1.986
ONC-DCless-H6-(P)FIBγ-TWK25	28,420	1.718
ONC-DCless-H6-(C)FIBγ-TWK25	28,420	1.717
ONC-DCless-H6-(P)GKY20	24,410	1.530
ONC-DCless-H6-(C)GKY20	24,410	1.530
Peptides		
(P)FIBα-GVV27	6,990	2.182
(P)FIBα-SFR22	1,490	0.560
(P)FIBβ-GVV28	17,990	4.991
(P)FIBβ-NWK23	12,490	4.120
(P)FIBγ-GII30	17,990	4.811
(P)FIBγ-TWK25	12,490	3.904
(C)FIBγ-TWK25	12,490	3.897
(P)GKY20	8,480	3.250
(C)GKY20	8,480	3.243

Table 1. Extinction coefficients of recombinant proteins and peptides calculated by the ProtParam tool.

2.4 Expression of recombinant proteins

E. coli strain BL21(DE3) was used to express recombinant proteins. Cells, transformed with pET recombinant plasmids, were grown in 10 mL of LB medium containing 100 µg/ml ampicillin, at 37°C up to an absorbance of 2 OD at 600 nm. These cultures were used to inoculate 1 L of LB/ampicillin medium containing 100 µg/ml ampicillin. Cultures were incubated at 37°C under shaking up to $OD_{600\ nm}$ of 1.5-2. Expression of recombinant proteins was induced by addition Isopropyl β-D-1-thiogalactopyranoside (IPTG) at a final concentration of 0.4 mM. Cells were harvested after 3 h induction by centrifugation at 6000 rpm for 10 min at 4°C. The bacterial pellet was suspended in 50 mM Tris-HCl, pH 7.4 and sonicated by ultrasonic processor on ice (15 x 1 min cycle; amplitude control set at 100%). The suspension was then centrifuged at 12000 rpm for 60 min at 4°C. Soluble and insoluble fractions were analyzed by SDS-PAGE.

2.5 Purification of fusion proteins

Recombinant proteins were purified by immobilized metal ion affinity chromatography (IMAC), using the Ni Sepharose™ 6 Fast Flow resin. Amounts of fusion proteins ranging from 100 mg to 140 mg were dissolved in 20 mL of denaturing buffer (5 M guanidine/HCl in 50 mM Tris-HCl, pH 7.4) and incubated on a rotary shaker at 37°C for 3 h under nitrogen atmosphere. Soluble fractions were collected by centrifugation and incubated with 5 mL of Ni Sepharose™ 6 Fast Flow resin equilibrated in denaturing buffer. The resin was shaken at 4°C for 16 h and then collected by centrifugation. The supernatant, containing the unbound proteins, was discarded. The resin was washed three times with 25 ml of denaturing buffer at 4°C for 30 min and then packed in a glass column. The fusion proteins were eluted with 30 ml of 0.1M sodium acetate buffer, pH 5.0, containing 5 M guanidine/HCl (elution buffer).
In the case of: *ONC-DCless-H6-(C)FIBγ-TWK25* and *ONC-DCless-H6-(C)GKY20* fusion proteins, IMAC purification was carried out in the presence of 1 mM Tris(2-carboxyethyl)phosphine hydrochloride (TCEP-HCl) as a thiol-free reducing agent to obtain the protein reduced form.
The eluate was extensively dialyzed against 0.1 M acetic acid at 4°C. Samples were stored at -80°C under nitrogen atmosphere. Purified fusion protein concentrations were determined by

spectrophotometric analysis using the extinction coefficients calculated using the ProtParam tool.

2.6 Cleavage of Asp-Pro and Asp-Cys peptide bonds

Cleavage of peptides from fusion proteins was performed in 0.1 M acetic acid at pH 2.0 (by addition of 18 mM HCl) incubating samples at 60°C for 24 h in a water bath under nitrogen atmosphere and by using 1 mM TCEP-HCl as scavenger of reactive oxygen species.
Cleavage percentages were estimated by densitometry analysis of SDSPAGEs using ImageJ software, available for free download at http://rsb.info.nih.gov/ij/ (Schneider et al. 2012).

2.7 Purification of recombinant peptides

A column-free purification procedure based on different solubility of carrier and peptides at pH 7 (Pane et al., 2016b) was first tested to evaluate solubility properties of each peptide in the experimental conditions. The hydrolysis mixtures were neutralized to pH 7-7.2 by adding NH_3 1 M. Samples were incubated for 1 h at 22 °C under nitrogen atmosphere in a water bath. Insoluble fusion proteins and carriers were separated from soluble peptides by 1 h centrifugation at 12000 rpm at 4 °C. Supernatants, containing soluble peptides, and insoluble fractions, containing carriers and uncleaved fusion proteins, were analyzed by SDS-PAGE. Peptide concentrations into soluble fractions were determined by spectrophotometric analyses using the extinction coefficients (Table 1) calculated by the ProtParam tool (accessible to the address http://web.expasy.org/protparam/) (Gasteiger et al., 2005). Peptides purified by selective precipitation of carrier were lyophilized and stored at -80°C. Peptides that co-precipitated with Onconase carrier at neutral pH were purified by reverse-phase chromatography (RP-HPLC).

2.8 RP-HPLC analyses

RP-HPLC were performed on a Jasco LC-4000 system equipped with PU-4086 semipreparative pumps and an MD-4010 photo diode array detector. The column was a C18 (25 × 1 cm, 5 µm particle size) Europa Protein 300Å (pore size) from Teknokroma (Barcelona, Spain).
The solvents were 0.05% trifluoracetic acid (TFA) in water (solvent A) and 0.05% TFA in acetonitrile (solvent B). Elution profiles were

recorded at 280 nm wavelength at a flow rate of 2 ml/min by linear gradients as follows:
Gradient 1: from 5% to 25% solvent B in 10 min, from 25% to 29% solvent B in 60 min, isocratic elution at 29% solvent B for 20 min, from 29% to 60% solvent B in 20 min, from 60% to 100% solvent B in 5 min, isocratic elution at 100% B for 10 min.
Gradient 2: from 5% to 20% solvent B in 10 min, from 20% to 25% solvent B in 60 min, isocratic elution at 25% solvent B for 20 min, from 25% to 60% solvent B in 20 min, from 60% to 100% solvent B in 5 min, isocratic elution at 100% solvent B for 10 min.
Gradient 3: isocratic elution at 5% solvent B for 10 min, from 5% to 30% solvent B in 5 min, from 30% to 38% solvent B in 40 min, from 38% to 100% solvent B in 10 min, isocratic elution at 100% solvent B for 10 min.
Gradient 4: from 5% to 27% solvent B in 10 min, from 27% to 31% solvent B in 60 min, isocratic elution at 31% solvent B for 60 min, from 31% to 100% solvent B in 20 min, isocratic elution at 100% solvent B for 20 min.
Gradients used for each peptide to perform analytical chromatography and large-scale purification procedures were reported in table 2.

Peptide	Cleavage analysis	Purification	Purity analysis
	Gradient number		
(P)FIBα-GVV27	1	1	3
(P)FIBα-SFR22	2	2	1
(P)FIBβ-GVV28	3	4	3
(P)FIBβ-NWK23	1	1	1
(P)FIBγ-GII30	3	4	3
(P)FIBγ-TWK25	1	1	1
(C)FIBγ-TWK25	1	1	1
Luc-FIBγ-TWK25	-	1	3

Table 2. Gradients used for RP-HPLC analyses.

2.9 Antibacterial assays: MIC, MBC and FIC index

The minimum Inhibitory Concentration (MIC) analyses were performed on Gram-positive and Gram-negative bacteria by broth microdilution method for antimicrobial peptides previously described (Pane et al., 2017) (Wiegand et al., 2008) with minor modifications.
In details, assays were carried out in Nutrient Broth 0.5x (Difco, Detroit, Mich.) using sterile 96-well polypropylene microtiter plates (cat. 3879, Costar Corp., Cambridge, MA). Bacterial strains were grown in Luria-Bertani (LB) medium overnight at 37°C and then diluted in Nutrient Broth at a final concentration of ~$5x10^5$ CFU/mL per well. Twofold serial dilutions of peptides were carried out in the test wells to obtain concentrations ranging from 50 μM to 0.05 μM.
In the case of INTb-AWT25 and INFk-AWE26 peptides, twofold serial dilutions start from 35.6 μM and 58.6 μM respectively, due to their limited solubility in water. Plates were incubated overnight at 37°C.
MIC value was taken as the lowest concentration at which growth was inhibited. Three independent experiments were performed for each MIC value. The peptide antibiotic polymyxin B and vancomycin (Merck KGaA, Darmstadt, Germany) were tested as control (twofold serial dilutions starting from 64 μg/mL concentration).
MIC values were measured on Gram-negative (*Pseudomonas aeruginosa* PAO1, *Escherichia coli* ATCC 25922, *Klebsiella pneumonia* ATCC 700603, *Acinetobacter baumanii* ATCC 17878, *Salmonella enteriditis* 706 RIVM, *Salmonella typhimurium* ATCC 14028, *Pseudomonas aeruginosa* PA14 and *Pseudomonas aeruginosa* RP73) and Gram-positive strains (*Staphylococcus aureus* ATCC 6538P, *Enterococcus faecalis* ATCC 29212 and *Bacillus globigii* TNO BM013).
To evaluate the bactericidal activity of the peptides the minimum bactericidal concentration (MBC) was determined from the broth dilution of MIC tests by subculturing cell mixtures on LB agar plates. The MBC was defined as the lowest concentration of antibacterial agent that kills ≥ 99.9% of bacterial cells. MBC values were measured on Gram-negative (*Pseudomonas aeruginosa* PAO1) and Gram-positive strains (Staphylococcus aureus ATCC 6538P).
Antibacterial agents are usually regarded as bactericidal if the MBC is no more than four times the MIC.
Synergy between CAMP/CAMP and CAMP/antibiotic combinations was assessed by the so called checkerboard assay, a broth

microdilution assay based on a two-dimensional array of serial dilutions of tested compounds. Experiments were carried out in 96-well plate on *Pseudomonas aeruginosa* PAO1 (Gram-negative) and *Staphylococcus aureus* ATCC 6538P (Gram-positive). Peptides were tested in several combinations CAMP/CAMP and CAMP/antibiotic, such as colistin, tobramycin and ciprofloxacin. The first antibiotic of the combination was serially diluted along the ordinate, while the second drug was diluted along the abscissa. The resulting checkerboard contains each combination of two antibiotics. Plates were incubated 16 h at 37°C. The fractional inhibitory concentration (FIC) index was calculated as follows: $FIC_A + FIC_B$, where FIC_A = MIC of drug A in combination/MIC of drug A alone, and FIC_B = MIC of drug B in combination/MIC of drug B alone. FIC index (FICI), reported in "Results and Discussion" section, refer to the combination of concentrations leading to the lowest FICI value.
As FICI interpretation model we used two similar models (Table 3). The more restrictive model proposed by Eucast (2000) assumes synergistic effects when FICI value≤0.5; additive when 0.5<FICI value≤1, indifferent when 1<FICI value<2 and antagonistic effect when FICI value≥2. The second model proposed by Fratini (2017) are less restrictive and propose a synergistic effect when FICI value < 1, additive when FICI value = 1, indifferent when 1 < FICI value ≤ 2 and antagonistic when FICI value > 2.

FICI value		**Effect**
Eucast model	**Fratini model**	
FICI≤ 0.5	FICI< 1	Synergistic
0.5 <FICI≤ 1	FICI= 1	Additive
1 <FICI< 2	1 < FICI≤ 2	Indifferent
FICI≥ 2	FICI> 2	Antagonist

Table 3. Interpretation model of FIC index

2.10 Antibiofilm activity

Antibiofilm activity of selected peptides was evaluated on pre-formed biofilm of *P. aeruginosa* PAO1 strains. Bacteria were grown overnight in Luria Bertani (LB) medium at 37°C. Overnight culture was dilute to 1×10^8 CFU/mL and incubated in BM2 biofilm-adjusted medium (Li J et al., 2013) (62 mM potassium phosphate buffer pH 7, 7 mM $(NH_4)_2SO_4$, 2 mM $MgSO_4$, 10 µM $FeSO_4$, 0.4% (wt/vol) glucose) in polystyrene 96-well microtiter plates (Corning®, USA) for 24 h at 37°C. One-day-old biofilm was then treated with increasing concentrations of the peptide under investigation (0.39-30 µM) to evaluate its eradication ability of pre-formed biofilm after 4 h incubation time at 37°C. At the end of the incubation, planktonic cultures were removed from the wells. After 3 washing steps with sterile PBS, biofilm mass was stained by 0.1% crystal violet for 20 min. The crystal violet excess was eliminated by three successive washes with sterile water. Finally, the crystal violet was solubilized with 30% acetic acid and sample optical absorbance values were determined at 595 nm by using a microtiter plate reader (Synergy™ H4, BioTek, USA).

To determine the percentage of viable bacteria after peptide incubation, biofilm was dissolved with 1% Triton X-100 for 10 min. Cells were serially diluted in LB medium and plated on LB/agar plates. After incubation for 16 h at 37°C, colony forming units were counted. Percentages of survival cells were calculated as follow: $(CFU_{\text{treated sample}}/CFU_{\text{untreated sample}})*100$.

The metabolic activity of cells after peptides treatment was evaluated by Cell Proliferation Kit II assay (XTT) (Merck KGaA, Darmstadt, Germany). Planktonic cells were removed and the plates were thoroughly washed three times with PBS. The assay was carried out in 100 µL of PBS added with 50 µL of XTT solution. Plates were incubated in the dark for 3-6 h at 37°C. The reduction of the tetrazolium salt into orange formazan dye by metabolically active cells was measured at 490 nm by using a microtiter plate reader. Viability was compared to controls carried out in absence of peptides. The medium was also set as negative control.

2.11 MTT assay

Cytotoxic effects of selected peptides on undifferentiated human monocytic cell line THP-1 (nonadherent cells) and on a human keratinocytes cell line HaCaT (adherent cells) were determined by

performing the 3-(4,5-dimethylthiazol-2-yl)-2,5 diphenyltetrazolium bromide reduction inhibition assay (MTT assay), designed to be used for the spectro-photometric quantification of cell proliferation.
2×104 cells were seeded into a 96-well plate (round-bottomed for undifferentiated nonadherent cells) and incubated at 37 °C in the presence of 5% CO_2.
After 16h, 96-well plate with nonadherent cells was centrifuged at 1000 rpm for 5 min and the media were replaced with fresh PBS. Cells were then again centrifuged at 1000 rpm for 5 min and PBS was replaced with 100 µL of fresh medium containing peptide solution at a final concentration ranging from 0.3 to 20 µM/well. Previously described cell washing and peptides administration steps have been carried out avoiding centrifugation steps for HaCaT cells since they are adherent cells.
After 24 h of incubation at 37 °C, the peptide-containing media were removed, and 100 µL of tetrazolium MTT diluted at 0.5 mg/mL in Dulbecco's modified Eagle's medium (DMEM) purchased from Lonza (Basel, Switzerland) without red phenol was added. After 4 h of incubation at 37 °C, the resulting insoluble formazan salts were solubilized in 0.04 M HCl in anhydrous isopropanol and quantified by measuring the absorbance at λ=570 nm, using an automatic plate reader spectrophotometer (Synergy™ H4, BioTek, USA). Cell survival was expressed as means of the percentage values compared to control. Analyses were performed at last 3 times.

2.12 Labeling and purification of peptides

mLuc-GKY20 and PyMPO-GKY20 peptides labeled by 6-methoxy-2-cyanobenzothiazole (CBT-OCH_3) and PyMPO maleimide (1-[2-(maleimido)ethyl]-4-[5-(4-methoxyphenyl)-2-oxazolyl]pyridinium triflate), respectively, were already available in the laboratory where this PhD work was carried out.
Peptide labeling by 6-hydroxy-2-cyanobenzothiazole (CBT-OH) and 6-amino-2-cyanobenzothiazole (CBT-NH_2) was performed following the procedure previously described (Pane et al., 2018b). Modification reactions were monitored by RP-HPLC on Europa Protein 300 C18 column with linear gradients (data not shown). Peptides were then purified through RP-HPLC with linear gradients (Table 2) (Siepi et al., 2021), lyophilized and dissolved in deionized water. Labeled peptide concentrations were determined using molar extinction coefficients reported in literature (luciferin: ε_{322nm} = 18,340

M^{-1} cm^{-1}; aminoluciferin: ε_{354nm} = 15,500 M^{-1} cm^{-1} (Monsees et al., 1994). Peptide concentrations were also confirmed by BCA assay. Purity of peptides was assessed by RP-HPLC on C18 column (data not shown).

2.13 Mass Spectrometry Analyses

Analyses were performed by Prof. Antimo Di Maro (University Vanvitelli, Caserta) on a MALDI-TOF micro MX spectrometer (Waters, Manchester, UK).

2.14 Steady-state fluorescence spectroscopy in water/organic solvent mixtures and SDS

Fluorescence spectra were recorded on a Fluoromax-4 fluorometer (Horiba, Edison, NJ, USA) using a 1 cm path length quartz cuvette at a temperature of 25 °C, using a peltier that can ensure an accuracy of ±0.1 °C. All experiments were carried out at a fixed peptide concentration (2 µM) in 10 mM sodium phosphate (NaP), pH 7.4, at 25 °C, unless otherwise stated. The excitation wavelengths were set to 330 nm (Luc-labeled peptides, phenol form), 400 nm (Luc-labeled peptides, phenolate form), 363 nm (aLuc-labeled peptides), 330 nm (mLuc-GKY20) and 408 nm for 1-[2-(maleimido)ethyl]-4-[5-(4-methoxyphenyl)-2-oxazolyl]pyridinium-labeled GKY20 [PyMPO-IGKY20]. The excitation spectra were recorded by varying the wavelength of excitation between 200 nm and 500 nm (em. = 539 nm). To evaluate the solvatochromic properties of labeled peptides, fluorescence spectra were recorded in the presence of NaP:methanol (50% v:v), NaP:isopropanol (50% v:v) and SDS (25 mM) under the experimental condition described above.

2.15 Steady-state fluorescence spectroscopy in the presence of liposomes

Experiments were carried out by Prof. Pompea Del Vecchio (University of Naples Federico II). Fluorescence spectra were recorded on a FluoroMax-4 fluorometer (Horiba, Kyoto, Japan). The emission spectra of Luc-labeled peptides were acquired, upon excitation at 330 nm, in the range 350–650 nm. For the aLuc-labeled peptides, the emission spectra were acquired in the range 380–700 nm, upon excitation at 363 nm. In addition, for Luc-labeled peptides, excitation spectra were also recorded. The excitation spectra were

recorded by varying the wavelength of excitation between 275 nm and 480 nm and monitoring the emission at 539 nm. All the spectra were recorded at a lipid-to-peptide ratio of 200 in 10 mM NaP, pH 7.4. The concentration of peptides was in the range of 2.2–3.6 μM.

2.16 Quantum-Yield determination

Experiments were carried out by Prof. Pompea Del Vecchio (University of Naples Federico II) as previously described (Siepi et al., 2021). Fluorescence quantum yields were determined for all the labeled peptides in 10 mM phosphate buffer, pH 7.4, in a mixture composed of phosphate buffer and isopropanol in the ratio 1:1 (v:v) and in acetate buffer, pH 5. Determination of the quantum yields was performed by comparing the fluorescence of samples to that of a standard, as previously described (Fery-Forgues et al., 1999). Fluorescein (in 0.1 M NaOH) was used as standard in the case of (a)Luc- and PyMPO-labeled peptides, whereas coumarin-6 (in pure ethanol) was used in the case of mLuc-labeled GKY20.

2.17 *pKa* Determination of Luc-Labeled Peptides

In order to measure pK_a values, phenolate concentration was evaluated by titrating a solution of Luc-labeled peptide (2 μM) as a function of pH (0.2 M sodium acetate, pH 4–6; 0.2 M sodium phosphate, pH 6–7.4; 0.2 M Tris/HCl, pH 7–9; 0.2 M Glycine /NaOH, pH 8–11). The excitation wavelength was set to 400 nm. Excitation spectra were recorded at 539 nm. pK_a values were determined by GraphPad Prism software (version 6, San Diego, CA, USA) by plotting variation of total fluorescence (450–700 nm) as a function of pH values.

2.18 Interaction of labeled CAMPs with LPS

Binding of CAMPs (2 μM) to LPS (200 μg/mL) from *E. coli* 0111:B4 (MW 10,000) (Yu L et al., 2006) was performed in 10 mM NaP buffer, pH 7.4. Mixtures were equilibrated at 25 °C for 10 min before recording emission (Luc-peptides, ex. = 330; aLuc-peptides, ex. = 363 nm) and excitation spectra (Luc-GKY20, em. = 516 nm; Luc-$ApoB_L$, em. = 508 nm) by means of a FluoroMax-4 fluorimeter. To test the influence of micellar and sub-micellar LPS concentration on CAMP fluorescence (2 μM), emission spectra (Luc-peptides, ex. = 330 or 400 nm; aLuc-peptides, ex. = 363 nm) were also recorded in the presence of increasing concentrations of LPS (0.62 e 200

μg/mL). Variation of total fluorescence (450–700 nm) was reported as a function of LPS concentration. The assays to determine K_d and binding stoichiometry of Luc-peptides toward LPS were carried out in 96-well polystyrene microtiter plates containing 100 μL of peptide/LPS mixtures. Spectra were recorded using a Synergy™ H4 microplate reader (BioTek Instruments Inc., Winooski, VT, USA) in 10 mM NaP buffer, pH 7.4, in the presence of 40 μg/mL (≈ 4 μM; MW 10,000) LPS and Luc-peptides (0.25–18 μM). Mixtures were incubated 15 min before emission spectra were recorded by excitation between 400 and 425 nm (phenolate form). Variation of total fluorescence (450–700 nm) was reported as a function of peptide concentration, and data were fitted to the model using Graphpad Prism (Siepi et al., 2021).

2.19 Interaction of labeled CAMPs with *E. coli* cells

Bacterial *E. coli* ATCC 25,922 strain was cultured in LB medium at 37 °C overnight. Culture was diluted 1:100 in fresh LB medium, and bacteria were grown until 1 OD_{600} optical density. Cells were collected by centrifugation at 8000× *g* for 5 min at 4 °C, washed three times in 10 mM NaP buffer, pH 7.4, and suspended at 1 OD_{600} concentration (10x cell stock solution) in the same buffer. The bacteria mixture was stored on ice until use. Binding of labeled CAMPs to *E. coli* cells was performed in 10 mM NaP buffer, pH 7.4, in the presence of 0.1 OD_{600} bacterial cells and 2 μM peptides. Mixtures were incubated at 25 °C for 20 min [(a)Luc-GKY20] and 120 min [(a)Luc-ApoB_L] before recording emission spectra (Luc-peptides, ex. = 330 and 400 nm; aLuc-peptides, ex. = 363 nm).

2.20 Kinetic analysis

Binding kinetic to LPS and *E. coli* cells was carried out in 10 mM NaP buffer, pH 7.4, in the presence of either 50 μg/mL LPS or 0.1 OD_{600} bacterial cells prepared as described above. Binding reactions were started by adding peptides (2 μM) and manually mixing the samples for 40 s. Binding was monitored, exciting at 400 nm and reading at 539 nm. One reading per minute was performed over 16 min observation time. Samples were not irradiated in the period between two readings in order to minimize peptide photobleaching. Photobleaching of peptides was also verified by control experiments carried out in the absence of LPS and cells.

2.21 Microscopy analysis of *E. coli* cells treated with the labeled peptides

Binding of labeled CAMPs (3 μM) to *E. coli* cells was performed in 10 mM NaP buffer, pH 7.4, in the presence of 0.1 OD_{600} bacterial cells. Fluorescence microscopy images of treated and untreated *E. coli* cells were taken over 50 min incubation at 25 °C. For this purpose, 10 μL of each sample was observed with an Olympus BX51 fluorescence microscope (Olympus, Tokyo, Japan) using DAPI (aLuc-labeled peptides) and FITC (Luc-labeled peptides) filters. Standard acquisition times were 1000 ms. Images were captured using an Olympus DP70 digital camera. The experiments were performed at least three times.

2.22 Determination of K_d values and stoichiometries

In order to determine the K_d value of Luc-labeled peptides for micellar LPS, we carried out the experiment at variable Luc-labeled peptide concentration and constant LPS concentrations (5 μg/mL corresponding to ~0.5 μM and 40 μg/mL corresponding to ~4 μM). The experimental data were fitted to the model described in Siepi et al. (Siepi et al., 2021).

Chapter 3 – RESULTS AND DISCUSSION

3.1 In silico identification of novel bioactive peptides

In order to achieve the first objective of this PhD work, new potential human CAMP-RPs and the corresponding cryptic CAMPs were identified using the *in silico* tool described in the Introduction (Pane et al., 2017). To maximize the chances of isolating cryptic CAMPs with the desired activities, in the first place we chose to analyse human secreted proteins, in fact, it is reasonable to assume that secreted proteins, being exposed to the extracellular environment, are more likely involved in host defence and, therefore, they should be richer in cryptic AMP-like sequences. In collaboration with Prof. Orlando Crescenzi (Department of Chemical Science, University of Naples Federico II) about 2000 sequences of human secreted proteins were obtained from the UniProt database and analyzed to generate a list of potential CAMP-RPs, i.e. proteins containing at least one high scoring peptide with an A.S. higher than 7, a score suggesting a moderate antimicrobial activity (MIC<~100 μM). Intriguingly, more than 10-15% of the analysed protein showed the presence of at least one peptide with an A.S. higher than the threshold (data not shown).
Given the very high number of potential CAMP-RPs and cryptic CAMPs, the list was manually analysed to select a number of peptides suitable for a preliminary experimental characterization. The most interesting candidates were selected according to the following criteria:

a) The presence of at least 1 high-scoring peptide not longer than 40-50 residues.

b) The physiological role, abundance and tissue specificity of the protein; abundant or widely distributed proteins involved in immune defence, coagulation, extracellular matrix formation/remodelling were considered particularly interesting for obvious reasons.

c) The position of the high-scoring peptide inside the primary structure of the protein; peptides at or close to the chain termini or to linker-regions of multi-domain proteins were considered particularly interesting as these peptides could be more easily released *in vivo* (thus suggesting the presence of a physiological CAMP with desirable activities).

D) The distribution of the hydrophobic and basic residues inside the peptide; peptides with long stretches of hydrophobic residues were discarded as these peptides could show low solubility, higher toxicity and could be difficult to synthesize.

e) A number of cysteine residues preferably ≤ 2; free cysteines are unstable and should be alkylated or mutated.

The manual screening of the raw pool of CAMP-RPs provided by the *in silico* analysis led to the selection of 17 human secreted proteins hosting 34 new potential cryptic CAMPs. The sequences of the 34 peptides are shown in Table 1 whereas the corresponding CAMP-RPs are briefly described below (the UniProt codes are in square parenthesis). For the sake of brevity, only the analysis of the fibrinogen subunits is discussed in details.

Human serum albumin (HSA) [P02768]

HSA is the main protein of plasma. Its main function is the regulation of the colloidal osmotic pressure of blood, but it also works as transporter of metal ions (zinc, calcium and magnesium), fatty acids, vitamins and several drugs. It binds the bacterial siderophore enterobactin and inhibits enterobactin-mediated iron uptake of *E. coli* from ferric transferrin, and may thereby limit the utilization of iron and growth of enteric bacteria such as *E. coli.*

The analysis of the HSA sequence showed the presence of four internal regions with high A.S. values. Intriguingly, these regions perfectly overlap to four helix-turn-helix motives in the fold of HSA. The corresponding selected peptides are shown in Table 1.

Fibrinogen alpha chain (FIBα) [P02671], beta chain (FIBβ) [P02675] and gamma chain (FIBγ) [P02679]

FIB is a major glycoprotein that circulates in the blood of vertebrates. In humans its concentration in blood plasma is about 3 mg/ml. During tissue and vascular injury it is converted enzymatically by thrombin to fibrin which aggregates thus starting the formation of blood clots. Therefore, FIB has a central role in blood coagulation.

The selected peptides are at the C-termini of each of the three subunits of FIB, Aα, Bβ and γ. The C-terminal domains of the three subunits are homologous, therefore it is not surprising that a CAMP-like peptide is present in each subunit at the same location. The similarity in the sequences of the three regions is evident in Table 1, where the sequences of the fibrinogen derived peptides are shown

aligned. However, differences in the number of positively charged and very hydrophobic residues determine significant differences in the A.S. values of the three cryptic peptides. Figure 1 shows a detailed analysis of the C-terminal region of the FIB subunits.

The isometric plots, reporting A.S. values as function of starting residue (x axis) and peptide length (y axis), clearly show the presence of an absolute maximum starting at the homologous residues FIB-Aα V822 (24 aa), FIB-Bβ V435 (24 aa) and FIB-γ I367 (28 aa). Moreover, a lower relative maximum is present at the end of a narrow crest on the left of the main peak and corresponding to the homologous residues FIB-Aα F827 (19 aa), FIB-Bβ W440 (19 aa) and FIB-γ W372 (23 aa).

It is Interesting to note that the 3 peptides corresponding to the absolute maxima include an N-terminal stretch of 4 consecutive hydrophobic and β-preferring residues not present in the peptides corresponding to the relative maxima: VVWV (FIB-Aα), VVWM (FIB-Bβ) and IIWA (FIB-γ). As the *in silico* tool scores the potential antimicrobial potency of a peptide but not other relevant properties like solubility, propensity to aggregate and bioavailability, the C-termini of FIB subunits were also analyzed by using three tools for the identifications of aggregation prone regions in proteins, namely TANGO (Rousseau et al., 2006; Fernandez-Escamilla et al., 2004), AmylPRED (Frousios et al., 2009) and AggreSCAN (Conchillo-Solé et al., 2007). The three tools identified an aggregation-prone region of 6-8 residues in each subunit centered around the four-residue hydrophobic regions mentioned above.

On the basis of these findings, both the longer and the shorter form of each potential cryptide were selected for the characterization in spite of the significant differences in the A.S. values.

It should be noted that in addition to the residues identified by the A.S. analysis few hydrophilic residues at the N- and C-termini were included in the peptides to be synthetized. T486-Q847 and P459-Q460-Q461 are the last residues of FIB-Aα and FIB-Bβ, respectively, so they were included in the peptides FIBα-GVV27, FIBα-SFR22, FIBβ-GVV28 and FIBβ-NWK28. The single Gly, Ser, Thr, Asn at the N-termini of the all the FIB derived-peptides and at the C-termini of FIB-γ derived peptides were arbitrarily included on the basis of the assumption that small uncharged residues may improve the interaction of the positively charged termini with the phospholipids heads thus improving membrane binding.

Von Willebrand factor (vWF) [P04275]

vWF is an abundant plasma glycoprotein synthesized in all vascular endothelial cells and megakaryocytes promoting adhesion of platelets.

The selected peptides are at position 627-670 out of 2050aa. However, it is known that ADAMTS13, a zinc protease, specifically hydrolyzes von Willebrand factor at position 842, therefore the potential antimicrobial region is not far from the C-terminus of the processed form.

Human signal peptide, cub and egf-like domain-containing proteins 1 (SCUB1) [q8iwy4], 2 (SCUB2) [q9nq36] and 3 (SCUB3) [q8ix30]

SCUB1 could function as an adhesive molecule. It is highly expressed in platelets and transferred to the cell surface upon activation and aggregation. SCUB2 is expressed in a broad spectrum of adult tissues is involved in angiogenesis. SCUB3 is involved in cell to cell signaling. The selected peptides are at the C-terminus. The peptides at the C-termini of SCUB1 and SCUB2 are identical.

Human probable carboxypeptidase x1 (CPX1) [q96sm3]

CPX1 may be involved in cell-cell interactions.

The selected peptides are close to the N-terminus.

Human napsin A precursor (NAPP) [o96009]

Napsin A is an aspartic-type endopeptidase involved in processing of pneumocyte surfactant precursors.

The selected peptide is the propeptide of the protease and is released to produce active napsin.

Human plasma serine protease inhibitor (PSPI) [p05154]

PSPI is a heparin-dependent serine protease inhibitor present in body fluids and secretions. It is localized in alpha granules in resting platelets and on the external plasma membrane in activated platelets.

The selected peptide is internal (residues 285-308 of 486 aa).

Human fibroblast growth factor 5 (FGF5) [p12034]

FGF5 is produced in the outer root sheath of the hair follicle as well as perifollicular macrophages.

The selected peptides are at the C-terminus.

Human secreted frizzled-related protein 1 (SFRP1) [q8n474]

SFRP1 is a matrix protein regulating cell growth and differentiation. It has antiproliferative effects on vascular cells, *in vitro* and *in vivo*, and can induce, *in vivo*, an angiogenic response.

The selected peptides are close to the C-terminus.

Human follicular dendritic cell secreted peptide (FDCSP) [Q8NFU4]

FDCSP is a cytokine abundantly expressed in tonsils, lymph nodes, and trachea and at lower levels in several other tissues. The aminoacidic composition of the selected peptide is intriguingly similar to those of proline rich cationic AMPs like drosocin and pyrrhocoricin two insect antimicrobial peptides with very high activity on Gram(-) strains.

The selected peptides are at the C-terminus.

Chemokine 9 (CXCL9) [Q07325]

CXCL9 affects the growth, movement, or activation state of cells that participate in immune and inflammatory response. It is chemotactic for activated T-cells.

The selected peptide is at the C-terminus.

Interferon beta (INTb) [P01574]

INTb has antiviral, antibacterial and anticancer activities.

The selected peptides are the two helices from the C-terminal helix-turn-helix motif.

Human interleukin-26 (IL26) [q9nph9]

IL26 may play a role in local mechanisms of mucosal immunity and seems to have a proinflammatory function.

The first selected peptide is internal (residues 44-77 of 171 aa) whereas the second one is close to the C-terminus.

Interferon kappa (INFk) [Q9P0W0]

INFk plays a role in the regulation of immune cell function and imparts cellular protection against viral infection in a species-specific manner.

The selected peptide is at the C-terminus.

Peptide name[a]	Sequence	nc[b]	Start/ lenght[c]	
HSA-TFL34	TFLKKYLYEIARRHPYFYAPELLFFAKRYKAAFT	5	133/585	Plasma / platelets
HSA-GKA38	GKASSAKQRLKCASLQKFGERAFKAWAVARLSQRFPKA	9	189/585	Plasma / platelets
HSA-YKF36	YKEQNALLVRYTKKVPQVSTPTLVEVSRNLGKVGSK	6	401/585	Plasma / platelets
HSA-KER30	KCRQIKKQTALVELVKHKPKATKEQLKAVM	6	519/585	Plasma / platelets
FIBα-GVV27	GVVWVSFRGADYSLRAVRMKIRPLVTQ	4	821/847	Plasma / platelets
FIBα-SFR22	SFRGADYSLRAVRMKIRPLVTQ	4	826/847	Plasma / platelets
FIBβ-GVV28	GVVWMNWKGSWYSMRKMSMKIRPFFPQQ	5	434/461	Plasma / platelets
FIBβ-NWK23	NWKGSWYSMRKMSMKIRPFFPQQ	5	439/461	Plasma / platelets
FIBγ-GII30	GIIWATWKTRWYSMKKTTMKIIPFNRLTIG	6	366/427	Plasma / platelets
FIBγ-TWK25	TWKTRWYSMKKTTMKIIPFNRLTIG	6	371/427	Plasma / platelets
vWF-PQR44	PQRMSRNFVRYVQGLKKKKVIVIPVGIGPHANLKQIRLIEKQAP	9	627/2050	Plasma / platelets
vWF-PQR29	PQRMSRNFVRYVQGLKKKKVIVIPVGIGP	7	627/2050	Plasma / platelets
vWF-PQR19	PQRMSRNFVRYVQGLKKKK	7	627/2050	Plasma / platelets
SCUB1-SKE25	SKEMFPRSFIKLLRSKVSRFLRPYK	7	936/988	Plasma / platelets
SCUB1-MFP22	MFPRSFIKLLRSKVSRFLRPYK	7	939/988	Plasma / platelets
SCUB3-KHK26	KHKEMLPKSFIKLLRSKVSSFLRPYK	7	942/993	Plasma / platelets
SCUB3-MLP22	MLPKSFIKLLRSKVSSFLRPYK	6	946/993	Plasma / platelets
CPX1-HVR43	HVRIRVIKKKKVIMKKRKKLTLTRPTPLVTAGPLVTPTPAGTL	12	43/714	Enzymes
CPX1-HVR25	HVRIRVIKKKKVIMKKRKKLTLTRP	12	43/714	Enzymes
NAPP-LIR38	LIRIPLHRVQPGRRILNLLRGWREPAELPKLGAPSPGD	4	1/38	Inhibitors
NAPP-LIR23	LIRIPLHRVQPGRRILNLLRGWR	6	1/38	Inhibitors
PSPI-KTL24	KTLRKWLKMFKKRQLELYLPKFSI	7	285/486	Signaling
FGF5-KKK33	KKKPPSPIKPKIPLSAPRKNTNSVKYRLKPRFG	11	216/248	Signaling
FGF5-KKK19	KKKPPSPIKPKIPLSAPRK	7	216/248	Signaling
SFRP1-FAL48	FALRMKIKEVKKMNGDKKIVPKKKKPLKLGPIKKKDLKKLVLYIKNGA	14	207/314	Signaling
SFRP1-KKI32	KKIVPKKKKPLKLGPIKKKDLKKLVLYIKNGA	12	223/314	Signaling
FDCSP-PYP41	PYPYPFRPLPPIPFPRFPWFRRNFPIPIPESAPTTPLPSEK	3	28/68	Signaling
FDCSP-PYP29	PYPYPFRPLPPIPFPRFPWFRRNFPIPIP	4	28/68	Signaling
CXCL9-VKE44	VKELIKKWEKQVSQKKKQKNGKKHQKKKVLKVRKSQRSRQKKTT	18	60/103	Signaling
INTβ-FTR26	FTRGKLMSSLHLKRYYGRILHYLKAK	7	111/166	Defense
INTβ-AWT25	AWTIVRVEILRNFYFINRLTGYLRN	3	142/166	Defense
IL26-ALY34	ALYIKAAWLKATIPEDRIKNIRLLKKKTKKQFMK	9	44/171	Defense
IL26-MKS37	MKSITRMKRIFYRIGNKGIYKAISELDILLSWIKKLL	7	131/171	Defense
INFk-AWE26	AWEIVRVEIRRCLYYFYKFTALFRRK	5	155/180	Defense

Coagulation

basic residues
hydrophobic residues
hydrophilic uncharged residues
borderline residues
histidine
acid residues

[a]Peptide names contain an abbreviation indicating the corresponding CAMP-RP, the first three amino acids of the peptide and its length; [b]net charge; [c]position of the peptide inside the CAMP-RP and length of the CAMP-RP.

Table 1. Sequence of the 34 selected cryptic peptides.

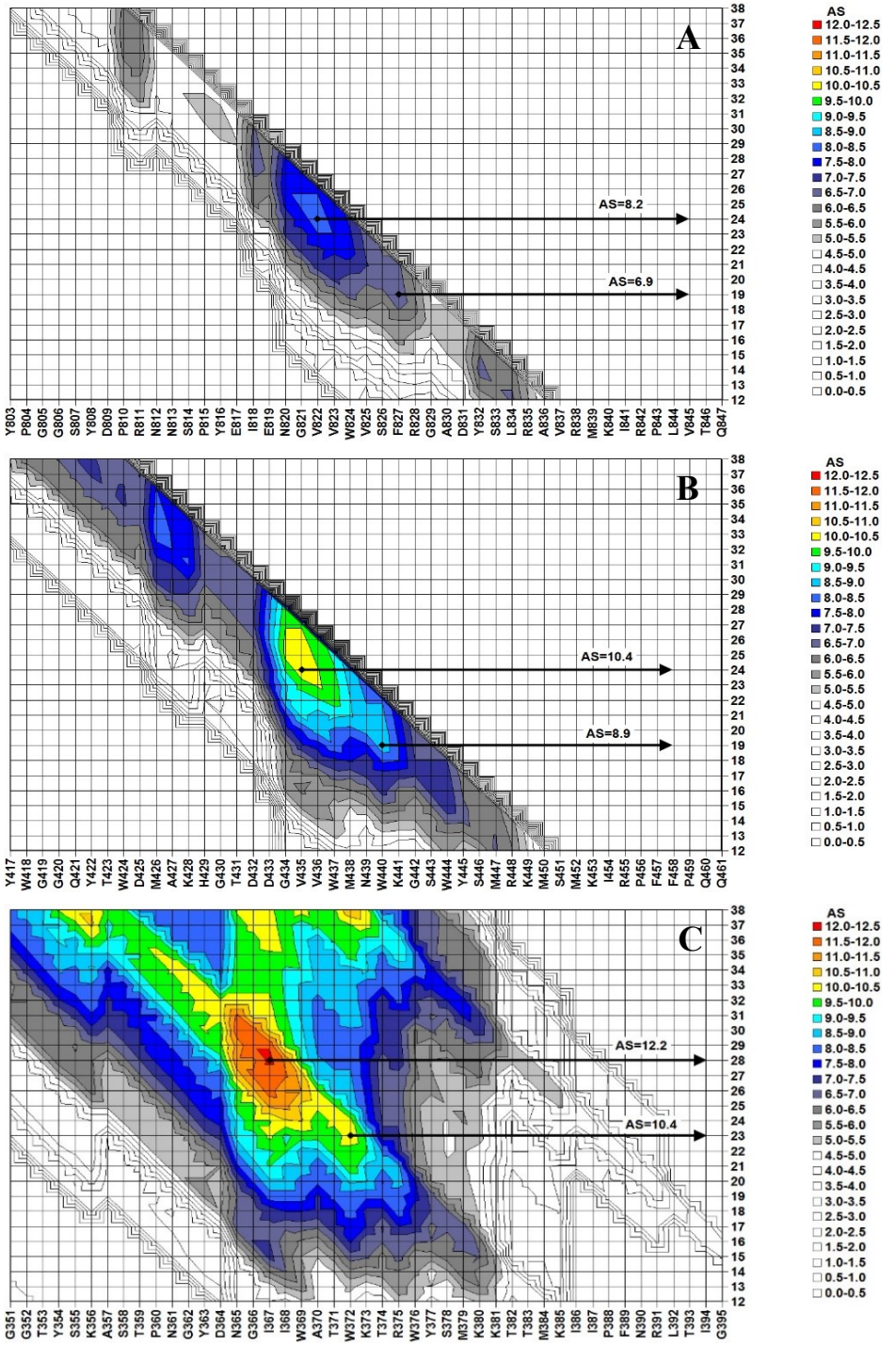

Figure 1. Detailed computational analysis of the C-terminal region of the FIB subunits: **A)** subunit Aα; **B)** subunit Bβ; **C)** subunit γ. The Isometric plots report Absolute Score values (AS) as function of starting position (x axis) and length (y axis) of the peptides.

3.1.1 Antimicrobial activity of the selected peptides

The 34 selected peptides shown in Table 1 were prepared by standard solid phase synthesis by the group of Prof. Cesar de la Fuente-Nuñez. Their antimicrobial activity was measured through the Minimum Inhibitory Concentration (MIC) assays on a panel of 10 strains of Gram-negative and Gram-positive clinically relevant pathogens (*Escherichia coli* ATCC 25922*; Klebsiella pneumoniae* ATCC 700603; *Acinetobacter baumannii* ATCC 17878; *Salmonella enteriditis* 706 RIVM; *Salmonella typhimurium* ATCC 14028; *Pseudomonas aeruginosa* PAO1; *Pseudomonas aeruginosa* PA14*; Pseudomonas aeruginosa* RP73*; Staphilococcus aureus* ATCC 6538P*; Enterococcus faecalis* ATCC 29212).
Very interestingly all the synthesized peptides displayed antimicrobial activity (Tab. 2) against all tested strains, similar to that of (P)GKY20 used as control peptide, with few exceptions (MIC values >50 μM). The MIC values were also measured by the research group of Prof. Cesar de la Fuente-Nuñez on a different panel of pathogenic and commensal strains (Torres et al., 2021). In general, the MIC values reported by Torres and co-workers were slightly higher than those shown in Table 2, likely due to different experimental conditions such as assay medium and in particular cell concentration ($5x10^5$ in the case of the MIC values in Table 2; 10^8 cfu/ml in the case of the MIC values reported by Torres et al., 2021). In spite of these limited differences, the preliminary characterization of the 34 selected peptides confirms the validity of the *in silico* prediction tool and suggests that the 17 human secreted proteins hosting these peptides are possible CAMP-RPs with a role in defence as source of HDPs.

Starting from these findings we decided to select a smaller panel of peptides for a more thorough characterization. The choice fell on peptides hosted in proteins participating in blood coagulation and/or secreted by platelets: fibrinogen subunits Aα, Bβ and γ; platelet proteins SCUB1 and 3; the von Willebrand factor. This choice was motivated by the fact that proteins involved in blood clotting, from a certain point of view, can be considered part of the host defence system moreover, it has been already demonstrated that several of these proteins host HDPs, as described in the introduction for the C-terminus of human thrombin and fibrinogen subunit Bβ itself.

The attention of our research group focused in particular on the peptides hosted by fibrinogen subunits (described in the next sections) and von Willebrand factor (that will be the subject of future research in the laboratory where this thesis has been prepared), whereas, Prof. de la Fuente-Nuñez and his collaborators decided to work on peptides derived from SCUB proteins: they demonstrated that SCUB1-SKE25 and SCUB3-MLP22 peptides, very active *in vitro* against a panel of both Gram-negative and Gram-positive strains (Tab. 2 and Torres et al., 2021), also show very high antimicrobial activity *in vivo* in a mouse model. Administration of SCUB1-SKE25 and SCUB3-MLP22 at the infection site (right thigh) decreased the bacterial load of *P. aeruginosa* and *A. baumannii* by four and two orders of magnitude, respectively, compared with untreated mice, especially when used in combination at their MIC values (Torres et al., 2021). Based on these finding it can be hypothesized that the cryptides from the C-termini of human SCUB proteins may find medical applications as antimicrobial agents.

Red: ≤1.6; Orange: 1.6 < MIC ≤ 4; Yellow: 4 < MIC ≤ 9; Green: 9 < MIC ≤ 18
Cyan: 18 < MIC ≤ 50; Blue: >50

	MIC (µM)									
	Gram negative								Gram positive	
PEPTIDE	*E.coli*	*K.pne.*	*A.bau.*	*S.ent.*	*S.typ.*	PAO1	PA14	RP73	*S.aur.*	*E.fae.*
HSA-TFL34	3,12	12,5	6,25	6,25	6,25	3,12	3,12	3,12	1,56	6,25
HSA-GKA38	3,12	3,12	3,12	3,12	1,56	1,56	1,56	1,56	1,56	3,12
HSA-YKF36	6,25	>50	6,25	>50	12,5	1,56	3,12	0,78	3,12	1,56
HSA-KER30	>50	>50	25	>50	>50	25	>50	12,5	12,5	>50
FIB?-GVV27	12,5	25	6,25	12,5	6,25	6,25	6,25	3,12	6,25	6,25
FIB?-SFR22	25	>50	25	50	50	12,5	12,5	12,5	12,5	6,25
FIB?-GVV28	6,25	25	6,25	12,5	12,5	6,25	6,25	6,25	3,12	6,25
FIB?-NWK23	6,25	25	6,25	12,5	12,5	3,12	3,12	6,25	3,12	6,25
FIB?-GII30	6,25	12,5	6,25	12,5	6,25	6,25	6,25	3,12	6,25	6,25
FIB?-TWK25	3,12	6,25	3,12	6,25	3,12	3,12	3,12	3,12	1,56	6,25
vWF-PQR44	3,12	12,5	1,56	3,12	1,56	0,78	1,56	1,56	0,78	1,56
vWF-PQR29	3,12	6,25	1,56	3,12	3,12	1,56	1,56	1,56	0,39	1,56
vWF-PQR19	3,12	12,5	3,12	6,25	3,12	1,56	3,12	1,56	0,39	25
SCUB1-SKE25	3,12	6,25	3,12	3,12	3,12	3,12	0,78	1,56	0,78	6,25
SCUB1-MFP22	3,12	6,25	1,56	3,12	1,56	1,56	0,78	1,56	0,78	6,25
SCUB3-KHK26	3,12	3,12	1,56	1,56	1,56	0,78	0,78	1,56	0,78	6,25
SCUB3-MLP22	3,12	3,12	1,56	3,12	1,56	1,56	0,78	1,56	0,78	6,25
CPX1-HVR43	3,12	3,12	1,56	1,56	1,56	3,12	1,56	1,56	0,39	1,56
CPX1-HVR25	3,12	3,12	1,56	1,56	0,78	1,56	1,56	0,78	0,19	1,56
NAPP-LIR38	6,25	25	3,12	12,5	6,25	3,12	0,78	3,12	1,56	12,5
NAPP-LIR23	3,12	12,5	3,12	3,12	3,12	1,56	3,12	1,56	0,78	6,25
PSPI-KTL24	3,12	3,12	1,56	3,12	1,56	1,56	3,12	1,56	0,78	3,12
FGF5-KKK33	1,56	1,56	1,56	1,56	1,56	0,78	1,56	0,78	0,39	3,12
FGF5-KKK19	12,5	>50	25	>50	25	12,5	25	6,25	6,25	25
SFRP1-FAL48	1,56	1,56	1,56	1,56	3,12	0,78	0,78	0,78	0,39	1,56
SFRP1-KKI32	1,56	1,56	1,56	1,56	1,56	0,78	0,78	0,78	0,19	1,56
FDCSP-PYP41	12,5	>50	3,12	>50	25	12,5	12,5	1,56	25	25
FDCSP-PYP29	12,5	25	3,12	12,5	3,12	3,12	12,5	1,56	3,12	6,25
CXCL9-VKE44	1,56	3,12	1,56	1,56	0,78	0,78	1,56	0,78	0,78	1,56
INTb-FTR26	3,12	3,12	1,56	1,56	1,56	3,12	1,56	1,56	0,78	3,12
INTb-AWT25*	17,8	>50	35,6	17,8	17,8	17,8	17,8	8,9	17,8	8,9
IL26-ALY34	6,25	3,12	3,12	3,12	3,12	1,56	3,12	1,56	1,56	3,12
IL26-MKS37	6,25	6,25	3,12	3,12	3,12	1,56	1,56	1,56	1,56	3,12
INFk-AWE26**	7,32	14,65	7,32	3,66	7,32	3,66	7,32	1,83	3,66	7,32
(P)GKY20	6,25	6,25	3,12	6,25	3,12	3,12	6,25	1,56	1,56	1,56

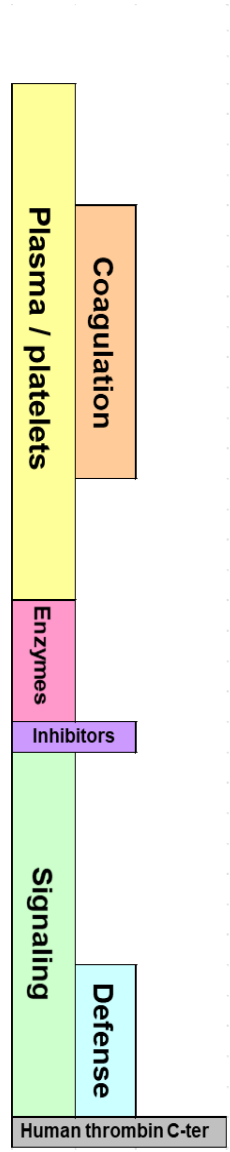

Horizontal lines are not present when the peptides are from the same region of the protein (i.e. they are short/long forms of the same peptide).
* Twofold serial dilutions starting from 35,6 µM.
** Twofold serial dilutions starting from 58,6 µM.

Table 2. Antimicrobial activity expressed as MIC (Minimum Inhibitory Concentration) values of chemically synthesized peptides. Data were obtained from a minimum of three independent experiments.

3.1.2 Expression of recombinant fusion proteins

As described in the previous section the six peptides hosted at the C-terminus of the three FIB subunits were selected for a deeper characterization. To this aim, the six peptides were prepared in the recombinant form by using the strategy based on ONC fusion proteins described in the Introduction (Pane et al., 2016b).

Accordingly, the following six recombinant fusion proteins were expressed in *E. coli* strain BL21DE3, using the pET22b(+) vector:

ONC-DCless-H6-(P)FIBα-GVV27

ONC-DCless-H6-(P)FIBα-SFR22

ONC-DCless-H6-(P)FIBβ-GVV28

ONC-DCless-H6-(P)FIBβ-NWK23

ONC-DCless-H6-(P)FIBγ-GII30

ONC-DCless-H6-(P)FIBγ-TWK25

By acidic hydrolysis these fusion proteins allowed, respectively, to isolate the recombinant peptides:

(P)FIBα-GVV27, *(P)FIBα-SFR22*, *(P)FIBβ-GVV28*, *(P)FIBβ-NWK23*, *(P)FIBγ-GII30*, *(P)FIBγ-TWK25.*

The “(P)” at the beginning of the peptide name highlights the fact that the recombinant peptides have an additional proline residue at the N-terminus deriving from the cleavage sequence “Asp-Pro” present in the fusion proteins.

Similarly, the recombinant protein *ONC-DCless-H6-(P)GKY20* was expressed to prepare the recombinant peptide *(P)GKY20* used as positive control.

Moreover, the recombinant proteins *ONC-DCless-H6-(C)GKY20 and ONC-DCless-H6-(C)FIBγ-TWK25* were expressed in *E. coli* strain BL21(DE3) to obtain the peptides named *(C)GKY20* and *(C)FIBγ-TWK25* with a cysteine residue at the N-terminus deriving from the cleavage sequence “Asp-Cys” whose sensitivity to acidic hydrolysis is just slightly lower than that of the sequence “Asp-Pro”. These two peptides were prepared to develop the fluorescent labelling strategy described in section 3.3. Among the six FIB derived peptides, *FIBγ-TWK25* was selected because it showed the highest antimicrobial activity (Tab. 2).

The seven fusion proteins for the production of fibrinogen derived peptides were expressed effectively in *E. coli* with high yields ranging from about 140 mg - 180 mg per liter of LB culture, as can be seen by SDS-PAGE analyses (Fig.2). Moreover, as expected, the fusion proteins were present exclusively in the insoluble fraction of cell lysates thus confirming that ONC is able to efficiently deliver peptides to inclusion bodies (Fig.2). *ONC-DCless-H6-(P)GKY20* and *ONC-DCless-H6-(C)GKY20* were expressed in inclusion bodies at very high expression levels of about 140 mg - 180 mg per liter of LB culture (data not showed) as already reported (Pane et al., 2016b; Pane et al., 2018b).

Recombinant proteins were purified by immobilized metal ion affinity chromatography (IMAC) carried out in denaturing conditions (5 M guanidine-HCl). In the case of *ONC-DCless-H6-(C)GKY20 and ONC-DCless-H6-(C)FIBγ-TWK25*, IMAC purification was carried out in the presence of 1 mM Tris(2-carboxyethyl)phosphine hydrochloride (TCEP-HCl), a thiol-free reducing agent, to obtain the proteins in the reduced form.

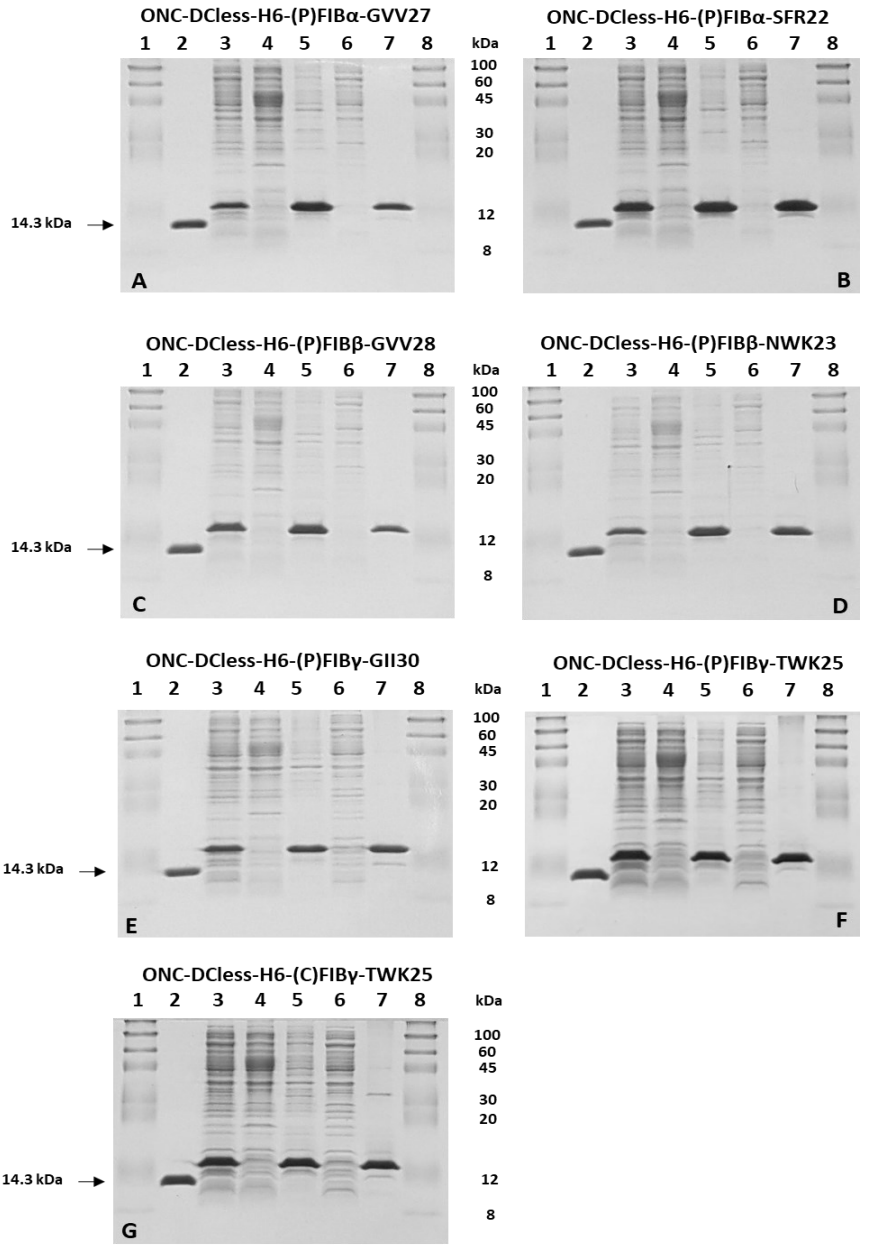

Figure 2. Expression and purification of recombinant proteins. SDS-PAGE (15%) expression analyses of **A)** ONC-DCless-H6-(P)FIBα-GVV27, **B)** ONC-DCless-H6-(P)FIBα-SFR22, **C)** ONC-DCless-H6-(P)FIBβ-GVV28, **D)** ONC-DCless-H6-(P)FIBβ-NWK23, **E)** ONC-DCless-H6-(P)FIBγ-GII30, **F)** ONC-DCless-H6-(P)FIBγ-TWK25, **G)** ONC-DCless-H6-(C)FIBγ-TWK25. Lanes 1,8: molecular markers (8-12-20-30-45-60-100-220 kDa proteins); lane 2: *Gallus gallus* lysozyme (14.3 kDa); lanes 3,4: cellular lysates of induced and non-induced cultures, respectively; lanes 5,6: insoluble and soluble fractions after cell lysis, respectively; lane 7: uncleaved fusion proteins.

3.1.3 Chemical cleavage and purification

The release of peptides from the fusion proteins was obtained by acid hydrolysis of the sequences Asp-Pro or Asp-Cys (Pane et al., 2016b) inserted between the carrier and the desired peptide
Purified proteins were first dialysed toward 0.1 M acetic acid and then incubated at 60°C for 24 h at pH 2, in the presence of 1 mM TCEP. By means of densitometric evaluation on SDS-PAGE (Fig.3), hydrolysis efficiencies of 95% and 75% were estimated for all the recombinant proteins containing the Asp-Pro and Asp-Cys sequences, respectively. Release of the peptides was also monitored by RP-HPLC carried out on C18 column. As can be observed in figure 4 (panel A-D), the hydrolysis of the four proteins carrying the peptides derived from the α and β isoforms provided two forms of each peptide with very close retention times. In particular chromatograms relative to *(P)FIBα-GVV27* (Fig.4A) and *(P)FIBα-SFR22* (Fig.4B) showed two peaks which represented 90% (form 1) and 10% (form 2) based on the analysis of the peak areas, whereas in the case of *(P)FIBβ-GVV28* (Fig.4C) and *(P)FIBβ-NWK23* (Fig.4D) form 1 and 2 represented respectively 82% and 18% of the total peptide. Mass spectrometry analyses (Tab. 3) of the major forms (form 1), confirmed that these are the expected peptides, whereas the experimental molecular masses of the minor forms (form 2) were one unit of mass higher than the theoretical expected molecular masses. A one unit difference between the expected and the experimental mass of a peptide is often due to the deamidation reactions of asparagine residues (more common) or, to a lesser extent, of glutamine residues. Since peptides derived from alfa [*(P)FIBα-GVV27* and *(P)FIBα-SFR22*] and beta [*(P)FIBβ-GVV28* and *(P)FIBβ-NWK23*] fibrinogens do not possess asparagine residues but possess 1 and 2 glutamine residues, respectively, at the C-terminal position(s) it can be hypothesized that “form 2” is the result of the deamidation of the C-terminal glutamine(s). The observed, unusually efficient, deamidation of glutamine residues might be due to the fact that, being at the C-terminus of the peptide, these residues are particularly mobile and solvent exposed, two conditions that could favour the deamidation reaction. It is worth noting that in the case of FIB-Aα derived peptides, with 1 glutamine residue, represent 10% of the total peptide, whereas in the case of FIB-Bβ derived peptides, with 2 glutamine residues, form 2 represent 18% of the total peptide.

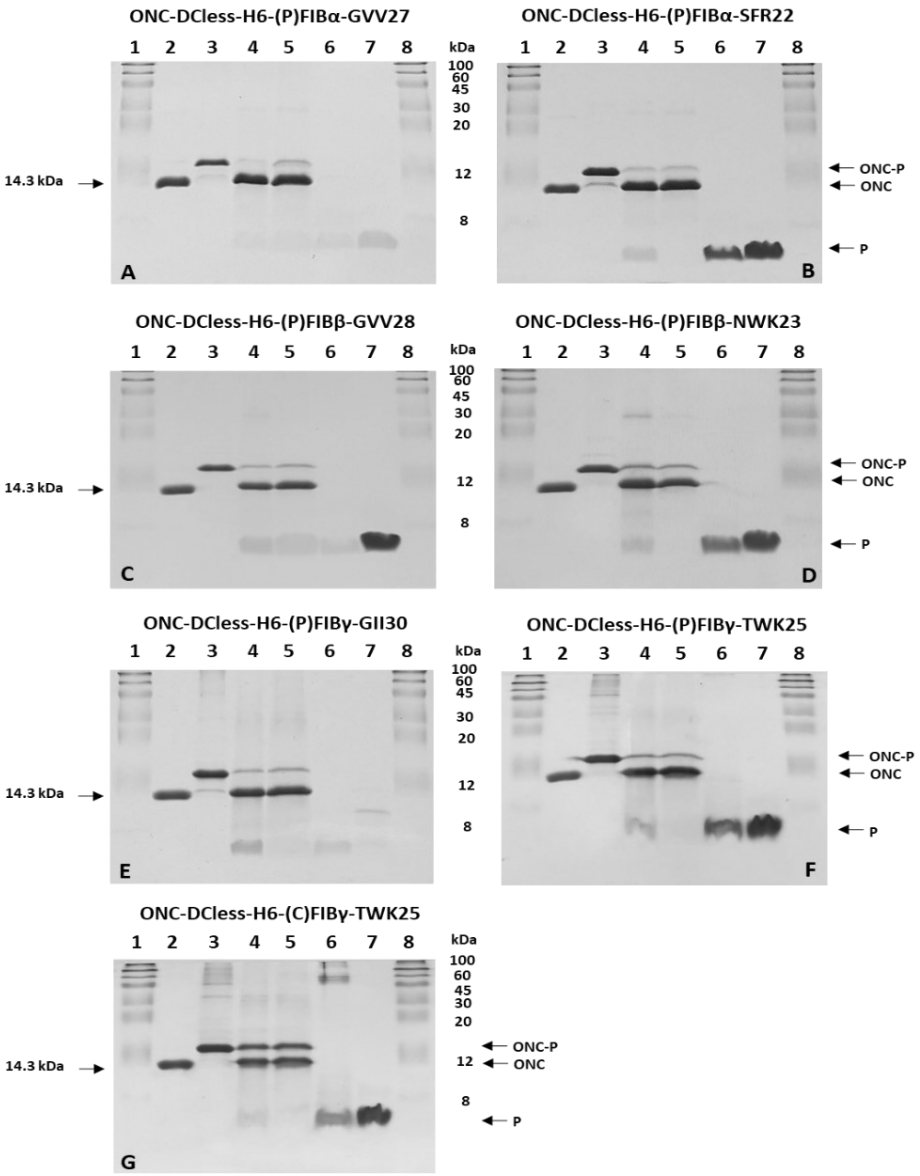

Figure 3. Large scale hydrolyses and selective precipitation of carriers and fusion proteins. SDS-PAGE (20 %) analysis of chemical cleavage carried out at 60°C for 24 h at pH 2 in the presence of TCEP reducing agent. **A)** ONC-DCless-H6-(P)FIBα-GVV27, **B)** ONC-DCless-H6-(P)FIBα-SFR22, **C)** ONC-DCless-H6-(P)FIBβ-GVV28, **D)** ONC-DCless-H6-(P)FIBβ-NWK23, **E)** ONC-DCless-H6-(P)FIBγ-GII30, **F)** ONC-DCless-H6-(P)FIBγ-TWK25, **G)** ONC-DCless-H6-(C)FIBγ-TWK25. Lanes 1,8: molecular markers (8-12-20-30-45-60-100-220 kDa proteins); lane 2: *Gallus gallus* lysozyme (14.3 kDa); lane 3: uncleaved fusion proteins; lane 4: fusion proteins after chemical cleavage; lanes 5,6: insoluble and soluble fractions after selective precipitation (pH 7.2 for 1 h at 28°C). Lane 7: RP-HPLC purified peptide. ONC-P: Onconase/Peptide fusion protein; ONC: Onconase carrier; P: peptide.

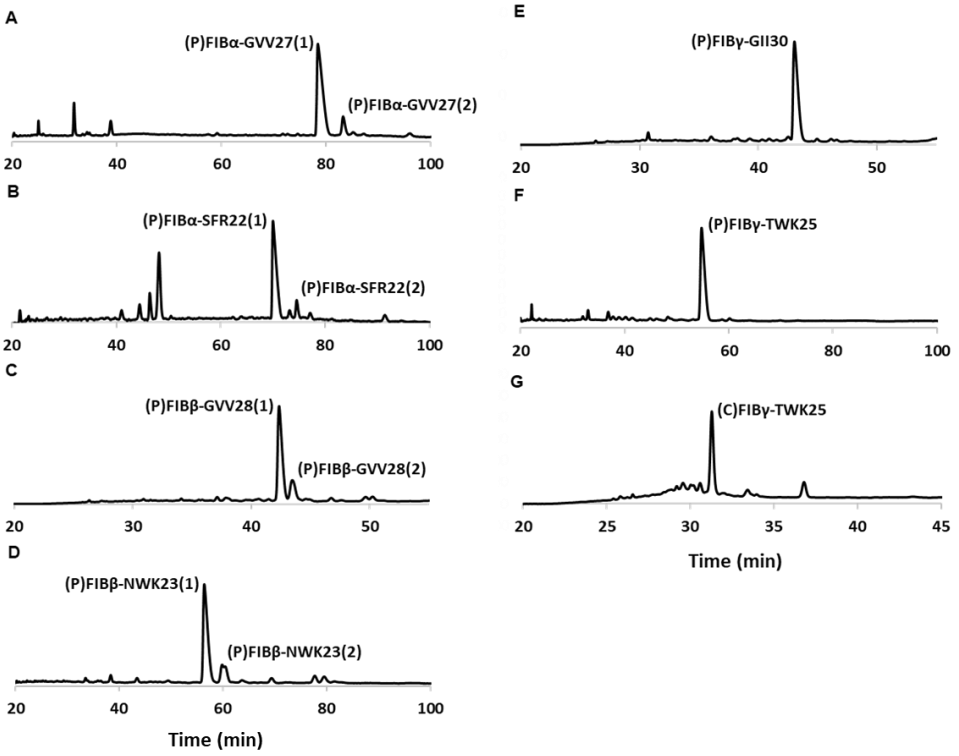

Figure 4. Chemical hydrolysis analyses. Hydrolysis mixtures were analyzed by RP-HPLC carried out on Europa Protein 300 C18 column. Chromatograms were recorded at 280 nm. **A)** ONC-(P)FIBα-GVV27 (gradient 1); **B)** ONC-(P)FIBα-SFR22 (gradient 2); **C)** ONC-(P)FIBβ-GVV28 (gradient 3); **D)** ONC-(P)FIBβ-NWK23 (gradient 1); **E)** ONC-(P)FIBγ-GII30 (gradient 3); **F)** ONC-(P)FIBγ-TWK25 (gradient 1); **G)** ONC-(C)FIBγ-TWK25 (gradient 3).

	[a] MW_{The} (Da)	[b] MW_{Exp} (Da)	[c] Length
PEPTIDE			
(P)FIBα-SFR22 (1)	2662.15	2662.42	23
(P)FIBα-SFR22 (2)	2662.15	2663.35	23
(P)FIBα-GVV27 (1)	3202.81	3202.64	28
(P)FIBα-GVV27 (2)	3202.81	3203.43	28
(P)FIBβ-NWK23 (1)	3031.61	3032.64	24
(P)FIBβ-NWK23 (2)	3031.61	3032.64	24
(P)FIBβ-GVV28 (1)	3604.33	3605.30	29
(P)FIBβ-GVV28 (2)	3604.33	3606.38	29

[a] Theoretical molecular mass; [b] Experimental molecular mass; [c] Amino acid number

Table 3. Mass spectrometry analyses. Theoretical and experimental molecular weights of fractions related to “form 1” and to “form 2” of peptides.

To purify recombinant peptides from hydrolysis mixtures, we firstly evaluated the possibility to selectively precipitate the carrier and the uncleaved fusion protein at pH 7 exploiting the fact that ONC is insoluble at pH higher than 5 (Pane et al., 2018b).
To this purpose, hydrolysis mixtures were neutralized by dropwise addition of diluted NH_3 and samples were incubated 1 h at 28°C.
Insoluble fusion proteins and ONC were separated from soluble peptides by centrifugation. Supernatants and insoluble fractions were analyzed by SDS-PAGE (Fig.3). Furthermore, concentration of peptides in the soluble fractions were determined by spectrophotometric analyses. These analyses allowed to estimate that 85% of *(P)FIBα-SFR22*, 63% of *(P)FIBα-GVV27*, 60% of *(P)FIBβ-NWK23*, 50% of *(P)FIBγ-TWK25,* 50% of *(C)FIBγ-TWK25* but only 12% *(P)FIBβ-GVV28* and 11% of *(P)FIBγ-GII30* were present in the supernatant. Therefore, the effectiveness of the selective precipitation strategy strongly depends on the peptide sequence, in particular *(P)FIBβ-GVV28* and *(P)FIBγ-GII30* proved to be particularly prone to aggregation and precipitation in agreement with the *in silico* analysis of the fibrillogenic sequences described in section 3.1.
Based on these findings, purification of *(P)FIBα-SFR22*, *(P)FIBα-GVV27* and *(P)FIBβ-NWK23* from was first performed by selective precipitation to remove the carrier and the uncleaved fusion protein. Hence, supernatants were furthermore purified by RP-HPLC.
The purifications of *(P)FIBβ-GVV28*, *(P)FIBγ-GII30*, *(P)FIBγ-TWK25* and *(C)FIBγ-TWK25* were instead performed directly by RP-HPLC on C18 column, obtaining, for all the recombinant peptides, final yields ranging between about 6-12 mg per liter of LB culture.
Purity of peptides, assessed by RP-HPLC, typically ranged from 95% to 99% (Fig.5). The identity of all the peptides was confirmed by mass spectrometry analyses of recovered peaks (Tab. 4).
These results confirm that the recombinant expression in *E. coli* is a very suitable strategy to prepare recombinant peptides allowing to produce the necessary amounts for further characterizations.

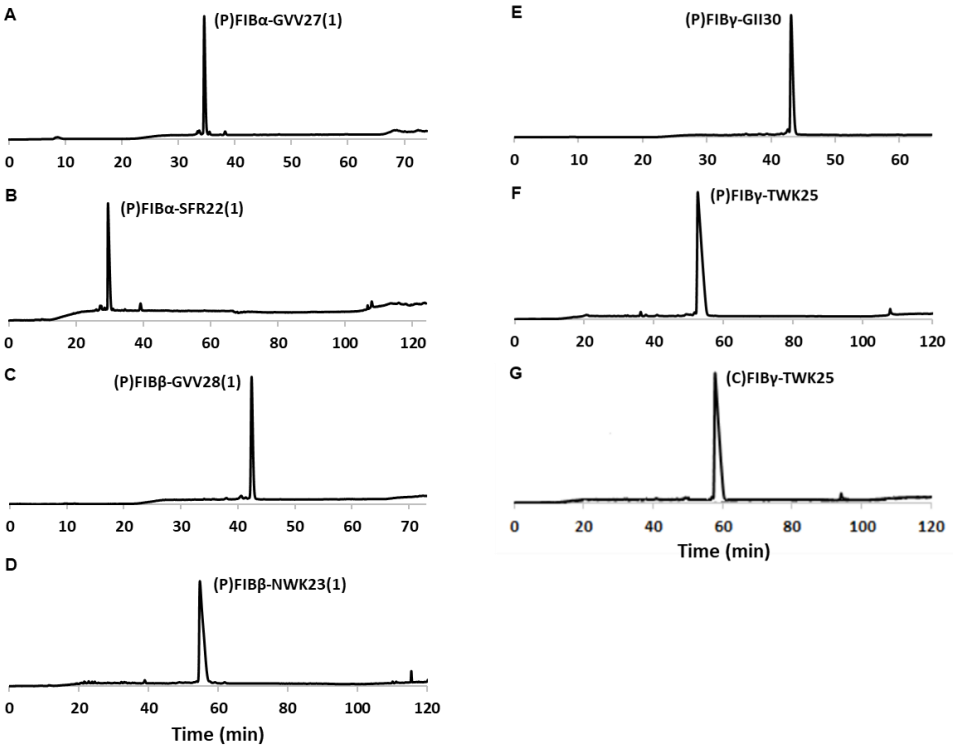

Figure 5. Peptide purity analyses. Peptides were analyzed by RP-HPLC carried out on Europa Protein 300 C18 column. Chromatograms were recorded at 280 nm. **A)** (P)FIBα-GVV27 (gradient 3); **B)** (P)FIBα-SFR22 (gradient 1); **C)** (P)FIBβ-GVV28 (gradient 3); **D)** (P)FIBβ-NWK23 (gradient 1); **E)** (P)FIBγ-GII30 (gradient 3); **F)** (P)FIBγ-TWK25 (gradient 1); **G)** (C)FIBγ-TWK25 (gradient 1).

	[a] MW_{The} (Da)	[b] MW_{Exp} (Da)	[c] Length
PEPTIDE			
(P)FIBα-SFR22	2662.15	2662.42	23
(P)FIBα-GVV27	3202.81	3202.64	28
(P)FIBβ-NWK23	3031.61	3032.64	24
(P)FIBβ-GVV28	3604.33	3605.30	29
(P)FIBγ-TWK25	3198.88	nd	26
(C)FIBγ-TWK25	3204.90	nd	26
(P)FIBγ-GII30	3739.54	3740.37	31

[a] Theoretical molecular mass. [b] Experimental molecular mass. [c] Amino acid number

Table 4. Mass spectrometry analyses. Theoretical and experimental molecular weights of peptides.

3.2 Biological activities of the peptides

The biological activities of the recombinant FIB-derived peptides were studied with particular attention to their direct antimicrobial activity, synergy of the peptides with conventional antibiotics, synergy of peptide/peptide combinations and antibiofilm activity on preformed biofilm. In addition, their LPS scavenging activity was also investigated.

3.2.1 Antimicrobial activity

The antimicrobial activity of the recombinant peptides was measured through the Minimum Inhibitory Concentration (MIC) assays on a panel of 8 Gram-negative and 2 Gram-positive bacterial strains (Tab. 5) and compared to that of the corresponding synthetic peptides provided by the research group of Prof. de la Fuente Nuñez. (P)GKY20 was included as positive control.

As shown in Table 5, synthetic and recombinant FIB-derived peptides showed very similar MIC values (with differences not greater than a single scalar dilution) thus confirming that the additional proline has no effect on the antimicrobial activity.

It is interesting to note that, even if all the peptides showed antimicrobial activity at a certain extent, significant differences were observed among the peptides from different FIB subunits but also between the long and short forms derived from the same subunit. In general, the activity of the peptides derived from subunit γ was higher than that of the peptides derived from the subunit Bβ and those of the peptides derived from subunit Aα was the lowest, in agreement with the A.S. values obtained through the *in silico* analysis. However, while the two peptides derived from subunit Bβ, *(P)FIBβ-GVV28* and *(P)FIBβ-NWK23*, showed essentially the same MIC values, *(P)FIBα-GVV27* was significantly more active than *(P)FIBα-SFR22* and *(P)FIBγ-GII30* was less active than *(P)FIBγ-TWK25*.

According to the A.S. values antimicrobial activity should follow the order:

(P)FIBα-SFR22 < (P)FIBα-GVV27 ≈ (P)FIBβ-NWK23 < (P)FIBβ-GVV28 ≈ (P)FIBγ-TWK25 < (P)FIBγ-GII30

In the case of *E. coli*, the observed order of antimicrobial activity is:

(P)FIBα-SFR22 < (P)FIBα-GVV27 < (P)FIBβ-GVV28 ≈ (P)FIBβ-NWK23 ≈ (P)FIBγ-GII30 < (P)FIBγ-TWK25.

In the case of *S. aureus*, the observed order of antimicrobial activity is very similar:

(P)FIBα-SFR22 < (P)FIBα-GVV27 ≈ (P)FIBγ-GII30 < (P)FIBβ-GVV28 ≈ (P)FIBβ-NWK23 < (P)FIBγ-TWK25.

With almost all the strains we found that *(P)FIBγ-TWK25*, and not *(P)FIBγ-GII30* as predicted, was the most active peptide. These differences might be due, at least in part, to the lower solubility (or a higher propensity to aggregate) of the longer peptides that could decrease their apparent activity (particularly in the case of *(P)FIBβ-GVV28* and *(P)FIBγ-GII30* that showed the highest propensity to precipitate during the purification as reported in section 3.1.3).

It is worth noting that the MIC values of *(P)FIBγ-TWK25* were found to be very similar to those of the reference peptide *(P)GKY20*, thus suggesting that *(P)FIBγ-TWK25* could be a promising candidate for biomedical applications.

	MIC (μM)									
	Gram negative								Gram positive	
PEPTIDE	*E.coli* [a]	*K.pne.* [b]	*A.bau.* [c]	*S.ent.* [d]	*S.typ.* [e]	PAO1 [f]	PA14 [g]	RP73 [h]	*S.aur.* [i]	*E.fae.* [l]
FIBα-GVV27	12.5	25	6.25	12.5	6.25	6.25	6.25	3.12	6.25	6.25
(P)FIBα-GVV27	12.5	50	6.25	12.5	6.25	6.25	6.25	3.12	6.25	6.25
FIBα-SFR22	25	>50	25	50	50	12.5	12.5	12.5	12.5	6.25
(P)FIBα-SFR22	25	>50	25	>50	25	12.5	12.5	6.25	12.5	6.25
FIBβ-GVV28	6.25	25	6.25	12.5	12.5	6.25	6.25	6.25	3.12	6.25
(P)FIBβ-GVV28	6.25	25	6.25	12.5	12.5	6.25	6.25	6.25	3.12	6.25
FIBβ-NWK23	6.25	25	6.25	12.5	12.5	6.25	3.12	6.25	3.12	6.25
(P)FIBβ-NWK23	6.25	25	6.25	12.5	6.25	6.25	3.12	3.12	3.12	6.25
FIBγ-GII30	6.25	12.5	6.25	12.5	6.25	6.25	6.25	3.12	6.25	6.25
(P)FIBγ-GII30	12.5	25	6.25	12.5	6.25	12.5	6.25	3.12	6.25	6.25
FIBγ-TWK25	3.12	6.25	3.12	6.25	3.12	3.12	3.12	3.12	1.56	6.25
(P)FIBγ-TWK25	3.12	6.25	3.12	3.12	3.12	3.12	3.12	3.12	1.56	3.12
(P)GKY20	6.25	6.25	3.12	6.25	3.12	3.12	6.25	1.56	1.56	1.56
ANTIBIOTIC	μg/mL									
Vancomicin									0.5	2
Polymixin B	0.5	0.5	0.5	0.5	0.12	0.25	0.25	0.12		

[a]***E.coli:*** *Escherichia coli* ATCC 25922; [b]***K.pne.:*** *Klebsiella pneumonia* ATCC 700603; [c]***A.bau.:*** *Acinetobacter baumanii* ATCC 17878; [d]***S.ent.:*** *Salmonella enteriditis* 706 RIVM; [e]***S.typ.:*** *Salmonella typhimurium* ATCC 14028; [f]***PAO1:*** *Pseudomonas aeruginosa* PAO1; [g]***PA14:*** *Pseudomonas aeruginosa* PA14; [h]***RP73:*** *Pseudomonas aeruginosa* RP73; [i]***S.aur:*** *Staphylococcus aureus* ATCC 6538P; [l]***E.fae.:*** *Enterococcus faecalis* ATCC 29212.

Table 5. Antimicrobial activity expressed as MIC (Minimum Inhibitory Concentration) values of Fibrinogen recombinant and chemically synthesized peptides. Data were obtained from a minimum of three independent experiments.

To further characterize, the antimicrobial activity of FIB-derived peptides, we determined the Minimum Bactericidal Concentration (MBC) by subculturing the content of the wells of the broth dilution test for the MIC determination to agar plates that did not contain the test agent. Differently from the MIC, MBC is the minimum concentration resulting in microbial death. Antibacterial agents are usually regarded as bactericidal if the MBC value is no more than four times higher than the MIC value.

As control antimicrobial agents, we tested (P)GKY20, LL-37, the sole human cathelicidin, colistin, a cyclic cationic polypeptide antibiotic from *Bacillus colistinus*, vancomycin, a branched tricyclic glycosylated non-ribosomal peptide, tobramycin, an aminoglycoside antibiotic, and ciprofloxacin, a quinolone antibiotic.

All the tested CAMPs showed MIC=MBC and bactericidal activity with MBC/MIC ratios of 1 on both *P. aeruginosa* PAO1 and *S. aureus*, thus indicating that they are fully bactericidal. The same ratio (MBC/MIC=1) was also observed for colistin and vancomycin, which alter bacterial-cell-membrane permeability, similarly to CAMPs. Tobramycin and ciprofloxacin, showed MBC/MIC ratios of 2.

Our data highlight that FIB-derived peptides have a behavior similar to that of the well characterized CAMPs (P)GKY20 and LL-37.

3.2.2 Antimicrobial Synergy of CAMP/CAMP and CAMP/antibiotic combinations

A very interesting strategy to reduce the risk of drug-resistance to antimicrobials is to use CAMPs in conjunction with conventional antibiotics, focusing on combinations that lead to effective synergy (Duong et al., 2021). Synergistic combinations of antimicrobials could be more lethal for bacteria, decreasing the likelihood that they develop resistance. Such combinations, targeting multiple pathways, would require independent and simultaneous sets of mutations before bacteria acquire an high resistance to the therapy.

Synergy has been observed not only between a CAMP and a conventional antibiotic but also between two different CAMPs (Yu G et al., 2016). Regarding cryptic CAMPs, it is particularly intriguing the possibility of synergistic interactions between peptides from the same body district that could be released simultaneously in response to a bacterial invasion (Torres et al. 2021).

For example, the fact that several proteins involved in blood clotting host cryptic CAMPs suggests that these peptides may be released simultaneously in the same site and cooperate to fight pathogens. In particular, it is likely that cryptides released from the C-terminus of thrombin – like GKY25, GKY20 and TCP_{99} – whose existence in human wound fluid has been already confirmed (Papareddy et al., 2010), coexist with FIB-derived cryptides. In fact, its long been known that thrombin binds to fibrin clots, and that fibrin acts as a reservoir for active thrombin (Liu et al., 1979).

Therefore, to assess possible synergistic interactions, we tested several combinations of CAMPs with antibiotics and other CAMPs. To this purpose, Fractional Inhibitory Concentration Indexes (FICI) were determined by checkerboard assay on *P. aeruginosa* PAO1 and *S. aureus*. As FICI interpretation methods we referred to two similar models: the more restrictive one proposed by Eucast (2000), that assumes synergistic effects when FICI are ≤0.5, and the one proposed by Fratini (Fratini et al., 2017) that assumes synergistic effects when FICI are <1.

As shown in Table 6, we found several combinations with FICI ≤ 0.5, which indicate synergy, according to both models.

When *P. aeruginosa* PAO1 strain was tested, we found FICI ≤ 0.5 only for the peptide couple (P)FIBy-GII30/(P)GKY20, however for all

the other couples, the FICI were lower than 1 thus indicating synergy at least according to Fratini et al., 2017. Clear synergy was also observed for all the combinations CAMP/colistin, with FICI in the range 0.18-0.31. Moreover, all the peptides showed synergy when combined to tobramycin, with FICI close to 0.5 in the case of (P)FIBβ-GVV28, (P)FIBβ-NWK23 and (P)FIBγ-GII30.

On the other hand, when *S. aureus* was tested, only (P)FIBγ-GII30/(P)GKY20 and (P)GKY20/tobramycin combinations showed FICI≤0.5. All the other combinations showed FICI between 0.5 and 1, indicating synergy only according to Fratini et al., 2017. Very interestingly when CAMP/ciprofloxacin mixtures were tested we observed FICI = 2, indicating antagonistic effect.

On the whole, our findings indicate that human fibrinogen and thrombin-derived cryptic CAMPs can cooperate efficiently, thus supporting the idea of a potential physiological cooperation among antimicrobial peptides released in the same site (wounds, in the specific case of the peptide reported in this study). More experiments will be required to address this hypothesis. It is also relevant to pharmacological applications that not all the CAMP/antibiotic combinations are equally effective. The strong synergy between CAMPs and colistin is not unexpected. Colistin is a cationic lipopeptide with a high and specific affinity for LPS, accordingly, its main target is the outer membrane of Gram-negative strains. CAMPs likely target all the membranes with lower selectivity and in addition they may reach intracellular targets. Therefore, when in combination, colistin disrupt the outer membrane thereby facilitating the access of the CAMPs to the inner membrane. Tobramycin, an aminoglycoside, targets ribosomes. It is well known that the limiting step for this class of antibiotics is cell wall crossing, therefore, CAMPs might facilitate the internalization of tobramycin (Zharkova MS et al., 2019). At the moment we have no clear explanation for the behavior of the CAMP/ciprofloxacin combinations.

Bacterial strains	Peptide / Peptide/Antibiotic	ΣFICI[a]						
		(P)FIBα-GVV27	(P)FIBα-SFR22	(P)FIBβ-GVV28	(P)FIBβ-NWK23	(P)FIBγ-GII30	(P)FIBγ-TWK25	(P)GKY20
Gram-negative strain *Pseudomonas aeruginosa* PAO1								
	(P)FIBα-GVV27	na[b]						
	(P)FIBα-SFR22	-	na					
	(P)FIBβ-GVV28	1	-	na				
	(P)FIBβ-NWK23	-	0.562	-	na			
	(P)FIBγ-GII30	0.625	-	0.56	-	na		
	(P)FIBγ-TWK25	-	1	-	0.75	-	na	
	(P)GKY20	0.75	-	0.625	-	0.5	0.562	na
	Colistin	0.312	0.25	0.187	0.312	0.156	0.187	0.187
	Tobramycin	0.625	0.75	0.526	0.516	0.5	0.625	0.75
	Ciprofloxacin	1	1	1	0.75	0.75	1	2
Gram-positive strain *Staphylococcus aureus* ATCC 6538P								
	(P)FIBα-GVV27	na						
	(P)FIBα-SFR22	-	na					
	(P)FIBβ-GVV28	2	-	na				
	(P)FIBβ-NWK23	-	0.75	-	na			
	(P)FIBγ-GII30	0.75	-	0.625	-	na		
	(P)FIBγ-TWK25	-	1	-	0.625	-	na	
	(P)GKY20	0.625	-	0.75	-	0.5	1	na
	Tobramycin	0.75	0.625	1	0.75	0.75	0.75	0.5
	Ciprofloxacin	2	2	2	2	2	2	2

[a]FICI: Fractional inhibitory Concentration index. Reported FICI values refer to the combination of concentrations leading to the lowest FICI value. Red values indicate synergistic effect according to Eucast model. Blu values indicate synergistic effect according to Fratini model. [b]Not applicable. (-) Not measured.

Table 6. Combination therapy analyses.

3.2.3 Antibiofilm activity

In addition to their activity against planktonic bacteria, many CAMPs also show antibiofilm activity. Many antimicrobial peptides have been used to control biofilm formation and to eradicate preformed biofilm. Natural and synthetic peptides have been shown to prevent colonization of surfaces, kill bacteria in the biofilm and disrupt the structure of the biofilm (Yasir et al., 2018).

On these basis the antibiofilm activity of FIB-derived peptides was tested on *P. aeruginosa* PAO1 as a model organism. In particular, the ability of the peptides to eradicate preformed biofilms, which represents an important therapeutic goal, was evaluated. The biofilm was allowed to grow in multiwell plates at 37°C for 24 h in BM2/glucose medium in the presence of $1x10^8$ CFU/mL. Peptides were added to the preformed biofilm at concentrations lower and higher than the MIC (0.39-30 μM), for 4 h at 37°C. At the end of the incubation, the mass of the biofilm was determined by crystal violet staining, the viability of the cells by XTT colorimetric assay and bacterial counts on LB/Agar plate.
As the activity of GKY20 on biofilm has not been reported before, in this case we used as control peptide LL-37, the human cathelicidin. This peptide strongly prevents bacterial biofilm formation and affects pregrown *P. aeruginosa* biofilms (Ridyard et al., 2021).

As shown in Figure 6A, LL-37 led to a progressive concentration dependent dispersion of the biofilm, as expected, with a residual biomass at 20 and 25 μM concentrations of 43% and 32%, respectively, compared to the control in the absence of peptide. On the other hand, no viable cells, measured by XTT assay, were observed at 20 and 25 μM. These data were confirmed by bacterial counts with 1.2% and 0.7% of surviving cells at peptide concentrations of 20 and 25 μM, respectively.

Also (P)GKY20 proved to be very effective (Fig. 6B). Similarly to LL-37, (P)GKY20 led to a concentration dependent dispersion of the biofilm, with 35% and 23% residual biomass at 20 and 25 μM, respectively. At the same time, a consistent decrease in cell viability, measured by XTT assay, was also observed, with cell survival of 4.4 and 0.8% at concentrations of 20 and 25 μM, respectively. These data were confirmed by bacterial counts with 5.5% and 8.8% of surviving cells at concentrations of 20 and 25 μM, respectively. The reported results show that (P)GKY20 is endowed with a significant

eradication activity of the preformed biofilm, a result comparable to that observed for the LL-37 model peptide.

A different and more complex behavior was observed in the case of the FIB-derived peptides. In particular, (P)FIBα-GVV27 (Fig. 6C) induced an increase in the biofilm matrix as a function of concentration and, at the same time, a decrease at about 60% of the metabolic residual activity, measured by XTT assay, at a concentration of 30 μM. On the other hand, the analysis of residual CFUs by plate counts showed that only 7-5% of the cells survived after 4 h of incubation in the presence of 20-30 μM peptide. These results suggest that the peptide is moderately active on the preformed biofilm but it also causes an increase in the amount of the extracellular matrix, likely due to a stress response by P. aeruginosa PAO1. It should be noted that the XTT analyses and the bacterial counts do not seem congruent. At this regard, it has been reported (Chavez-Dozal et al., 2016) that the data obtained by XTT assay may not be tightly correlated to the number of cells, rather they might be better correlated to the viability state of the cells. Therefore, our data could be interpreted by assuming that cells survived to the toxic effect of the peptides exhibited increased metabolic activity synthesizing new matrix in an attempt to defend themselves from the action of the peptide.

As for (P)FIBβ-GVV28 (Fig. 6D), no biofilm mass eradication was observed until 30 μM peptide concentration. However, a constant value of 70% residual vitality was measured by XTT assay between 20 and 30 μM peptide concentrations. On the other hand, the bacterial plate counting method indicated no decrease of viable bacteria respect to the control in the absence of peptide.

All the other peptides (Fig. 6E-H) did not show any ability to eradicate biofilm after 4 h incubation.

Confocal microscopy studies are currently underway to confirm the antibiofilm properties of the peptides.

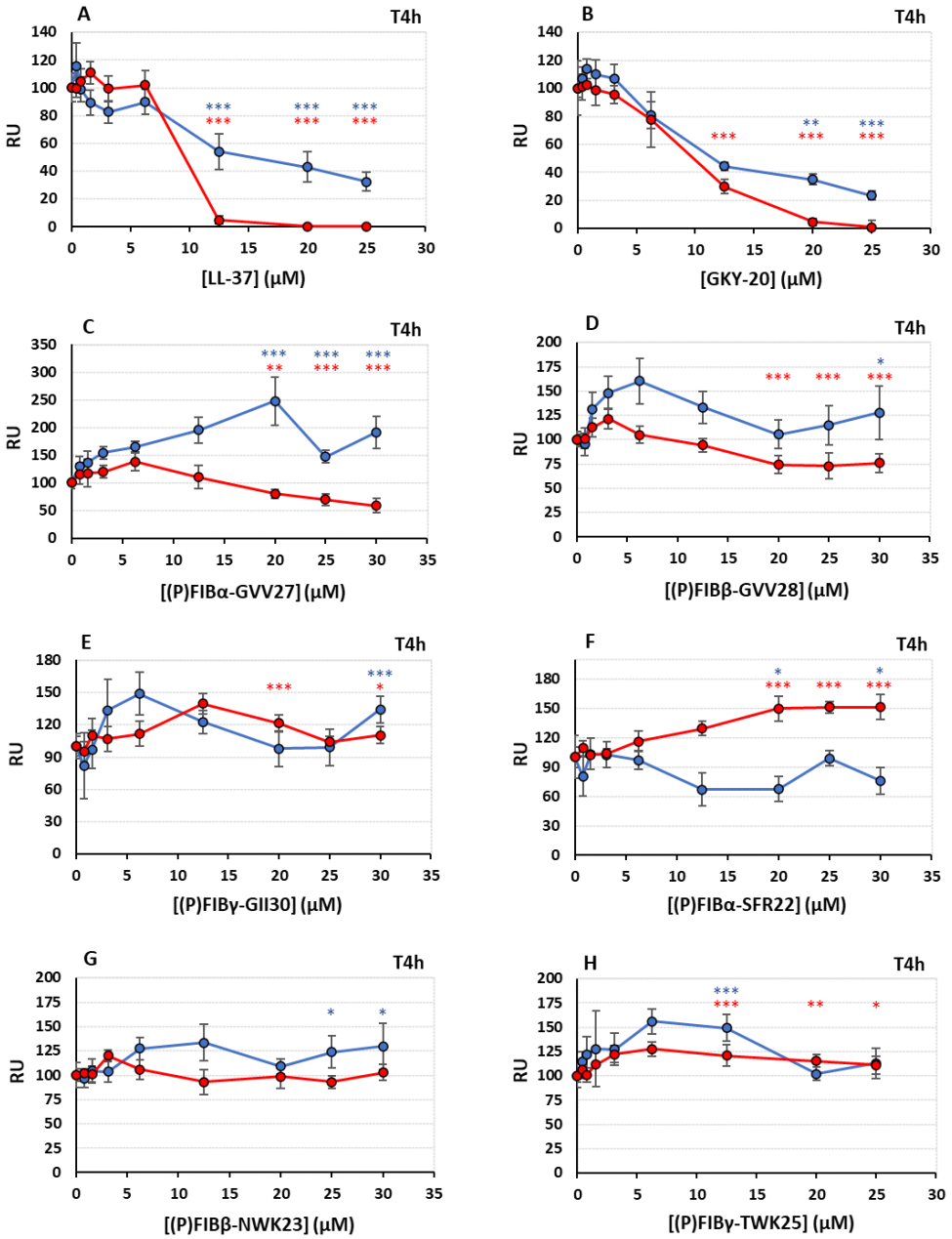

Figure 6. Antibiofilm activity of fibrinogen derived peptides against *P. aeruginosa* PAO1 strain. The effects of increasing concentrations of selected peptides were evaluated on pre-formed biofilm after 4h incubation time. Biofilm was stained with crystal violet and measured at 595 nm. The effects of increasing concentrations of selected peptides on cell viability was evaluated by XTT colorimetric assay and bacterial counts on LB/Agar plate. Presented data are mean values ± standard deviation (SD). Each value was compared to the untreated control and considered statistically significant according to Student's t-test (∗p< 0.05, ∗∗p< 0.005, ∗∗∗p< 0.0005). **A)** LL-37; **B)** GKY-20; **C)** (P)FIBα-GVV27; **D)** (P)FIBβ-GVV28; **E)** (P)FIBγ-GII30; **F)** (P)FIBα-SFR22; **G)** (P)FIBβ-NWK23; **H)** (P)FIBγ-TWK25. (red line: % viable bacteria; blue line: % biofilm mass).

3.2.4 Cytotoxicity assays on THP-1 and HaCaT line cells

Even if FIB-derived peptides are endogenous CAMPs, before hypothesizing a potential pharmacological application, it is necessary to verify their safety. To this purpose we studied the cytotoxic effect of the six peptides on two human cell lines, namely THP-1, undifferentiated human monocytes, and HaCaT, human immortalized keratinocytes. In the case of the THP-1 cells no significant toxicity was observed except for a slightly decrease in cell viability at the highest concentration tested of *(P)FIBβ-GVV28* and *(P)FIBγ-GII30* (Fig. 7). *(P)FIBγ-GII30* and *(P)FIBγ-TWK25* toxicity was also measured on HaCaT cells. As shown in Figure 8, also in this case *(P)FIBγ-TWK25* did not result, in any significant reduction in cell viability whereas *(P)FIBγ-GII30* caused a slightly decrease in cell viability starting from 10 μM.

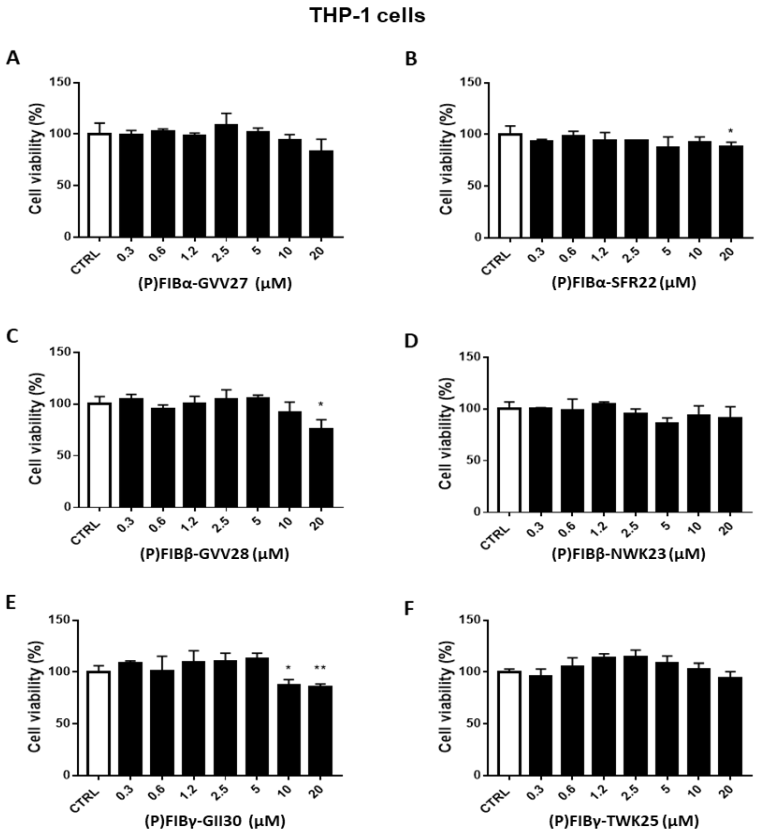

Figure 7. Cytotoxicity analyses on THP-1 human monocyte cells (MTT assay).
Cytotoxicity was analyzed incubating THP-1 cells for 24 h with increasing concentration of peptide (from 0.3 to 20 μM). **A)** (P)FIBα-GVV27; **B)** (P)FIBα-SFR22; **C)** (P)FIBβ-GVV28; **D)** (P)FIBβ-NWK23; **E)** (P)FIBγ-GII30; **F)** (P)FIBγ-TWK25. Each value was compared to the untreated control and considered statistically significant according to Student's t-test (∗p< 0.05, ∗∗p< 0.005, ∗∗∗p< 0.0005).

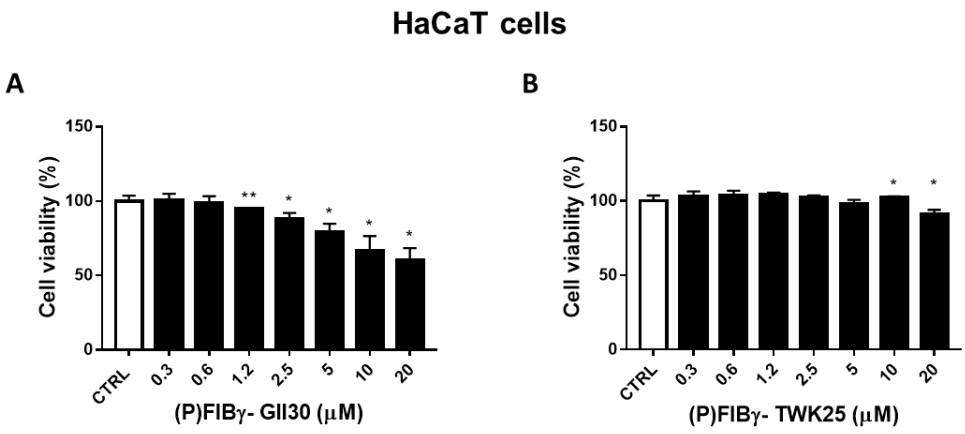

Figure 8. Cytotoxicity analyses on HaCaT human keratinocyte cells (MTT assay). Cytotoxicity was analyzed incubating HaCaT cells for 24 h with increasing concentration of peptide (from 0.3 to 20 μM). **A)** (P)FIBγ-GII30; **B)** (P)FIBγ-TWK25. Each value was to the untreated control and considered statistically significant according to Student's t-test (∗p< 0.05, ∗∗p< 0.005, ∗∗∗p< 0.0005).

3.3 Fluoroscence properties

Environment-sensitive fluorophores are very valuable tools in the study of molecular and cellular processes. When used to label proteins and peptides, they allow the monitoring of even small variations in the local microenvironment, thus acting as reporters of conformational variations and binding events.

To evaluate the suitability of luciferin (Luc) and aminoluciferin (aLuc) as environment-sensitive fluorescent labels, in addition to the GKY20, described in the previous sections, we selected three additional, well-known bioactive peptides: $ApoB_L$ (37 residues), p53pAnt (37 residues) and RGD (6 residues) (Fig.9) (Siepi et al., 2021).

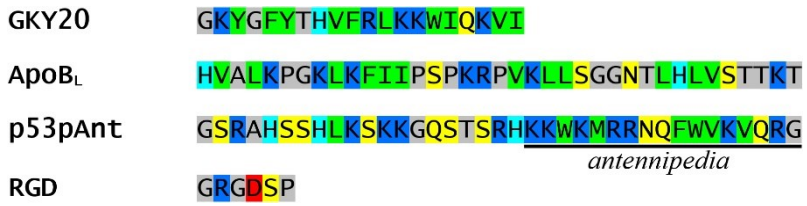

Figure 9. Peptide sequences colored by residue type (blue, basic; cyan, histidine; red, acidic; green, hydrophobic; yellow polar; gray borderline).

$ApoB_L$ (Gaglione et al., 2017), like GKY20, is a cryptic CAMP able to bind bacterial membranes (Wiesner et al., 2010; Pizzo et al., 2018) and LPS. p53pAnt (also spelled p53p-Ant) is a designed antitumor peptide containing a sequence at the N-terminus that induces apoptosis by interacting with p53, as well as a "cell-penetrating peptide" (CPP) at the C-terminus that derived from the Antennapedia protein homeodomain, which can drive peptides inside eukaryotic cells both by directly crossing the cytoplasmic membrane and by mediating endocytosis (Selivanova et al., 1997; Li Y et al., 2002). RGD is a natural ligand of integrins, cell surface proteins involved in adhesion to the extracellular matrix (Pierschbacher et al., 1984; Ruoslahti, 1996), and it is very different from the other three peptides, because it is very short, hydrophilic and uncharged. RGD interaction with eukaryotic cell membranes depends on binding to a protein receptor rather than on a direct

interaction with membrane lipids, as in the case of CAMPs and CPPs. Immobilized RGD-like peptides are frequently used to promote the adhesion of eukaryotic cells to surfaces, polymers, hydrogels, etc. Moreover, they may find applications in diagnostic and imaging fields (Knetsch et al., 2015; Karimi et al., 2018).

Peptides GKY20, $ApoB_L$ and p53pAnt with an additional cysteine residue at the N-terminus – named (C)GKY20, (C)$ApoB_L$ and (C)p53pAnt – were prepared by the ONC-based strategy described in the Introduction and separated from the carrier exploiting the sensitivity of the Asp-Cys sequence to the acidic hydrolysis (Pane et al., 2018b). Peptide RGD with an additional cysteine residue at the N-terminus—(C)RGD—was obtained by chemical synthesis.

The four peptides were labeled with either a Luc or an aLuc moiety at the N-terminus (Siepi et al., 2021) by incubation with a slight molar excess of 6-hydroxy-2-cyanobenzothiazole or 6-amino-2-cyanobenzothiazole, respectively. As expected, based on the well-known high efficiency of this reaction, Luc-labeled peptides (Luc-GKY20, Luc-$ApoB_L$, Luc-p53pAnt and Luc-RGD) and aLuc-labeled peptides (aLuc-GKY20, aLuc-$ApoB_L$, aLuc-p53pAnt and aLuc-RGD) were obtained with yields close to 100% after very short incubation times (30–60 min).

(C)GKY20 was also treated with 6-methoxy-2-cyanobenzothiazole to obtain an mLuc-labeled peptide (mLuc-GKY20) and with PyMPO maleimide, the thiol-reactive version of PyMPO, a widely used photostable solvatochromic fluorophore (Litak et al., 1994; Wakabayashi et al., 2013), to obtain the peptide PyMPO-(C)GKY20. SDS-PAGE analysis of labeled GKY20, $ApoB_L$ and p53pAnt showed their bright fluorescence under UV light (365 nm) and their solvatochromic nature appreciable even by the naked eye (Fig.10).

In addition to the labelled peptides described above, using similar procedures the labelled peptide Luc-FIBγ-TWK25 was prepared starting from the recombinant peptide (C)FIBγ-TWK25, whose preparation has been described in section 3.1.2.

The spectrofluorimetric properties of the labelled peptides were studied in different conditions and in the presence of different

interactors (liposomes, SDS, LPS and *E. coli* cells) to verify the suitability of Luc and aLuc as fluorescent label for peptides.

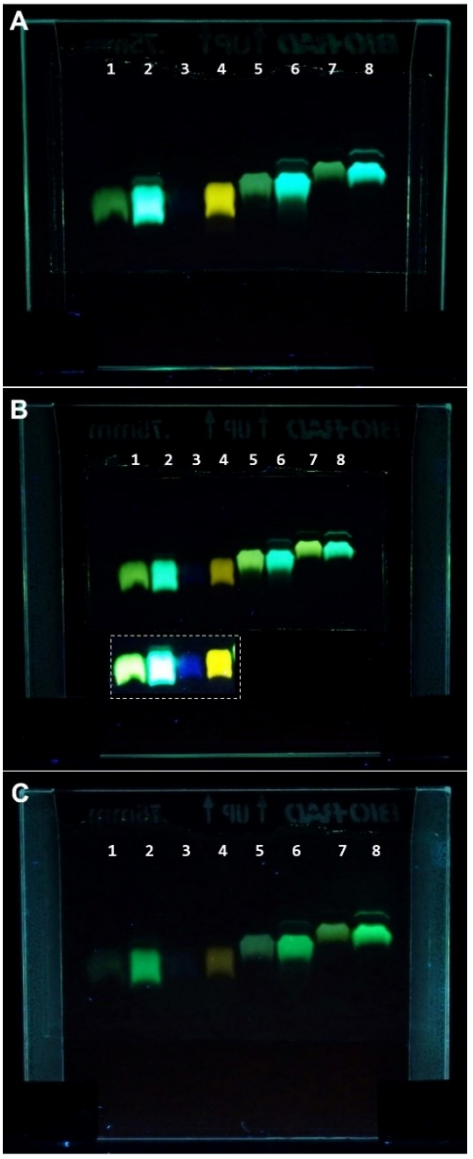

Figure 10. SDS-PAGE analysis of the labeled peptides. Lanes 1-8, Luc-GKY20, aLuc-GKY20, mLuc-GKY20, PyMPO-(C)GKY20, Luc-ApoB$_L$, aLuc-ApoB$_L$, Luc-p53pAnt, aLuc-p53pAnt. The gel was photographed immediately after the analysis in the running buffer containing SDS (**A**), after repeated washes in isopropanol/water (40% v:v) to remove SDS (**B**) and after repeated washes in water to remove isopropanol (**C**). The inset in (**B**) shows lanes 1-4 with increased contrast to highlight the weak blue fluorescence of mLuc-GKY20.

3.3.1 Antimicrobial activity of labeled peptides

When choosing the best fluorophore to label a peptide, in addition to excitation and emission wavelengths, other relevant parameters are (photo)stability and molecular features, which might influence the biological activity of the peptide to be labeled (molecular weight, charge, hydrophobicity, etc.).

In order to determine the influence of Luc labels on the antimicrobial activity of the peptides, we compared the activity of labeled GKY20 and $ApoB_L$ peptides with those of the corresponding unlabeled recombinant peptides, (P)GKY20 (Pane et al., 2016b) and (P)$ApoB_L$ (Gaglione et al., 2017). The MIC values of Luc-GKY20 and aLuc-GKY20 were found to be identical to those measured for (P)GKY20 on Gram-negative and Gram-positive strains (Tab. 7). The MIC values of Luc-$ApoB_L$ and aLuc-$ApoB_L$ were found to be very similar to those measured for (P)$ApoB_L$ (the observed differences, not higher than one dilution, are generally considered not significant in the microdilution assay).

	Strain		
	Escherichia coli 25922 ATCC	**Staphylococcus aureus ATCC 6538P**	**Bacillus globigii TNO BM013**
Peptide	**MIC (μM)[a]**		
(P)GKY20	6.25	1.56	nd[b]
Luc-GKY20	3.12	1.56	nd
aLuc-GKY20	6.25	1.56	nd
(P)ApoBL	2.5	nd	2.5
Luc-ApoBL	2.5	nd	1.25
aLuc-ApoBL	5.0	nd	5.0
Antibiotic	**MIC (μg/mL)[a]**		
Vancomycin	nd	0.5	2.0
Polymyxin B	0.5	nd	nd

[a]Data were obtained from a minimum of three independent experiments. The highest value was accepted as MIC. A difference of one scalar dilution is generally considered not significant.
[b]Not determined.

Table 7. Antimicrobial activity expressed as MIC values.

3.3.2 Response of the labeled peptides to Solvent Polarity Changes

Most solvatochromic fluorophores show an increase in fluorescence emission and a blue shift of the λ_{max} as solvent polarity decreases. Therefore, we measured emission spectra of the labeled peptides in sodium phosphate 10 mM, pH 7.4 (NaP) and in the same buffer containing 50% (v:v) either isopropanol or methanol. Quantum yield (QY), was also measured by Prof. Del Vecchio and co-workers (University of Naples, “Federico II”).

The emission spectra in NaP of the Luc- and aLuc-labeled peptides showed maximum emission at 539 and 526 nm, respectively (Fig. 11 and Tab. 8). As expected, all the labeled peptides showed a blue shift of the λ_{max} in the presence of the organic solvents (Tab. 8). The blue shift was less in the case of Luc-labeled peptides (6–7 nm) and greater in the case of aLuc-labeled peptides (9–15 nm). Furthermore, aLuc-labeled peptides showed a considerably greater blue shift in isopropanol than in methanol, thus confirming that aLuc is a probe more sensitive to solvent polarity compared to Luc. mLuc-GKY20 showed blue-shift values very similar to those of aLuc-GKY20, whereas PyMPO-(C)GKY20 showed a 5 nm blue shift only in the presence of isopropanol.

Intriguingly, emission intensities (Fig. 11) and QY values (Tab. 9) showed complex and partially unexpected variation characteristic of each peptide. For example, all the variants of GKY20 showed very large increases in emission intensities and QY values in the presence of the organic solvent (2.5–6 times higher in 50% isopropanol than in water). On the contrary, Luc-p53pAnt and aLuc-p53pAnt showed a 30–35% reduction in QY. Both labeled variants of $ApoB_L$ and RGD showed little or no variation in emission intensities (Fig. 11) and QY (Tab. 9). These puzzling variations are likely the result of a very well-known phenomenon, i.e., the quenching of fluorophores bound to protein/peptides. Even if several mechanisms can contribute to quenching, the most common is photoinduced electron transfer (PET), a reversible light-triggered transfer of electrons from amino-acid residues to the fluorophore (Doose et al., 2009). The most efficient donors are tryptophan and tyrosine, although to a lesser extent, histidine and methionine can also contribute significantly to quenching (Chen H et al., 2010). Obviously, the redox potential of a fluorophore and therefore its

propensity to accept electrons, influences its sensitivity to quenching (Doose et al., 2009).

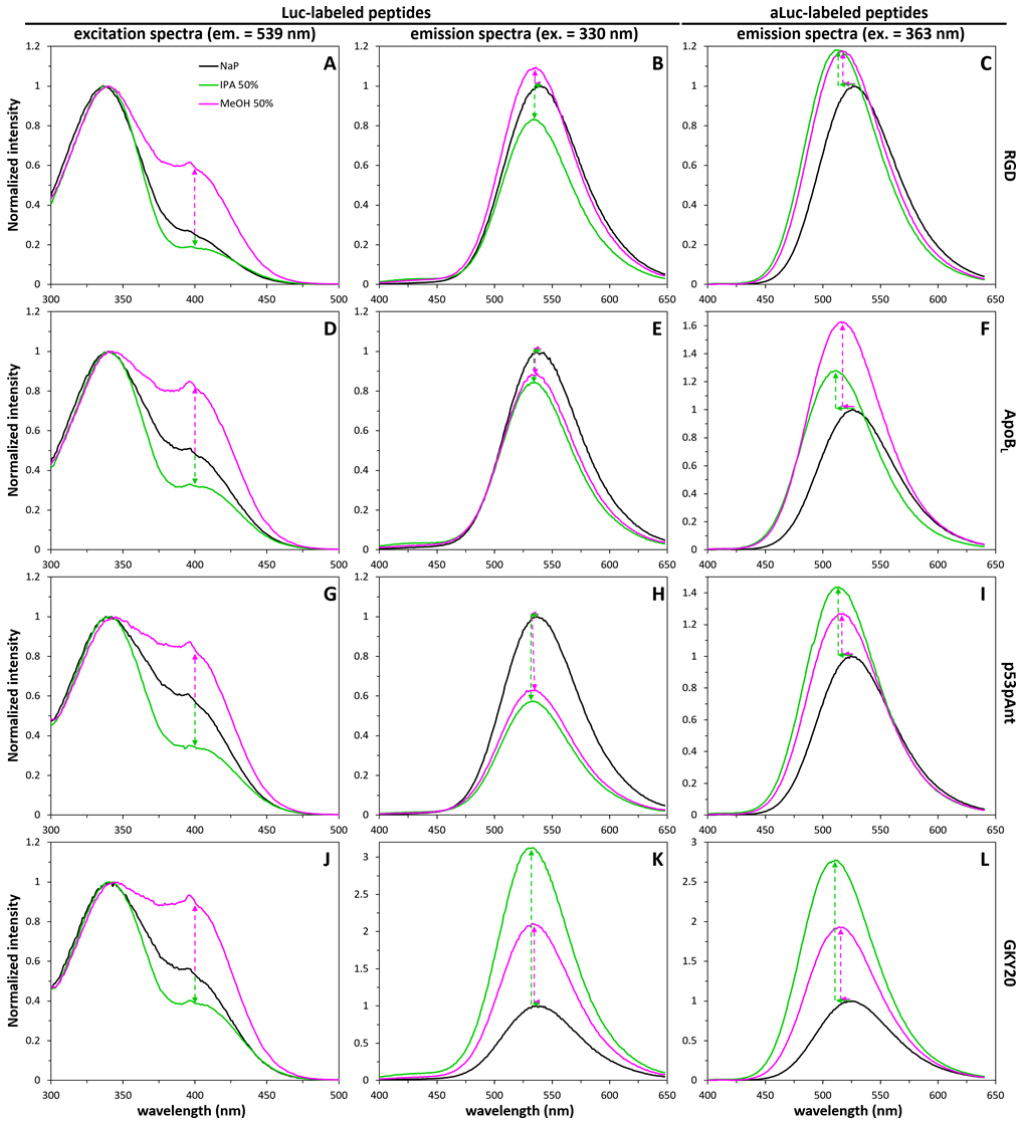

Fig. 11. Fluorescence of labeled peptides in 50% methanol or isopropanol in NaP pH 7.5 (v:v). Emission spectra recorded in the presence of organic solvents were normalized to the corresponding spectra in NaP. Arrows highlight the main changes with respect to NaP.

Peptide	λ_{max} (nm) [a]							
	NaP pH 7.4	MeOH 50%	IPA 50%	SDS (25 mM)	POPC +POPG	POPC	LPS (200 µg/mL)	*E. coli* cells
Luc-GKY20	538	533 (5)	531 (7)	526 (12)	520 (19)	520 (19)	516 (23)	522 (16)
Luc-ApoB$_L$	539	533 (6)	533 (6)	526 (13)	522 (17)	539 (0)	508 (31)	534 (5)
Luc-p53pAnt	539	533 (6)	533 (6)	526 (13)	522 (17)	539 (0)	nd [b]	nd
Luc-RGD	539	533 (6)	533 (6)	533 (6)	539 (0)	539 (0)	nd	nd
aLuc-GKY20	525	515 (10)	510 (15)	506 (19)	499 (26)	499 (26)	503 (22)	509 (16)
aLuc-ApoB$_L$	527	516 (11)	512 (15)	505 (22)	497 (27)	527 (0)	486 (41)	518 (9)
aLuc-p53pAnt	526	516 (10)	515 (11)	504 (22)	499 (25)	526 (0)	nd	nd
aLuc-RGD	526	517 (9)	513 (13)	510 (16)	526 (0)	526 (0)	nd	nd
mLuc-GKY20	439	429 (10)	424 (15)	422 (17)	nd	nd	nd	nd
PyMPO-(C)GKY20	563	563 (0)	558 (5)	556 (7)	535 (28)	541 (22)	nd	nd

[a] Blue-shift values with respect to the λ_{max} in NaP are shown in parenthesis. [b] nd = not determined.

Table 8. λ_{max} and blue-shift values of the labeled peptides.

Peptide	QY [a] (variation relative to NaP pH 7.4)		
	NaP pH 7.4	IPA 50% [b]	NaAc [c] pH 5.0
PyMPO-GKY20	0.080	0.373 (4.66)	nd[d]
mLuc-GKY20	0.008	0.021 (2.63)	nd
Luc-GKY20	0.111	0.639 (5.76)	0.269 (2.42)
aLuc-GKY20	0.202	0.969 (4.80)	nd
Luc-ApoB$_L$	0.365	0.389 (1.07)	0.450 (1.23)
aLuc-ApoB$_L$	0.574	0.757 (1.32)	nd
Luc-p53pAnt	0.261	0.184 (0.70)	0.418 (1.60)
aLuc-p53pAnt	0.432	0.274 (0.63)	nd
Luc-RGD	0.519	0.443 (0.85)	0.510 (0.98)
aLuc-RGD	0.937	1.040 (1.11)	nd

[a] Errors ≤ 5% of the reported values. [b] Isopropanol:NaP pH 7.4 (1:1, *v*/*v*). [c] Sodium acetate 20 mM. [d] nd = not determined.

Table 9. Relative quantum yield of the labeled peptides.

PET is also very sensitive to distance and orientation of the donor/acceptor couple, so the quenching efficiency can be influenced even by minor variations in the conformation of the labeled protein/peptide. In fact, PET-mediated quenching is a powerful tool for detection of conformational variations in proteins and peptides (Doose et al., 2009).

Very interestingly, the peptides that show the largest variations, namely GKY20 and p53pAnt, contain several residues with strong quenching ability (tryptophan, histidine and two tyrosines in GKY20; two tryptophans, three histidines and a methionine in p53pAnt; Fig. 9).

The QY values of the Luc-labeled peptides were also measured in sodium acetate at pH 5.0 to induce the protonation of the histidine residues. Protonation of histidine residue can influence PET quenching both directly, by reducing the donor ability of the imidazole ring, and indirectly, by inducing conformational changes. As expected, significant increases in QY values were observed only for the three peptides containing histidine residues: GKY20, p53pAnt and $ApoB_L$ (Tab. 9). To date, it has not been possible to determine the relative contribution of the direct and indirect effect of histidine protonation on quenching.

3.3.3 Response of Luc-Labeled Peptides to pH

Luc has a phenolic hydroxyl, which behaves as a weak acid, with a pK_a of about 8.7 (Morton et al., 1969). As Luc and its phenolate have quite different excitation spectra, with maxima at 330 and 395 nm, respectively, the excitation spectra of the Luc-labeled peptides recorded at pH 7.4 show a characteristic shoulder at 390–400 nm originating from the small amount of phenolate ion present at this pH (Fig.12). It should be noted that the shoulder is also visible in the presence of organic solvents (Fig. 11). On the other hand, the shoulder disappears in buffers with pH values below 6, as Luc becomes protonated, whereas the peak at 400 nm prevails at pH values greater than 8.5 (Fig.12). By recording the emission at 539 nm of the Luc-labeled peptides after excitation at 400 nm in buffers with different pH values, we determined the actual pK_a values of the Luc moieties which were found to be: 8.40 ± 0.03 (Luc-RGD), 8.13 ± 0.04 (Luc-GKY20), 8.11 ± 0.04 (Luc-ApoBL) and 7.97 ± 0.03 (Luc-p53pAnt). All pK_a values were slightly lower than that of free Luc,

with small differences among the peptides, likely due to differences in the net charge and distribution of positively charged residues.

The possibility of selectively exciting the phenolic or phenolate form of Luc not only makes Luc a useful pH probe for the pH range of 7–8 but also allows for monitoring of the formation of peptide/ligand complexes in which the ionization of the Luc moiety is suppressed or altered. The next sections show some applications of this peculiar feature of Luc.

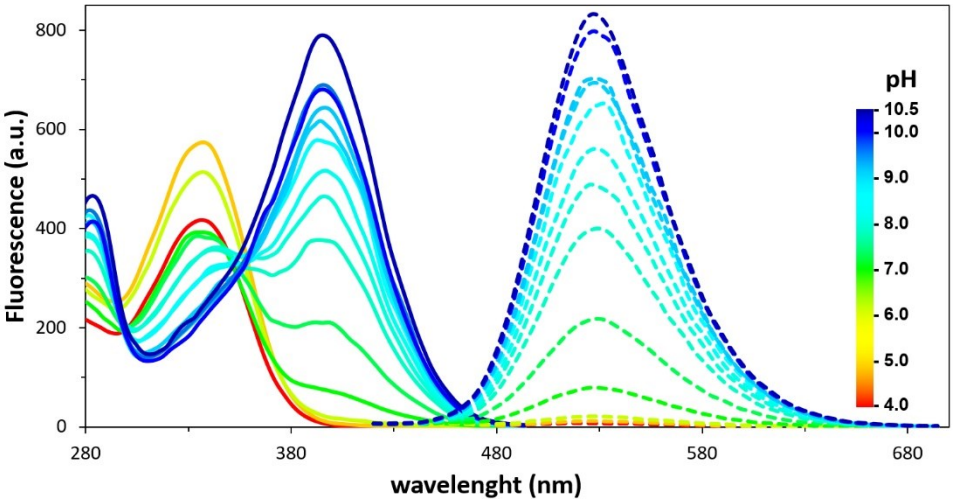

Figure 12. Response of Luc-labeled peptides to pH. Excitation (solid lines) and emission (dashed line) spectra of Luc-GKY20 as function of pH. Excitation spectra were recorded at 539 nm; emission spectra were recorded after excitation at 400.

3.3.4 Interaction of labeled Peptides with Liposomes

Both CAMPs and CPPs are able to interact with biological membranes, and this interaction is essential to their properties. Therefore, in order to verify whether Luc-labeling can be used to investigate peptide/membrane interaction, we studied the behavior of the labeled peptides in the presence of liposomes (carried out by Prof. Pompea Del Vecchio, University of Naples Federico II) composed either of pure palmitoyl-oleoyl-phosphatidylcholine (POPC) or of a mixture of POPC and palmitoyl-oleoyl-phosphatidylglycerol (POPG) at a molar ratio of 4:1. As the POPC head group is zwitterionic, liposomes composed only of this lipid are neutral and are usually considered mimetic of eukaryotic cell membranes. On the contrary, POPG-containing liposomes are negatively charged and are considered a simplified model of bacterial cell membranes.

The short, hydrophilic and negatively charged labeled RGD was used as a negative control. As expected, the excitation and emission spectra of Luc-RGD were essentially identical in NaP and in the presence of the two types of liposomes (Fig. 13). The same result was obtained in the case of the emission spectrum of aLuc-RGD (Fig. 13). On the contrary, in the case of Luc-ApoB$_L$, the excitation spectrum in the presence of POPC/POPG liposomes was clearly different from the spectra in NaP and in the presence of POPC liposomes, completely lacking a shoulder at 400 nm (Fig. 13). This suggests that in the presence of POPC/POPG liposomes, the deprotonation of the Luc phenolic group is inhibited. Two mechanisms could explain this finding: (i) embedding of the phenolic group of Luc among the lipids would directly prevent deprotonation; or (ii) binding of the Luc probe to the surface of the negatively charged POPC/POPG liposomes could prevent deprotonation as a consequence of the more acidic local environment. In fact, it is well-known that polyanionic surfaces and polymers determine the formation of acidic local environments by attracting protons from the bulk solution (Goldstein et al., 1964; Maurel et al., 1976). Further information was obtained from analysis of the emission spectra. Once more, the emission spectrum in the presence of POPC/POPG liposomes was very different from the other two spectra, showing the presence of a large shoulder at 425–430 nm (Fig. 13). As mentioned above, this blue emission is characteristic of the phenolic

form of Luc and can only be observed when Luc is in an environment with very low water content, a condition able to suppress the photoinduced dissociation. Therefore, the presence of a blue shoulder in the emission spectrum of Luc-ApoB$_L$ is a clear indication that the Luc moiety is deeply embedded into the POPC/POPG bilayer.

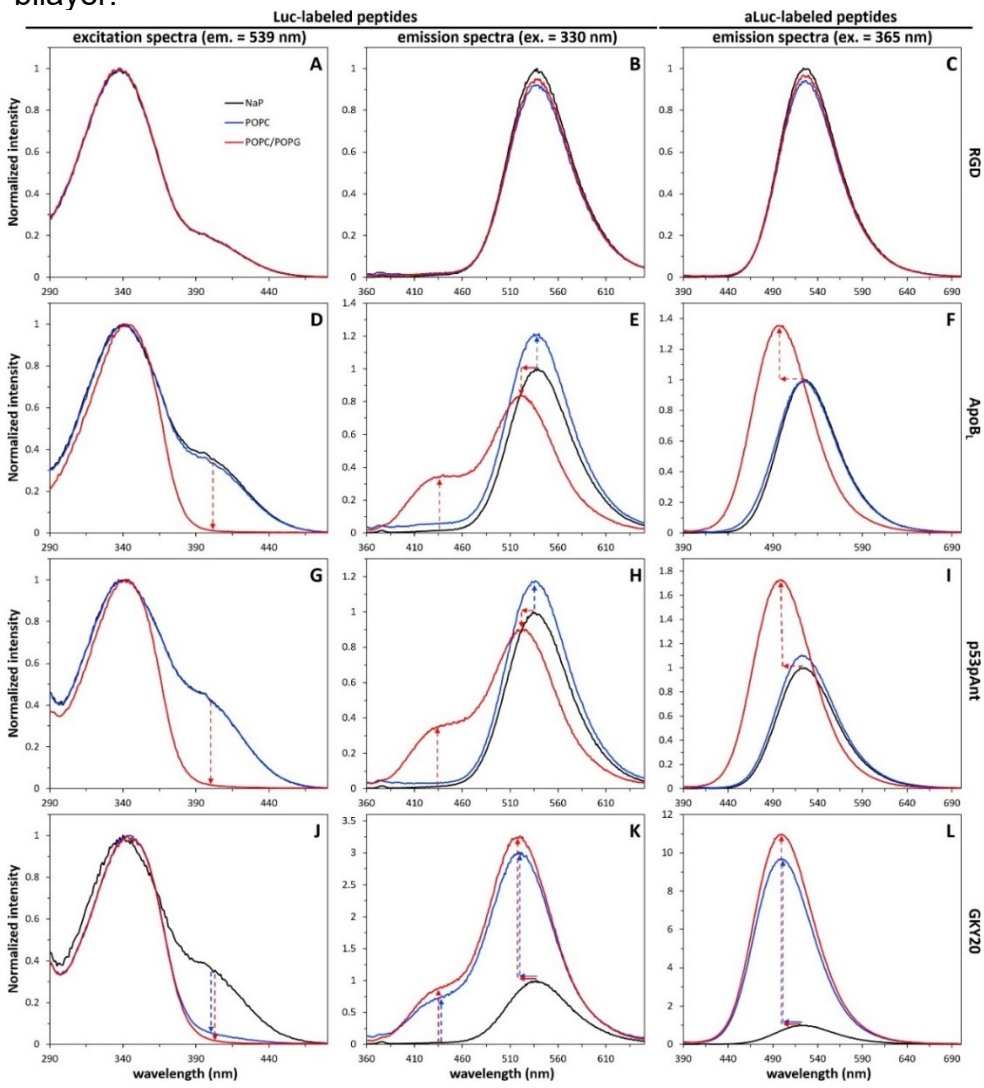

Figure 13. Fluorescence of labeled peptides in the presence of liposomes of POPC or POPC/POPG (5:1). Excitation spectra of luciferin (left), emission spectra of luciferin (center) and emission spectra of aminoluciferin (right) were recorded for peptides RGD (**A–C**), ApoB$_L$ (**D–F**), p53pAnt (**G–I**) and GKY20 (**J–L**). Spectra recorded in the presence of liposomes were normalized to the corresponding spectra in NaP. Arrows highlight the main changes with respect to NaP.

This is further confirmed by the 16–18 nm blue shift (from 539 to about 522 nm) of the peak in the green region (Tab. 8). The analysis of the emission spectra of aLuc-ApoB$_L$ is simpler but not less informative. This peptide shows a considerable increase in the fluorescence emission and a 27–28 nm blue shift (from 525 to about 497 nm) only in the presence of POPC/POPG liposomes (Fig. 13 and Tab. 8). Given the solvatochromic nature of aLuc, this is an indication that, only in the case of negatively charged liposomes, the probe is embedded in a hydrophobic environment. Therefore, three different and independent phenomena confirm binding and embedding of labeled ApoB$_L$ into the POPC/POPG bilayer: (i) inhibition of the deprotonation of Luc; (ii) inhibition of the photoinduced dissociation of Luc; (iii) the blue shift of Luc and aLuc emission peaks. In this regard, it is worth noting that the interaction of ApoB$_L$ with anionic liposomes of phosphatidylcholine and phosphatidylglycerol has been recently demonstrated by using differential scanning calorimetry (Gaglione et al., 2021).

Labeled p53pAnt showed a behavior essentially similar to labeled ApoB$_L$ (Fig. 13), whereas GKY20 showed that it can interact with both types of liposomes. Indeed, the emission spectra of Luc and aLuc-GKY20 and the excitation spectra of Luc-GKY20 in the presence of POPC and POPC/POPG liposomes are very similar (Fig. 13). All the emission spectra show a large blue shift compared to those recorded in NaP (Tab. 8). Furthermore, the emission spectra of Luc-GKY20 show a blue shoulder, thus indicating that the (a)Luc moiety is embedded in a less polar environment. The spectra of PyMPO-(C)GKY20 in the presence of liposomes were found to be very similar to those of aLuc-GKY20 (Fig. 14), thus demonstrating that the binding to both liposome types is not an artifact due to (a)Luc. These findings agree with previous studies performed using unlabeled GKY20 and the same model membranes (Oliva et al., 2019). We do not have a straightforward explanation for the observed varying behavior of the two CAMPs. However, very interestingly, further analyses conducted on labeled GKY20 and ApoB$_L$ evidence several additional differences, as described in the next sections.

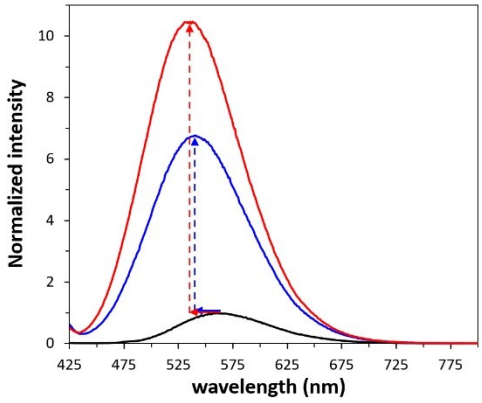

Figure 14. Fluorescence of PyMPO-(C)GKY20 in the presence of liposomes. Black line, NaP pH 7.5; blue line, POPC; red line, POPC/POPG (5:1). Spectra recorded in the presence of liposomes were normalized to the corresponding spectra in NaP. Arrows highlight the main changes with respect to NaP.

3.3.5 Interaction of labeled CAMPs with SDS micelles

In order to further confirm the ability of Luc probes to reveal the interaction of peptides with lipidic structures, we also recorded fluorescence spectra in the presence of 25 mM SDS (Fig. 15A–C). At this concentration, well above the critical micelle concentration (CMC) of about 8 mM, SDS forms micelles containing an average of 60 molecules (Aniansson et al., 1976). For this reason, SDS has been frequently used as a membrane mimetic, such as for determination of the NMR structure of membrane-binding peptides. However, it should be remembered that SDS is a strong detergent able to interact unspecifically with peptides. Accordingly, in the presence of SDS, not only labeled GKY20, $ApoB_L$ and p53pAnt but also labeled RGD showed spectral behavior, suggesting interaction with micelles (Fig. 15A–C). Nonetheless, the spectra of labeled RGD were not completely superimposable to those of the other three peptides. For example, in the excitation spectra of Luc-RGD in the presence of SDS, a tail at 400–420 nm is still visible, indicating that not all of the peptide is strongly associated to the micelles (Fig. 15A–C). In the emission spectrum of Luc-RGD, the blue peak is less evident than in the corresponding spectra of the other three peptides (Fig. 15A–C), and the ratio between the area of the peaks in the blue (380–465 nm) and green (466–640 nm) regions was 0.16, whereas

the same ratio for Luc-GKY20, Luc-ApoB$_L$ and Luc-p53pAnt was 0.27, 0.36 and 0.33, respectively. It is also evident that the peak in the green region is less blue-shifted than in the case of Luc-GKY20, Luc-ApoB$_L$ and Luc-p53pAnt (Fig. 15A–C and Tab. 8).

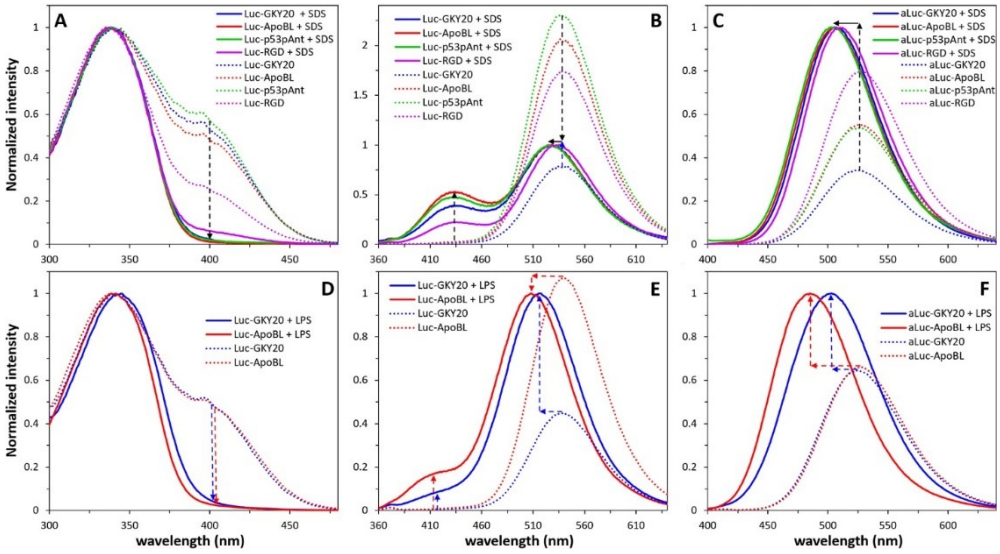

Figure 15. Fluorescence of labeled peptides in the presence of SDS or LPS micelles. (**A**), (**D**) Excitation spectra of Luc-labeled peptides (em. = 539; Luc-GKY20 + LPS, em. = 516 nm; Luc-ApoBL + LPS, em. = 508 nm). (**B**), (**E**) Emission spectra of Luc-labeled peptides (ex. = 330 nm). (**C**), (**F**) Emission spectra of aLuc-labeled peptides (ex. = 363 nm). Solid line, spectra recorded in the presence of SDS or LPS; dotted line, spectra recorded in NaP. In (**B**), (**C**), (**E**) and (**F**), spectra recorded in NaP were normalized to the corresponding spectra recorded in the presence of SDS or LPS. Arrows highlight the main changes with respect to NaP.

As in the case of the emission spectra recorded in the presence of liposomes, the spectra of aLuc-labeled peptides recorded in the presence of SDS also showed a significant increase in emission intensity, as well as a blue shift. However, again, the blue shift was smaller in the case of aLuc-RGD (Fig. 15A–C and Tab. 8). These results indicate that the hydrophilic RGD peptide interacts less tightly with the SDS micelles than Luc-GKY20, Luc-ApoB$_L$ and Luc-p53pAnt.

3.3.6 Interaction of labeled CAMPs with LPS micelles

As already mentioned in the previous chapters of this thesis, the ability to work as very effective LPS-scavengers is one of the most interesting properties of CAMPs (Rosenfeld et al., 2006). Therefore, the development of effective yet simple tools to study the CAMP/LPS interaction is of outstanding importance. Accordingly, we studied the interaction of labeled GKY20 and $ApoB_L$ by using a commercially available LPS from *E. coli* strain 0111:B4. Firstly, we recorded the excitation and the emission spectra of Luc-GKY20 and Luc-$ApoB_L$ in the presence of 200 µg/mL LPS, a concentration well above the CMC of this LPS (about 1.3–1.6 µM corresponding to 13–16 µg/mL) (Yu L et al., 2006). As expected, the binding of the two peptides to LPS caused the disappearance of the shoulder at 400 nm in the excitation spectra (Fig. 15D–F). The emission spectra of Luc-GKY20 and Luc-$ApoB_L$ show the expected blue shift of the peak in the green region—even larger than those observed in the presence of SDS and liposomes (Tab. 8) However, surprisingly, only a very low shoulder was observed in the blue region, especially in the case of Luc-GKY20 (Fig. 15D–F). The ratio between the area of the peaks in the blue (365–435 nm) and green (436–640 nm) regions is 0.046, and 0.095 for Luc-GKY20 and Luc-$ApoB_L$, respectively, i.e., even lower than the ratio observed for the Luc-RGD peptide in the presence of SDS. Very interestingly, the peak in the blue region is also blue-shifted (about 20 nm) with respect to the same peak observed in the case of liposomes and SDS. Finally, the emission spectra of aLuc-GKY20 and aLuc-$ApoB_L$ show, as expected, an increase in emission intensity and a large blue shift, particularly in the case of aLuc-$ApoB_L$ (41 nm). These findings suggest that the orientation of the Luc moiety when the peptides are bound to LPS is very different from that adopted when the peptides are bound to liposomes and SDS micelles. The high blue-shift values suggest that the (a)Luc moiety is in a very non-polar environment, while the very weak emission in the blue region indicate that the phenolic OH group of Luc points toward the solvent or a proton acceptor in the LPS (e.g., a basic group in the lipid A of LPS). Possible orientations of the Luc moiety in LPS and SDS or liposomes explaining the observed variations in excitation and emission spectra are schematically drawn in Figure 16.

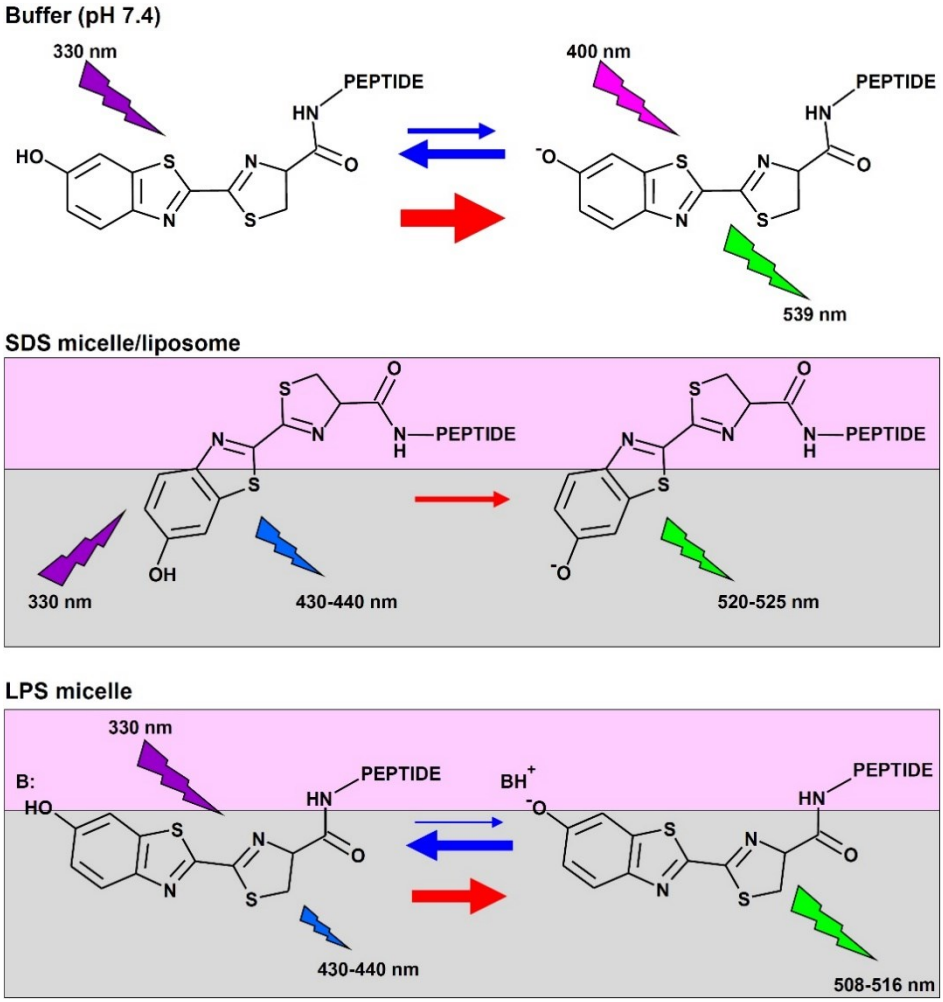

Figure 16. Possible orientations of Luc-labeled peptides bound to SDS micelles/liposomes or LPS. Gray and pink boxes represent, respectively, the inner hydrophobic region and the hydrophilic surface of liposomes and micelles. Blue and red arrows indicate acid-base equilibria and photoinduced ionization events, respectively. "B:" is a generic proton acceptor (either a solvent molecule or a group in the polar portion of the lipide A); the proton acceptor might be different in the case of the acid base equilibrium and the photoinduced ionization. In SDS micelles/liposomes the luciferin moiety is less buried than in LPS micelles but the hydroxyl group is better shielded from proton acceptors thus reducing the efficiency of the photoinduced dissociation and increasing the intensity of the blue fluorescence (430-440 nm).

3.3.7 Interaction of labeled CAMPs with Non-Micellar LPS

Next, we recorded the emission spectra of Luc-GKY20, Luc-ApoB$_L$, aLuc-GKY20 and aLuc-ApoB$_L$ at a constant peptide concentration in the presence of increasing concentrations of LPS (Fig. 17). All peptides showed a turn-off of the fluorescence associated with a considerable blue shift of λ_{max} values for LPS concentrations up to 10–20 µg/mL, followed by a turn-on phase with smaller changes in λ_{max} values. The biphasic nature of the process is clearly visible by plotting the area beneath the spectra and the λ_{max} values as a function of the LPS concentration (Fig. 17B,D,F,H). Only in the case of (a)Luc-ApoB$_L$, a turn-on phase with no shift in λ_{max} values was visible at very low LPS concentrations (0–2 µg/mL).

A similar behavior has been previously described for GKY25, HVF18 and VFR12, three CAMPs derived, like GKY20, from the C-terminus of human thrombin. In particular, GKY25 is a variant of GKY20, with five additional residues at the C-terminus (Saravanan et al., 2018). In that case, the authors, exploiting the intrinsic fluorescence of the single tryptophan residue present in all the thrombin-derived CAMPs, observed a biphasic process with a turn-off phase for LPS concentrations below 10 µg/mL and a turn-on phase at higher concentrations. Therefore, the turn-off/turn-on switch seems to be independent of the nature and position of the fluorophore. As the CMC of *E. coli* LPS is about 16 µg/mL, it can be speculated that the turn-off and turn-on phases might be the result of the binding to free and micellar LPS, respectively. The additional turn-on phase observed at very low LPS concentrations only in the case of (a)Luc-ApoB$_L$ might be due to a conformational change in this peptide induced by the presence of small amounts of LPS.

We also recorded the emission spectra of Luc-GKY20 and Luc-ApoB$_L$ after excitation at 400 nm in order to follow the binding process by monitoring the disappearance of the phenolate form in the solution (Fig. 18). As expected for a saturable binding process, we observed a progressive reduction in the fluorescence, which reached a minimum at about 50 µg/mL LPS for both peptides.

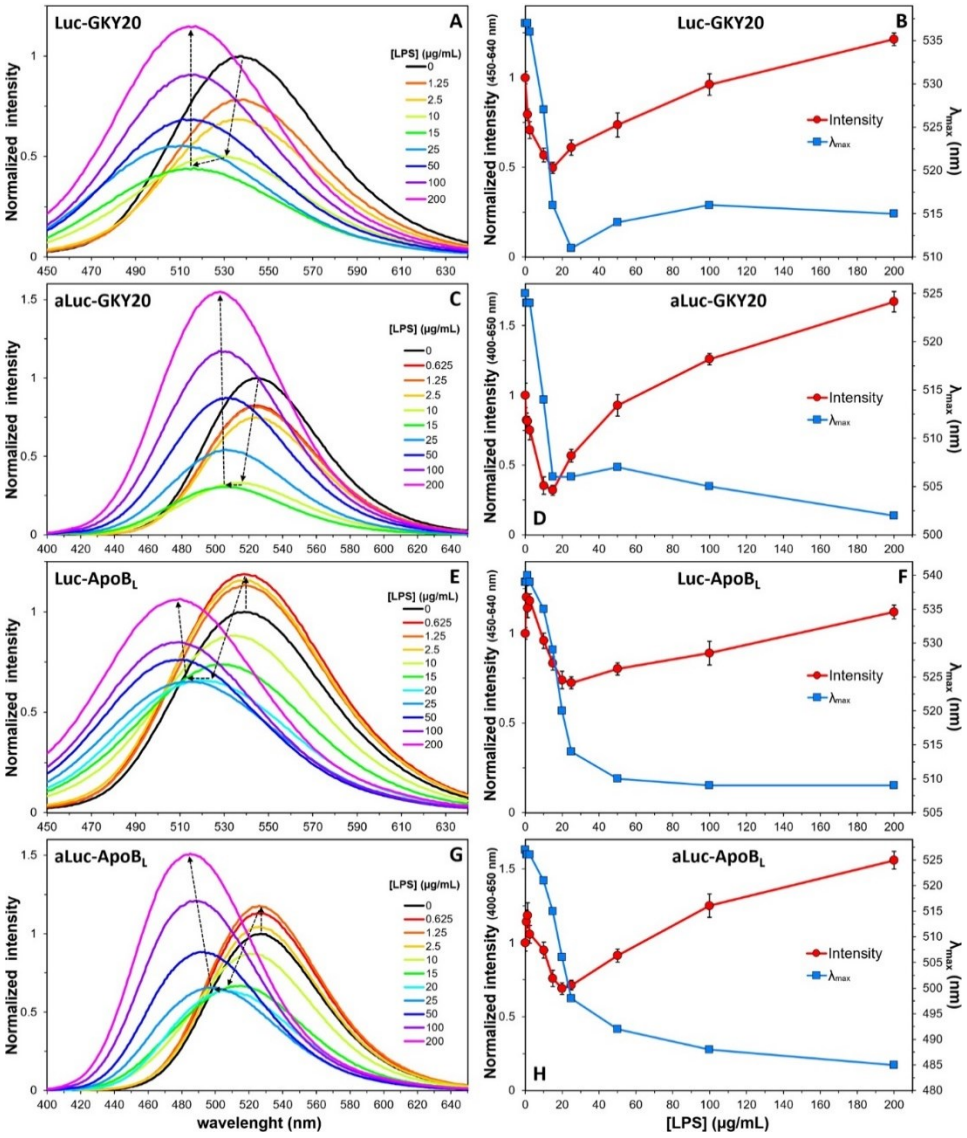

Figure 17. Fluorescence of the labeled peptides in the presence of increasing concentrations of LPS (0–200 µg/mL). (**A**), (**C**), (**E**), (**G**) Emission spectra of the peptides recorded after excitation at 330 nm (Luc-labelled peptides) and 363 nm (aLuc-labelled peptides). Spectra recorded in the presence of LPS were normalized to the corresponding spectra recorded in NaP (black lines). Arrows highlight the main changes with respect to NaP. (**B**), (**D**), (**F**), (**H**) Variation of total fluorescence (in the indicated ranges) and of the λ_{max} values as a function of LPS concentration.

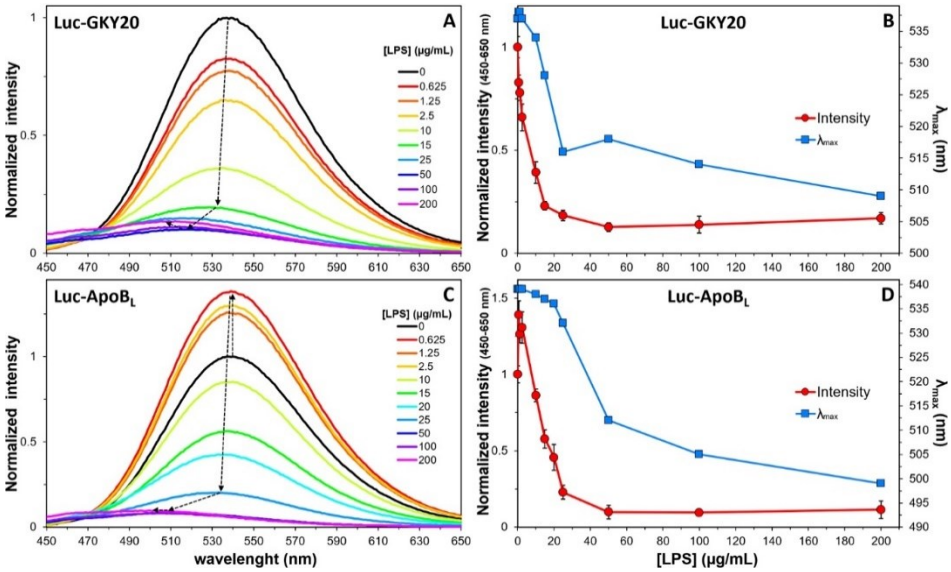

Figure 18. Fluorescence of the Luc-labeled peptides in the presence of increasing concentrations of LPS (0–200 μg/mL). (**A**), (**C**) Emission spectra of Luc-labeled peptides recorded after excitation at 400 nm. Spectra recorded in the presence of LPS were normalized to the corresponding spectra recorded in NaP. Arrows highlight the main changes with respect to NaP. (**B**), (**D**) Variation of total fluorescence (in the indicated ranges) and of the λ_{max} values as a function of LPS concentration.

3.3.8 Quantitative analysis of the Peptide/LPS interaction

The curves measured at constant peptide concentration and variable LPS concentration could be used to determine K_d values. However, as such K_d values would be the result of measurements obtained using concentrations below and above the CMC of LPS, their meaning would be questionable. In order to determine the K_d value of Luc-labeled peptides for micellar LPS, we repeated the experiment at variable Luc-labeled peptide concentration and constant LPS concentration (40 μg/mL corresponding to ~4 μM). The experimental data were fitted to the model described in Siepi et al. (Siepi et al., 2021). The model allows for the estimation not only the K_d value but also the number of binding sites and hence the stoichiometry of binding. The spectra and the fittings are shown in Figure 19. Luc-GKY20, Luc-ApoB$_L$, Luc-p53pAnt show K_d values in the range 50–400 nM. As expected, Luc-RGD did not bind to LPS, and the resulting plot of the fluorescence emission as function of the peptide concentration was a straight line (Fig. 19). The fact that the anticancer peptide Luc-p53pAnt binds to LPS with affinity

comparable to those of the two CAMPs is not surprising, considering that it has an amino-acid composition similar to that of the CAMPs (Fig. 9) and that it is the most cationic of the three peptides.

On the other hand, the three peptides show very different binding stoichiometries (Fig. 19). Only Luc-ApoB$_L$ binds to LPS in a 1:1 ratio. In the case of Luc-GKY20 three molecules of the peptide bind to two molecules of LPS, whereas in the case of Luc-p53pAnt, two molecules of the peptide bind to three molecules of LPS. The higher number of binding sites found for Luc-GKY20 might be due to the fact that this peptide is considerably shorter than the other two. However, Luc-ApoB$_L$ and Luc-p53pAnt have exactly the same length; therefore, the different stoichiometry might be due to a different mode of binding or a different fold adopted by the peptides upon binding.

Finally, we studied the interaction of Luc-FIBγ-TWK25 with LPS. In this case we determined K_d values and stoichiometry both at 40 µg/mL LPS and at 5 µg/mL, a concentration below the CMC. At 40 µg/mL LPS Luc-FIBγ-TWK25 showed parameters very similar to those of GKY20 (Fig. 20A). Very interestingly at 5 µg/mL LPS, we found a K_d value similar to that measured with micellar LPS but the peptide:LPS ratio increased from 1.5:1 to 4:1 (Fig. 20B). This finding might be due to the fact that, at concentration below the CMC, LPS molecules are not associated thereby exposing a higher portion of their molecular surface, in particular the fatty acid chains of lipid A which would be free to interact with the peptides. This analysis shows that FIBγ-TWK25 binds to LPS with a high affinity, therefore, supporting the hypothesis that it might act as an LPS scavenger similarly to other CAMPs like GKY20 and ApoB$_L$.

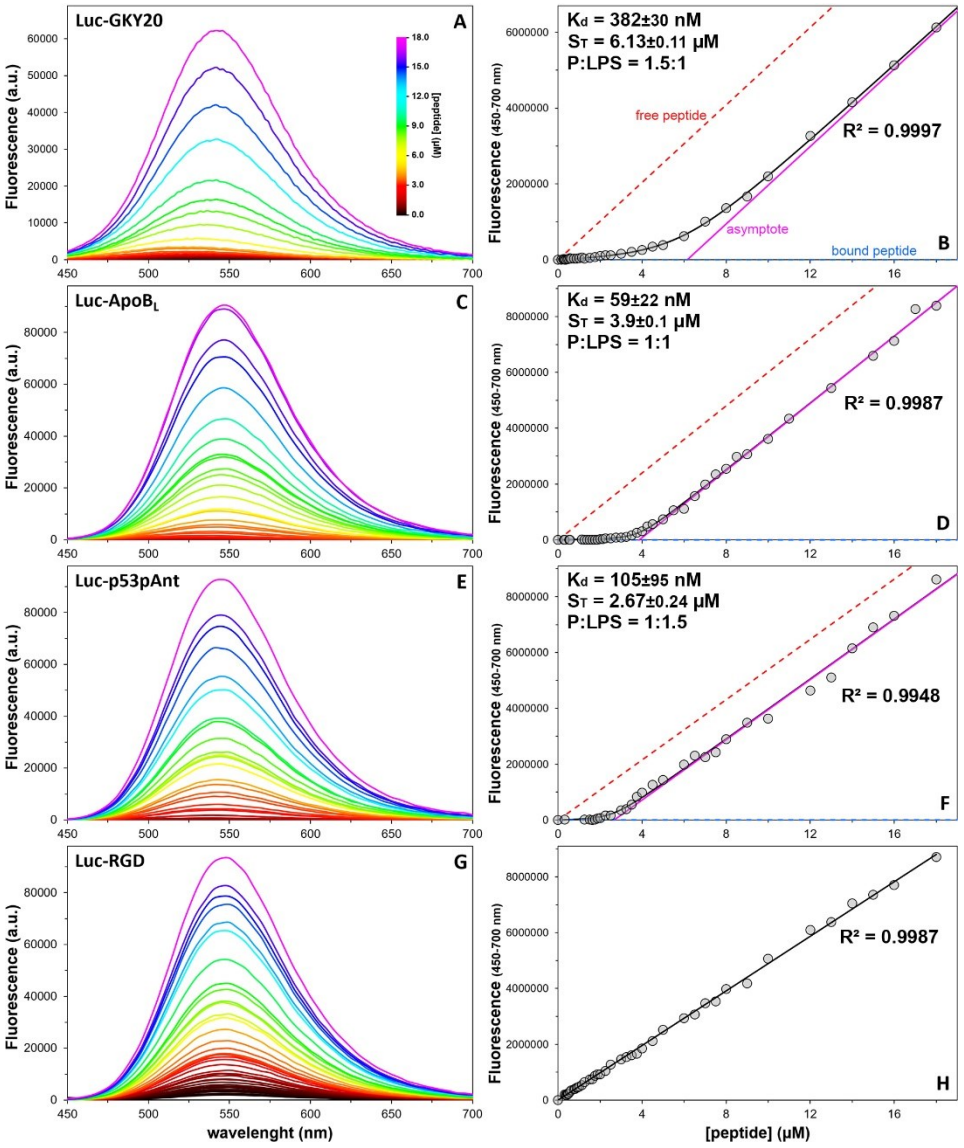

Figure 19. Determination of the K_d values and stoichiometry for the peptide/micellar LPS interaction. (**A**), (**C**), (**E**), (**G**) Emission spectra of Luc-labeled peptides (0–18 μM) in the presence of 40 μg/mL LPS (ex. = 400, 415, 425 and 410 nm, respectively). (**B**), (**D**), (**F**), (**H**) Variation of total fluorescence (450–700 nm) as a function of peptide concentration. The dashed lines are the expected fluorescence of the free and bound peptide, respectively. Black lines, K_d and stoichiometry (S_T) values were obtained using the equation described in Supplementary Methods. The ratio P:LPS was calculated from S_T, assuming that *E. coli* LPS has an average molecular weight of 10 kDa. In (**H**), data were fitted to a straight line.

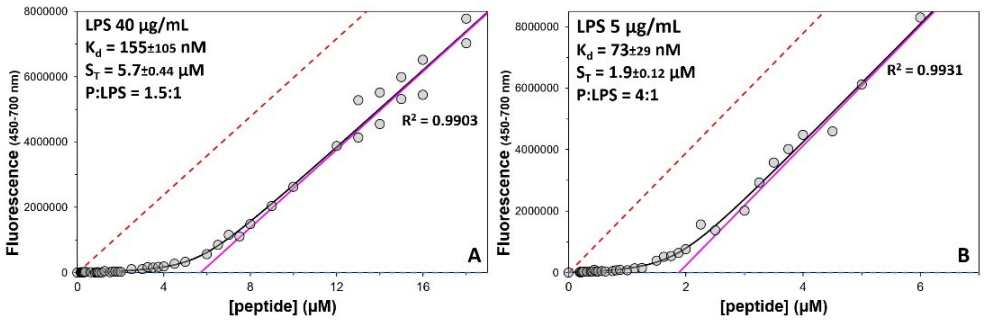

Figure 20. Determination of the K_d values and stoichiometry for the Luc-FIBγ-TWK25 / LPS interaction at 40 µg/mL (**A**) and 5 µg/mL (**B**). Color code as in Figure 19.

3.3.9 Interaction of labeled CAMPs with *E. coli* cells

In order to study the interaction of GKY20 and $ApoB_L$ with whole bacterial cells, we recorded the emission spectra of the labeled peptides in the presence of *E. coli* cells at an optical density of 0.1 OD_{600} (corresponding to about 0.63 × 10^9 CFU/mL). The emission spectra of Luc-GKY20 and Luc-$ApoB_L$ obtained after excitation at 330 nm show that in both cases, binding to *E. coli* cells causes a moderate decrease in the fluorescence emission (Fig. 21A), accompanied by a blue shift of 16 nm in the case of Luc-GKY20 (a value slightly lower than those observed in the case of liposomes and micellar LPS) and of only 5 nm in the case of Luc-$ApoB_L$ (Tab. 8). In the blue region, the emission of Luc-GKY20 was higher than that of Luc-$ApoB_L$, which is the opposite of what was observed in the case of LPS (Fig. 21B). The differences between the spectra of the labeled peptides in the presence of whole bacterial cells and those obtained in the presence of liposomes and purified LPS might be due to the fact that the outer membrane of Gram-negative bacteria is a very complex mixture of LPS, phospholipids and proteins.

The emission spectra of Luc-GKY20 and Luc-$ApoB_L$ obtained after excitation at 400 nm show a strong decrease in fluorescence emission (Fig. 21C), likely due to a reduced hydrolysis of the Luc hydroxyl group of the cell-bound peptides.

Finally, *E. coli* cells caused a significant increase in the fluorescence emission of aLuc-GKY20 and a slight decrease in the fluorescence emission of aLuc-$ApoB_L$ (Fig. 21D). In the case of aLuc-labeled

peptides, we also observed a blue shift lower than that observed in the case of liposomes and micellar LPS (Tab. 8).

The spectra shown in Figure 21 were recorded after an incubation time of 20 min in the case of labeled GKY20 and of 120 min in the case of labeled $ApoB_L$. The different incubation times were necessary for an unexpected difference in the binding kinetic of the two peptides, as shown in Figure 21E. In the case of Luc-GKY20, the slope of the curve obtained by plotting fluorescence intensity (ex. = 400 nm; em. = 539 nm) as a function of time was about 6.7 times higher than that observed in the case of Luc-$ApoB_L$. Intriguingly, in the case of purified LPS, the binding process was complete within the preparation time of the samples (about 60 sec) for both peptides. The reasons for such differences were not further investigated. Nonetheless, these results highlight another useful application of Luc labeling.

We also observed *E. coli* cells treated with the labeled peptides (3 μM) using a fluorescence microscope equipped with a mercury arc lamp (Fig. 22 and 23). In the case of GKY20-treated cells, in addition to homogeneously labeled cells, we observed several cells with a heterogeneous labeling pattern (Fig. 22K,N and 23E). The same pattern was observed in *E. coli* cells treated with PYMPO-(C)GKY20, indicating that heterogeneous labeling is not an artifact of Luc labeling (Fig. 22A–D). For incubation times longer than 30 min, we observed an increased amount of highly fluorescent and large bodies (Fig. 23), likely aggregates of cell debris and/or dead cells. This is not surprising, as GKY20 and $ApoB_L$, like many CAMPs, cause cell lysis (Kasetty et al., 2011; Gaglione et al., 2019a).

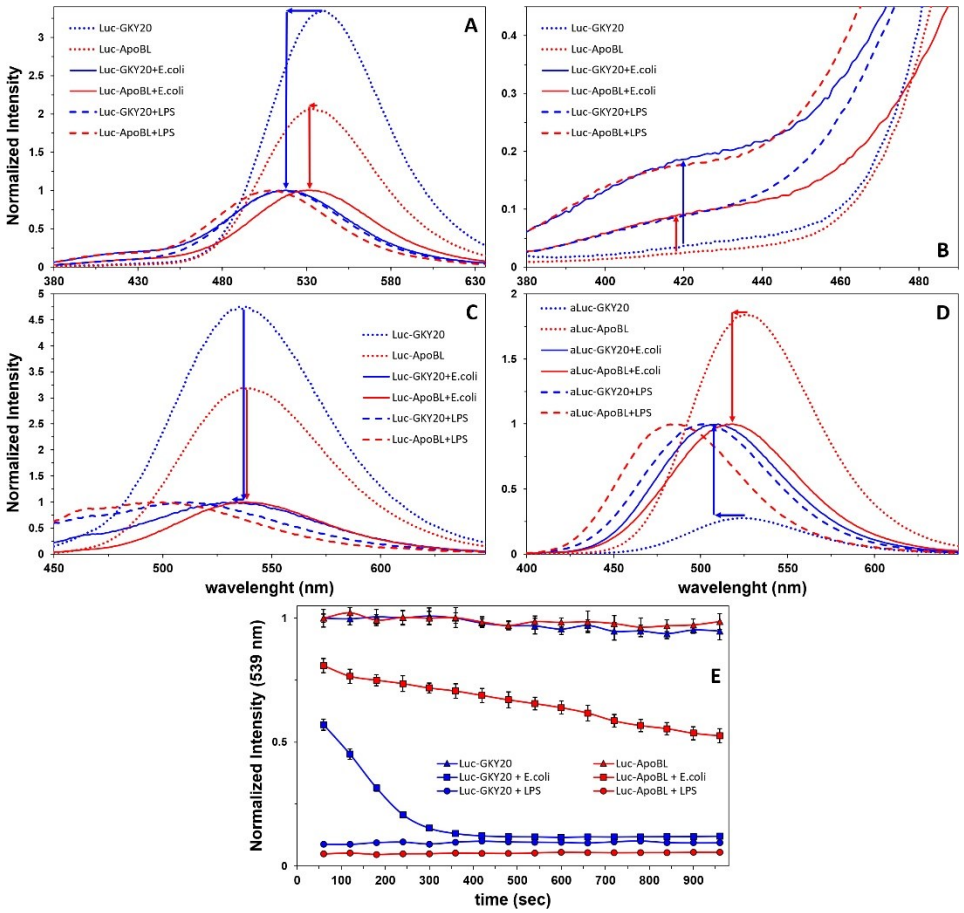

Figure 21. Emission spectra of labeled peptides in the presence of *E. coli* cells (0.1 O.D.). (**A**) Emission spectra of Luc-labeled peptides excited at 330 nm. (**B**) Close up of the blue region of the spectra in (**A**). (**C**) Emission spectra of Luc-labeled peptides excited at 400 nm. (**D**) Emission spectra of aLuc-labeled peptides excited at 363 nm. Spectra recorded in NaP (dotted lines) were normalized to the corresponding spectra recorded in the presence of *E. coli* cells. Arrows highlight the main changes with respect to NaP. (**E**) Variation of fluorescence (ex. 400 nm; em. 539 nm) as function of the incubation time.

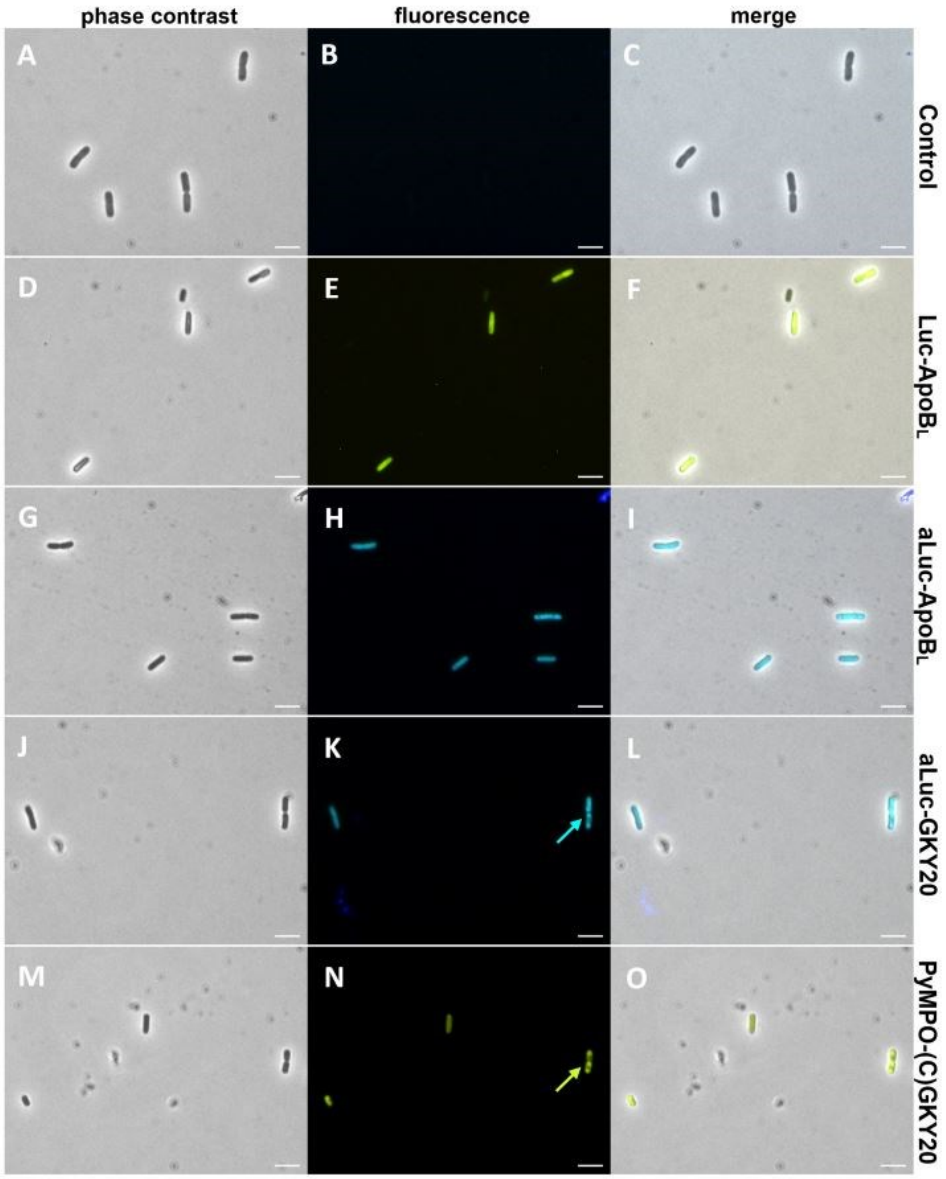

Figure 22. Fluorescence microscopy images of *E. coli* cells treated with labeled GKY20 and $ApoB_L$. *E. coli* was incubated with peptides (3 μM) for 15 min and observed without further treatments. Cyan and yellow arrows highlight dividing cells with a heterogeneous staining. Bar, 2 μm.

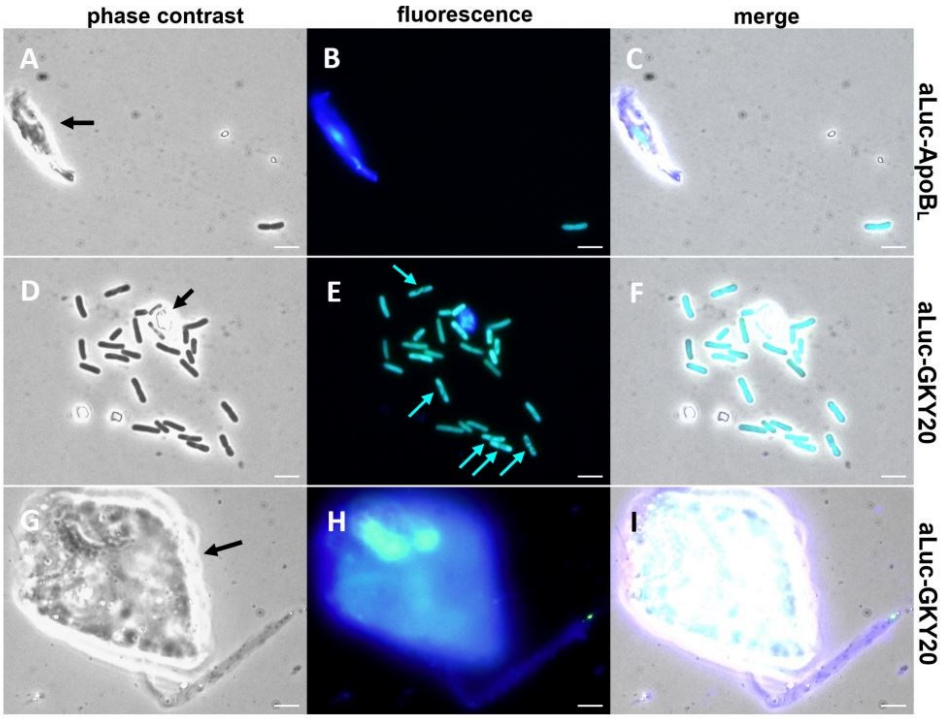

Figure 23. Fluorescence microscopy images of *E. coli* cells treated with labeled GKY20 and $ApoB_L$. *E. coli* was incubated with peptides (3 µM) for 30 min (**A-F**) or 50 min (**G-I**). Cyan arrows highlight dividing cells with a heterogeneous staining. Black arrows highlight fluorescent aggregates. Bar, 2 µm.

Chapter 4 – CONCLUSIONS

Among the many different classes of antimicrobial agents, HDP and in particular CAMPs have peculiar features that make very promising their use in several fields. These include pharmacology and veterinary but also agriculture, food and cosmetic industry, moreover, they may find applications in the biomaterial industry and as agents for the functionalization of prosthesis and medical implants and devices. However, they also have drawbacks common to other agents with a polypeptide nature: high production costs, low stability/short half-life, possible immunogenicity (at least for some applications). So far this has hampered the exploitation of their full potential. For this reason, the general aim of the laboratory where this PhD Thesis has been prepared is to develop a platform that could help to fully exploit CAMPs. The realization of the present thesis work has allowed to move some further steps toward this goal. *In silico* screening of human secretome allowed to identify several tens of new potential CAMP-RP, i.e. proteins hosting one or more cryptic CAMPs. An exhaustive manual examination of the list allowed to select 34 cryptic CAMPs from 17 CAMP-RPs. The experimental characterization of the 34 CAMPs showed that almost all the selected peptides have direct antimicrobial activity, at least at some extent. This result has two relevant implications:

- it confirms the validity of the *in silico* analysis method, so far applied just to few proteins;
- together with the seven cryptic CAMPs previously identified using the same method, it has allowed to define a library of selected human bioactive peptides for the development of biomedical applications.

As a further step, in collaboration with the group of Prof. de la Fuente-Nuñez, we decided to perform a more thorough characterization of the peptides hosted in the proteins participating in blood coagulation and/or secreted by platelets. This choice was motivated by the fact that coagulation proteins play a special role in defense and that their role as source of bioactive peptides has already been demonstrated. While the group of Prof. de la Fuente-Nuñez has demonstrated that 4 of the 34 selected peptides, namely those hosted at the C-terminus of platelet protein SCUB1-3, are active also *in vivo* in a murine model of cutaneous infection, the analysis reported in this thesis has shown that the peptides hosted

at the C-terminus of the three subunits of fibrinogen have wide spectrum antimicrobial activity and that their effect is bactericidal. At least two of the peptides, those deriving from the fibrinogen subunits α and β, also showed a significant antibiofilm activity on preformed biofilm of *P. aeruginosa* PAO1. However, the most interesting finding is that fibrinogen-derived peptides show synergic activity when combined with each other and with GKY20, a CAMP derived from the C-terminus of thrombin. This in turn suggests that cryptic CAMPs from the same body district can cooperate, a particularly relevant finding considering that several proteins involved in blood clotting host cryptic CAMPs.

The results reported in the present work are very intriguing for two different but complementary reasons.

On one hand, our results confirm the existence of an “antimicrobial cryptome” thus shedding new light also on our view of innate immunity. Even if in humans there is just one cathelicidin, the well-known LL37, now we know that in addition to this CAMP there is a still undefined number of cathelicidin-like cryptides often deriving from proteins apparently not involved directly in defense, namely coagulation factors, serum proteins, extracellular matrix components, proteases, cytokines and peptide hormones. How great is the contribution of these potential HDPs to host defense remain to be determined, however, it very interesting to note that the existence of an “antimicrobial cryptome” could help to solve the so-called MIC paradox. The MIC values of most natural CAMPs is in the range 5-50 μM but only rarely a single natural CAMPs reaches such high concentrations in physiological conditions. However, if tens of HDPs of different origin – “conventional” and “cryptic” – coexist *in vivo*, the global concentration of these peptides could reach values significant from the point of view of the direct antimicrobial activity. At this regard the demonstration that cryptic CAMPs from the same body district can cooperate is even more relevant.

On the other hand, we have defined a wide panel of bioactive peptides that could be used alone or in combination to develop biomedical applications. The fact that all these peptides are of human origin reduces the concerns about possible immune compatibility issues. Even if apparently similar, all the newly

identified CAMPs differ for length, charge, hydrophobicity, solubility, propensity to aggregate or to form fibrils and, likely, in their affinity towards relevant bacterial toxic components like LPS and LTA. Moreover, they might also differ in their toxicity and biological effects on human cells. In principle, once characterized more in deep, human cryptic CAMPs might be used to develop mixture of peptides with the desired pharmacological activities, not limited to direct antimicrobial and antibiofilm activity. In addition, the fact that many cryptic CAMPs may show synergy with conventional antibiotics also suggests the possibility to design combined CAMP/antibiotic therapies. Obviously, the development of formulations based on mixture of peptides require the availability of effective and cheap methods for their preparation on an industrial scale. At this regard it is worth mentioning that the fibrinogen-derived peptides were prepared with high yields and purity using the ONC based strategy previously developed as part of the platform. This confirms the validity of the tool and the fact that fibrinogen-derived peptides may be prepared on an industrial scale. Very intriguingly, as already shown (Pane et al., 2018a), our recombinant strategy could be also used to prepare peptide mixtures instead of single peptides.

Finally, this thesis work has substantially contributed to the development of a new and very useful tool for the platform. This tool exploits the unusual, and, from some point of view, unique fluorescence properties of luciferin and aminoluciferin to prepare environment-sensitive fluorescent peptides that can be used to study the binding with a wide panel of interactors including model membranes, SDS, endotoxins like LPS and lipoteichoic acid, DNA and acidic polysaccharides like alginate as well as bacterial and eukaryotic cells. These applications, useful in a variety of fields, are particularly relevant in the case of CAMPs. For example, using the new labelling strategies it is possible:

- to measure the binding kinetics of peptides with bacterial cells;
- to determine the K_d values and binding stoichiometries for endotoxins, thus allowing to study quantitatively the endotoxin-scavenging activity of the peptides;
- to study qualitatively and quantitatively the interaction of CAMPs with a variety of extracellular polymers commonly

found in the extracellular matrix of biofilms (e.g. DNA and alginate).

Moreover, as discussed more thoroughly in (Siepi et al., 2021), luciferin and aminoluciferin should not significantly change the properties (size, hydrophobicity, charge, etc.) of the peptides to be labeled thus minimizing the risk of altering their chemical-physical behavior and/or biological activity. In fact, only NBD, bimane and unsubstituted coumarin dyes are smaller than luciferin. Moreover, several widely used solvatochromic and not-solvatochromic fluorophores are either quite hydrophobic or very hydrophilic and with several charged groups, whereas luciferin and aminoluciferin are uncharged and neither too hydrophobic nor particularly hydrophilic. Therefore, it can be reasonably anticipated that the new labelling strategy not only will improve and speed up the characterization of CAMPs but it will also make easier the rational optimization of CAMP-based antimicrobial, antibiofilm and antiendotoxin formulations.

REFERENCES

Ando Y, Akiyama H. **PH-dependent fluorescence spectra, lifetimes, and quantum yields of firefly-luciferin aqueous solutions studied by selective-excitation fluorescence spectroscopy.** *Jpn. J. Appl. Phys.* 2010, *49*, 117002.

Aniansson EAG, Wall SN, Almgren M, Hoffmann H, Kielmann I, Ulbricht W, Zana R, Lang J, Tondre C. **Theory of the kinetics of micellar equilibria and quantitative interpretation of chemical relaxation studies of micellar solutions of ionic surfactants.** *J. Phys. Chem.* 1976, *80*, 905–922.

Baltzer SA1, Brown MH. **Antimicrobial peptides: promising alternatives to conventional antibiotics.** J Mol Microbiol Biotechnol. 2011;20(4):228-35.

Beadell B., Powell T.R., Berton R., Porter E. **The antimicrobial peptides HNP-1 and HBD-2 act against Mycobacterium smegmatis independent from their chirality.** Southern California Conferences for Undergraduate Research; 2017.

Bellacchio E. **Mutations Causing Mild or No Structural Damage in Interfaces of Multimerization of the Fibrinogen γ-Module More Likely Confer Negative Dominant Behaviors.** *International Journal of Molecular Sciences*. 2020; 21(23):9016.

Belmadani A, Semlali A, Rouabhia M. **Dermaseptin-S1 decreases Candida albicans growth, biofilm formation and the expression of hyphal wall protein 1 and aspartic protease genes.** J Appl Microbiol. 2018;125(1):72-83.

Boparai JK, Sharma PK. **Mini Review on Antimicrobial Peptides, Sources, Mechanism and Recent Applications.** Protein Pept Lett. 2020;27(1):4-16.

Bosso A, Pirone L, Gaglione R, Pane K, Del Gatto A, Zaccaro L, Di Gaetano S, Diana D, Fattorusso R, Pedone E, Cafaro V, Haagsman HP, van Dijk A, Scheenstra MR, Zanfardino A, Crescenzi O, Arciello A, Varcamonti M, Veldhuizen EJA, Di Donato A, Notomista E, Pizzo E. **A new cryptic host defense peptide identified in human 11-hydroxysteroid dehydrogenase-1 β-like: from in silico identification to experimental evidence**. Biochim Biophys Acta Gen Subj. 2017 Sep;1861(9):2342-2353.

Bowdish DM, Davidson DJ, Hancock RE. **Immunomodulatory properties of defensins and cathelicidins.** Curr Top Microbiol Immunol. 2006;306:27-66.

Brancatisano FL, Maisetta G, Di Luca M, Esin S, Bottai D, Bizzarri R, Campa M, Batoni G. **Inhibitory effect of the human liver-derived antimicrobial peptide hepcidin 20 on biofilms of polysaccharide intercellular adhesin (PIA)-positive and PIA-negative strains of Staphylococcus epidermidis.** Biofouling. 2014;30(4):435-46.

Brogden KA. **Antimicrobial peptides: pore formers or metabolic inhibitors in bacteria?** Nat Rev Microbiol. 2005 Mar;3(3):238-50.

Cardoso P, Glossop H, Meikle TG, Aburto-Medina A, E.Conn C, Sarojini V, Valery C. **Molecular engineering of antimicrobial peptides: microbial targets, peptide motifs and translation opportunities.** Biophys Rev 13, 35–69 (2021).

Cederlund A1, Gudmundsson GH, Agerberth B. **Antimicrobial peptides important in innate immunity.** FEBS J. 2011 Oct;278(20):3942-51.

Chavez-Dozal AA, Nourabadi N, Erken M, McDougald D, Nishiguchi MK. **Comparative analysis of quantitative methodologies for Vibrionaceae biofilms.** Folia Microbiol (Praha). 2016 Nov;61(6):449-453.

Chen H, Ahsan SS, Santiago-Berrios MB, Abruña HD, Webb WW. **Mechanisms of quenching of alexa fluorophores by natural amino acids.** *J. Am. Chem. Soc.* 2010, *132*, 7244–7245.

Chen KT, Leritano C, Seimbille Y. **Early-Stage Incorporation Strategy for Regioselective Labeling of Peptides using the 2-Cyanobenzothiazole/1,2-Aminothiol Bioorthogonal Click Reaction**. *ChemistryOpen* 2018, *7*, 256–261.

Chen L, Jia L, Zhang Q, Zhou X, Liu Z, Li B, Zhu Z, Wang F, Yu C, Zhang Q, Chen F, Luo SZ. **A novel antimicrobial peptide against dental-caries-associated bacteria.** Anaerobe. 2017 Oct;47:165-172.

Chen X, Zhou L, Wu D, Huang W, Lin Y, Zhou B, Chen J. **The Effects of Titanium Surfaces Modified with an Antimicrobial Peptide GL13K by Silanization on Polarization, Anti-Inflammatory, and Proinflammatory Properties of Macrophages.** Biomed Res Int. 2020 Jul 24;2020:2327034.

Conchillo-Solé O, de Groot NS, Avilés FX, Vendrell J, Daura X, Ventura S. **AGGRESCAN: a server for the prediction and evaluation of "hot spots" of aggregation in polypeptides.** *BMC Bioinformatics* 8, 65 (2007).

Costa F, Carvalho IF, Montelaro RC, Gomes P, Martins MC. **Covalent immobilization of antimicrobial peptides (AMPs) onto biomaterial surfaces.** Acta Biomater. 2011 Apr;7(4):1431-40.

Cui L, Rao J. **2-Cyanobenzothiazole (CBT) condensation for site-specific labeling of proteins at the terminal cysteine residues.** Methods Mol Biol. 2015;1266:81-92.

de la Fuente-Núñez C, Reffuveille F, Mansour SC, Reckseidler-Zenteno SL, Hernández D, Brackman G, Coenye T, Hancock RE. **D-enantiomeric peptides that eradicate wild-type and multidrug-resistant biofilms and protect against lethal Pseudomonas aeruginosa infections.** Chem Biol. 2015 Feb 19;22(2):196-205.

Delavat F, Miyazaki R, Carraro N, Pradervand N, van der Meer JR. **The hidden life of integrative and conjugative elements.** FEMS Microbiol Rev. 2017;41(4):512-537.

Di Somma A, Moretta A, Canè C, Cirillo A, Duilio A. **Antimicrobial and Antibiofilm Peptides. Biomolecules.** 2020 Apr 23;10(4):652.

Dib JR, Wagenknecht M, Farías ME, Meinhardt F. **Strategies and approaches in plasmidome studies-uncovering plasmid diversity disregarding of linear elements?.** Front Microbiol. 2015;6:463. Published 2015 May 26.

Dominiczak MH, Caslake MJ. **Apolipoproteins: metabolic role and clinical biochemistry applications.** Annals of Clinical Biochemistry. 2011;48(6):498-515.

Donadio G, Di Martino R, Oliva R, Petraccone L, Del Vecchio P, Di Luccia B, Ricca E, Isticato R, Di Donato A, Notomista E**. A new peptide-based fluorescent probe selective for zinc(II) and copper(II).** *J. Mater. Chem. B* 2016, *4*, 6979–6988.

Doose S, Neuweiler H, Sauer M. **Fluorescence quenching by photoinduced electron transfer: A reporter for conformational dynamics of macromolecules.** *ChemPhysChem* 2009, *10*, 1389–1398.

Dubnau D, Blokesch M. **Mechanisms of DNA Uptake by Naturally Competent Bacteria.** Annu Rev Genet. 2019;53:217-237.

Duong L, Gross SP, Siryaporn A**. Developing Antimicrobial Synergy With AMPs.** Mini-review 2021. published: 12 March 2021**.** Frontiers in Medical Technology Volume 3.

EUCAST, 2000. **Terminology relating to methods for the determination of susceptibility of bacteria to antimicrobial agents.** Clin. Microbiol. Infect. 6,503–508.

Falanga A, Galdiero S. **Emerging therapeutic agents on the basis of naturally occurring antimicrobial peptides.** Peptides and Proteins: Volume 42, 2017

Fernandez-Escamilla AM, Rousseau F, Schymkowitz J, Serrano L. **Prediction of sequence-dependent and mutational effects on the aggregation of peptides and proteins.** Nat Biotechnol. 2004 Oct;22(10):1302-6.

Fery-Forgues S, Lavabre D. **Are Fluorescence Quantum Yields So Tricky to Measure? A Demonstration Using Familiar Stationery Products.** *J. Chem. Educ.* 1999, *76*, 1260.

Fischbach MA, Walsh CT. **Antibiotics for emerging pathogens.** Science. 2009 Aug 28;325(5944):1089-93.

Fratini F, Mancini S, Turchi B, Friscia E, Pistelli L, Giusti G, Cerri D. **A novel interpretation of the Fractional Inhibitory Concentration Index: The case Origanum vulgare L. and Leptospermum scoparium J. R. et G. Forst essential oils against Staphylococcus aureus strains.** Microbiol Res. 2017 Jan;195:11-17.

Fritsche TR, Rhomberg PR, Sader HS, Jones RN. **Antimicrobial activity of omiganan pentahydrochloride tested against contemporary bacterial pathogens commonly responsible for catheter-associated infections**. *Journal of Antimicrobial Chemotherapy*, Volume 61, Issue 5, May 2008, Pages 1092–1098.

Frousios KK, Iconomidou VA, Karletidi CM, Hamodrakas SJ. **Amyloidogenic determinants are usually not buried.** *BMC Struct Biol* 9, 44 (2009).

Gaglione R, Cesaro A, Dell'Olmo E, Della Ventura B, Casillo A, Di Girolamo R, Velotta R, Notomista E, Veldhuizen EJA, Corsaro MM, et al. **Effects of human**

antimicrobial cryptides identified in apolipoprotein B depend on specific features of bacterial strains. *Sci. Rep.* 2019a, *9*, 1–13.

Gaglione R, Dell'Olmo E, Bosso A, Chino M, Pane K, Ascione F, Itri F, Caserta S, Amoresano A, Lombardi A, Haagsman HP, Piccoli R, Pizzo E, Veldhuizen EJA, Notomista E, Arciello A. **Novel human bioactive peptides identified in Apolipoprotein B: Evaluation of their therapeutic potential.** Biochemical Pharmacology Volume 130, 15 April 2017, Pages 34-50.

Gaglione R, Pane K, Dell'Olmo E, Cafaro V, Pizzo E, Olivieri G, Notomista E, Arciello A. **Cost-effective production of recombinant peptides in Escherichia coli.** N Biotechnol. 2019a Jul 25;51:39-48.

Gaglione R, Smaldone G, Cesaro A, Rumolo M, De Luca M, Di Girolamo R, Petraccone L, Del Vecchio P, Oliva R, Notomista E, Pedone E, Arciello A. **Impact of a Single Point Mutation on the Antimicrobial and Fibrillogenic Properties of Cryptides from Human Apolipoprotein B. Pharmaceuticals (Basel).** 2021 Jun 29;14(7):631.

Gasteiger E, Hoogland C, Gattiker A, Duvaud S, Wilkins M, Appel RD, Bairoch AM. **Protein identification and analysis tools on the ExPASy server.** In: Walker JM, editor. The Proteomics Protocols Handbook. Humana Press; 2005 p. 571-607.

Gharsallaoui A, Oulahal N, Joly C, Degraeve P. **Nisin as a Food Preservative: Part 1: Physicochemical Properties, Antimicrobial Activity, and Main Uses.** Crit Rev Food Sci Nutr. 2016 Jun 10;56(8):1262-74.

Goldstein L, Levin Y, Katchalski E. **A Water-insoluble Polyanionic Derivative of Trypsin. II. Effect of the Polyelectrolyte Carrier on the Kinetic Behavior of the Bound Trypsin.** *Biochemistry* 1964, *3*, 1913–1919.

Gomes D, Santos R, S Soares R, Reis S, Carvalho S, Rego P, C Peleteiro M, Tavares L, Oliveira M. **Pexiganan in Combination with Nisin to Control Polymicrobial Diabetic Foot Infections.** Antibiotics (Basel). 2020 Mar 20;9(3):128.

Green MR, Hughes H, Sambrook J, MacCallum P. **Molecular cloning: a laboratory manual.** 4th edn. New York: Cold Spring Harbor Laboratory Press; 2012. p. 1890.

Guilhelmelli F, Vilela N, Albuquerque P, Derengowski Lda S, Silva-Pereira I, Kyaw CM. **Antibiotic development challenges: the various mechanisms of action of antimicrobial peptides and of bacterial resistance.** Front Microbiol. 2013;4:353. Published 2013 Dec 9.

Haiko J, Suomalainen M, Ojala T, Lahteenmaki K, Korhone TK, 2009. **Invited review: breaking barriers–attack on innate immune defences by omptin surface proteases of enterobacterial pathogens.** Innate Immun. 15, 67–80.

Han J, Burgess K. **Fluorescent Indicators for Intracellular pH**. *Chem. Rev.* 2010, *110*, 2709–2728, doi:10.1021/cr900249z.

Hancock RE, Sahl HG, **Antimicrobial and host-defense peptides as new anti-infective therapeutic strategies**, Nat. Biotechnol. 24 (2006) 1551–1557.

Hancock RE. **Cationic peptides: effectors in innate immunity and novel antimicrobials.** Lancet Infect Dis. 2001;1(3):156-164.

Hancock RE, Alford MA, Haney EF. **Antibiofilm activity of host defence peptides: complexity provides opportunities.** *Nat Rev Microbiol* **19,** 786–797 (2021).

Haney EF, Trimble MJ, Cheng JT, Vallé Q, Hancock REW. **Critical Assessment of Methods to Quantify Biofilm Growth and Evaluate Antibiofilm Activity of Host Defence Peptides.** Biomolecules. 2018 May 21;8(2):29.

Hansen FC, Kalle-Brune M, van der Plas MJ, Strömdahl AC, Malmsten M, Mörgelin M, Schmidtchen A. **The Thrombin-Derived Host Defense Peptide GKY25 Inhibits Endotoxin-Induced Responses through Interactions with Lipopolysaccharide and Macrophages/Monocytes.** J Immunol. 2015 Jun 1;194(11):5397-406.

Harris F, Dennison SR, Phoenix DA. **Anionic antimicrobial peptides from eukaryotic organisms.** Curr Protein Pept Sci. 2009;10(6):585-606.

Hilchie AL, Wuerth K, Hancock RE, **Immune modulation by multifaceted cationic host defense (antimicrobial) peptides**, Nat. Chem. Biol. 9 (2013) 761–768.

Ibrahim HR, Hamasaki K, Miyata T. **Novel peptide motifs from lysozyme suppress pro-inflammatory cytokines in macrophages by antagonizing toll-like receptor and LPS-scavenging action.** Eur J Pharm Sci. 2017 Sep 30;107:240-248.

Ibrahim HR, Imazato K, Ono H. **Human lysozyme possesses novel antimicrobial peptides within its N-terminal domain that target bacterial respiration.** J Agric Food Chem. 2011 Sep 28;59(18):10336-45.

Izadi N, Keikha M, Ghazvini K, Karbalaei M. (2020). **Oral antimicrobial peptides and new therapeutic strategies for plaque-mediated diseases.** *Gene Reports*, 100811.

Jeon J, Shen B, Xiong L, Miao Z, Lee KH, Rao J, Chin FT. **Efficient method for site-specific 18F-labeling of biomolecules using the rapid condensation reaction between 2-cyanobenzothiazole and cysteine.** Bioconjug Chem. 2012 Sep 19;23(9):1902-8.

Johnson EC, Malito E, Shen Y, Pentelute B, Rich D, Florián J, Tang WJ, Kent SB. **Insights from atomic-resolution X-ray structures of chemically synthesized HIV-1 protease in complex with inhibitors.** J Mol Biol. 2007 Oct 26;373(3):573-86.

Johnston C, Martin B, Fichant G, Polard P, Claverys JP. 2014. **Bacterial transformation: distribution, shared mechanisms and divergent control.** Nat Rev Microbiol 12:181–196.

Kakiuchi M, Ito S, Yamaji M, Viviani VR, Maki S, Hirano T. **Spectroscopic**

Properties of Amine-substituted Analogues of Firefly Luciferin and Oxyluciferin. *Photochem. Photobiol.* 2017, *93*, 486–494.

Karimi F, O'Connor AJ, Qiao GG, Heath DE. **Integrin Clustering Matters: A Review of Biomaterials Functionalized with Multivalent Integrin-Binding Ligands to Improve Cell Adhesion, Migration, Differentiation, Angiogenesis, and Biomedical Device Integration.** *Adv. Healthc. Mater.* 2018, *7*, 1–28.

Kasetty G, Papareddy P, Kalle M, Rydengård V, Mörgelin M, Albiger B, Malmsten M, Schmidtchen A. **Structure-activity studies and therapeutic potential of host defense peptides of human thrombin.** Antimicrob Agents Chemother. 2011 Jun;55(6):2880-90.

Kattula S, Byrnes JR, Wolberg AS. **Fibrinogen and Fibrin in Hemostasis and Thrombosis.** Arterioscler Thromb Vasc Biol. 2017 Mar;37(3):e13-e21.

Khare T, Anand U, Dey A, Assaraf YG, Chen ZS, Liu Z, Kumar V. **Exploring Phytochemicals for Combating Antibiotic Resistance in Microbial Pathogens.** Front Pharmacol. 2021 Jul 21;12:720726.

Klymchenko AS. **Solvatochromic and Fluorogenic Dyes as Environment-Sensitive Probes: Design and Biological Applications**. *Acc. Chem. Res.* 2017, *50*, 366–375.

Knetsch PA, Zhai C, Rangger C, Blatzer M, Haas H, Kaeopookum P, Haubner R, Decristoforo C. **[68Ga]FSC-(RGD)3 a trimeric RGD peptide for imaging αvβ3 integrin expression based on a novel siderophore derived chelating scaffold-synthesis and evaluation.** *Nucl. Med. Biol.* 2015, *42*, 115–122.

Koczulla R, Degenfeld G, Kupatt C, Krotz F, Zahler S, Gloe T, Issbrucker K, Unterberger P, Zaiou M, Lebherz C, Karl A, Raake P, Pfosser A, Boekstegers P, Welsch U, Hiemstra PS, Vogelmeier C, Gallo RL, Clauss M, Bals R, **An angiogenic role for the human peptide antibiotic LL-37/hCAP-18**, J. Clin. Invest. 111 (2003) 1665–1672.

Kuchlyan J, Banik D, Roy A, Kundu N, Sarkar N. **Excited-state proton transfer dynamics of fireflys chromophore d-luciferin in DMSO-water binary mixture.** *J. Phys. Chem. B* 2014, *118*, 13946–13953.

Kumar P, Kizhakkedathu JN, Straus SK. **Antimicrobial Peptides: Diversity, Mechanism of Action and Strategies to Improve the Activity and Biocompatibility In Vivo.** Biomolecules. 2018 Jan 19;8(1):4.

Laemmli UK. **Cleavage of structural proteins during the assembly of the head of bacteriophage T4.** Nature. 1970 Aug 15;227(5259):680-5.

Lee J, Lee DG. **Antimicrobial Peptides (AMPs) with Dual Mechanisms: Membrane Disruption and Apoptosis.** J Microbiol Biotechnol. 2015;25(6):759-764.

Lee TH, Hall KN, Aguilar MI. **Antimicrobial Peptide Structure and Mechanism of Action: A Focus on the Role of Membrane Structure.** Curr Top Med Chem. 2016;16(1):25-39.

Legrand D. **Overview of lactoferrin as a natural immune modulator.** J Pediatr 2016; 173(Suppl.): S10-5.

Li J, Kleintschek T, Rieder A, Cheng Y, Baumbach T, Obst U, Schwartz T, Levkin PA. **Hydrophobic liquid-infused porous polymer surfaces for antibacterial applications.** ACS Appl Mater Interfaces. 2013 Jul 24;5(14):6704-11.

Li S, Ruan Z, Zhang H, Xu H. **Recent achievements of bioluminescence imaging based on firefly luciferin-luciferase system.** *Eur. J. Med. Chem.* 2021, *211*, 113111.

Li Y, Rosal RV, Brandt-Rauf PW, Fine RL. **Correlation between hydrophobic properties and efficiency of carrier-mediated membrane transduction and apoptosis of a p53 C-terminal peptide.** *Biochem. Biophys. Res. Commun.* 2002, *298*, 439–449.

Litak PT, Kauffman JM. **Syntheses of reactive fluorescent stains derived from 5(2)-aryl-2(5)-(4-pyridyl)oxazoles and bifunctionally reactive linkers.** *J. Heterocycl. Chem.* 1994, *31*, 457–479.

Liu CY, Nossel HL, Kaplan KL. **The binding of thrombin by fibrin.** J Biol Chem. 1979 Oct 25;254(20):10421-5.

Lohner K. **Membrane-active antimicrobial peptides as template structures for novel antibiotic agents.** Curr. Top. Med. Chem. 2017;17(5):508–519.

Lönnerdal B. **Infant formula and infant nutrition: bioactive proteins of human milk and implications for composition of infant formulas.** Am J Clin Nutr. 2014 Mar;99(3):712S-7S.

Loving GS, Sainlos M, Imperiali B. **Monitoring protein interactions and dynamics with solvatochromic fluorophores**. *Trends Biotechnol.* 2010, *28*, 73–83.

Luz C, Calpe J, Saladino F, Luciano FB, Fernandez-Franzón M, Mañes J, Meca G. **Antimicrobial packaging based on ε-polylysine bioactive film for the control of mycotoxigenic fungi in vitro and in bread.** J Food Process Preserv. 2018 Jan;42(1):e13370.

Malmsten M. **Interactions of Antimicrobial Peptides with Bacterial Membranes and Membrane Components.** Curr Top Med Chem. 2016;16(1):16-24.

Mangoni ML, McDermott AM, Zasloff M, **Antimicrobial peptides and wound healing: biological and therapeutic considerations**, Exp. Dermatol. 25 (2016) 167–173.

Mansour SC, Pena OM, Hancock RE. **Host defense peptides: front-line immunomodulators.** Trends Immunol. 2014 Sep;35(9):443-50.

Maróti G, Kereszt A, Kondorosi E, Mergaert P. **Natural roles of antimicrobial peptides in microbes, plants and animals.** Res Microbiol. 2011;162(4):363-374.

Martin L, van Meegern A, Doemming S, Schuerholz T. **Antimicrobial Peptides in Human Sepsis.** Front Immunol. 2015 Aug 20;6:404.

Maurel P, Douzou P. **Catalytic implications of electrostatic potentials: The lytic activity of lysozyme as a model.** *J. Mol. Biol.* 1976, *102*, 253–264.

Mookherjee N, Anderson MA, Haagsman HP, Davidson DJ (2020) **Antimicrobial host defence peptides: functions and clinical potential.** Nat Rev Drug Discov 19:311–332.

Monsees T, Miska W, Geiger R. **Synthesis and characterization of a bioluminogenic substrate for alpha-chymotrypsin.** Anal Biochem. 1994 Sep;221(2):329-34.

Morton RA, Hopkins TA, Seliger HH. **Spectroscopic properties of firefly luciferin and related compounds; an approach to product emission.** *Biochemistry* 1969, *8*, 1598–1607.

Mueller LK, Baumruck AC, Zhdanova H, Tietze AA. **Challenges and Perspectives in Chemical Synthesis of Highly Hydrophobic Peptides.** Front Bioeng Biotechnol. 2020 Mar 4;8:162.

Munita JM, Arias CA. **Mechanisms of Antibiotic Resistance**. Microbiol Spectr. 2016 Apr;4(2):10.1128/microbiolspec.VMBF-0016-2015.

Niyonsaba F, Iwabuchi K, Someya A, Hirata M, Matsuda H, Ogawa H, Nagaoka I. **A cathelicidin family of human antibacterial peptide LL-37 induces mast cell chemotaxis.** Immunology. 2002;106(1):20-26.

Okuda K, Zendo T, Sugimoto S, Iwase T, Tajima A, Yamada S, Sonomoto K, Mizunoe Y. **Effects of bacteriocins on methicillin-resistant Staphylococcus aureus biofilm.** Antimicrob Agents Chemother. 2013 Nov;57(11):5572-9.

Oliva R, Del Vecchio P, Grimaldi A, Notomista E, Cafaro V, Pane K, Schuabb, V, Winter R, Petraccone L. **Membrane disintegration by the antimicrobial peptide (P)GKY20: Lipid segregation and domain formation.** *Phys. Chem. Chem. Phys.* 2019, *21*, 3989–3998.

Overhage J, Campisano A, Bains M, Torfs EC, Rehm BH, Hancock RE. **Human host defense peptide LL-37 prevents bacterial biofilm formation.** Infect Immun. 2008 Sep;76(9):4176-82.

Oyekale AS, Oyekale TO. **Healthcare waste management practices and safety indicators in Nigeria.** BMC Public Health. 2017;17(1):740. Published 2017 Sep 25.

Pachón-Ibáñez ME, Smani Y, Pachón J, Sánchez-Céspedes J. **Perspectives for clinical use of engineered human host defense antimicrobial peptides.** FEMS Microbiol Rev. 2017;41(3):323-342.

Påhlman LI, Mörgelin M, Kasetty G, Olin AI, Schmidtchen A, Herwald H. (2013).**Antimicrobial activity of fibrinogen and fibrinogen-derived peptides- a novel link between coagulation and innate immunity.** *Thrombosis and haemostasis,109 5*, 930-9.

Pane K, Cafaro V, Avitabile A, Torres MT, Vollaro A, De Gregorio E, Catania MR, Di Maro A, Bosso A, Gallo G, Zanfardino A, Varcamonti M, Pizzo E, Di Donato A, Lu TK, de la Fuente-Nunez C, Notomista E. **Identification of Novel Cryptic**

Multifunctional Antimicrobial Peptides from the Human Stomach Enabled by a Computational-Experimental Platform. ACS Synth Biol. 2018a Sep 21;7(9):2105-2115.

Pane K, Durante L, Crescenzi O, Cafaro V, Pizzo E, Varcamonti M, Zanfardino A, Izzo V, Di Donato A, Notomista E. **Antimicrobial Potency of Cationic Antimicrobial Peptides can be Predicted from their Amino Acid Composition: Application to the Detection of "Cryptic" Antimicrobial Peptides.** J Theor Biol. 2017 Apr 21;419:254-265.

Pane K, Durante L, Pizzo E, Varcamonti M, Zanfardino A, Sgambati V, Di Maro A, Carpentieri A, Izzo V, Di Donato A, Cafaro V, Notomista E. **Rational Design of a Carrier Protein for the Production of Recombinant Toxic Peptides in Escherichia coli.** PLoS One. 2016b Jan 25;11(1):e0146552.

Pane K, Sgambati V, Zanfardino A, Smaldone G, Cafaro V, Angrisano T, Pedone E, Di Gaetano S, Capasso D, Haney EF, Izzo V, Varcamonti M, Notomista E, Hancock RE, Di Donato A, Pizzo E. **A new cryptic cationic antimicrobial peptide from human apolipoprotein E with antibacterial activity and immunomodulatory effects on human cells.** FEBS J. 2016a Jun;283(11):2115-31.

Pane K, Verrillo M, Avitabile A, Pizzo E, Varcamonti M, Zanfardino A, Di Maro A, Rega C, Amoresano A, Izzo V, Di Donato A, Cafaro V, Notomista E. **Chemical Cleavage of an Asp-Cys Sequence Allows Efficient Production of Recombinant Peptides with an N-Terminal Cysteine Residue.** Bioconjug Chem. 2018b Apr 18;29(4):1373-1383.

Papareddy P, Rydengård V, Pasupuleti M, Walse B, Mörgelin M, Chalupka A, Malmsten M, Schmidtchen A. **Proteolysis of human thrombin generates novel host defense peptides.** PLoS Pathog. 2010 Apr 22;6(4):e1000857.

Pasupuleti M, Schmidtchen A, and Malmsten M (2012). **Antimicrobial peptides: key components of the innate immune system.** Crit. Rev. Biotechnol. 32, 143–171.

Perez RH, Ishibashi N, Inoue T, Himeno K, Masuda Y, Sawa N, Zendo T, Wilaipun P, Leelawatcharamas V, Nakayama J, Sonomoto K. **Functional Analysis of Genes Involved in the Biosynthesis of Enterocin NKR-5-3B, a Novel Circular Bacteriocin.** J Bacteriol. 2015;198(2):291-300. Published 2015 Oct 26.

Petrlova J, Hansen FC, van der Plas MJA, Huber RG, Mörgelin M, Malmsten M, Bond PJ, Schmidtchen A. **Aggregation of thrombin-derived C-terminal fragments as a previously undisclosed host defense mechanism.** Proc Natl Acad Sci U S A. 2017 May 23;114(21):E4213-E4222.

Pfalzgraff A, Brandenburg K, Weindl G. **Antimicrobial Peptides and Their Therapeutic Potential for Bacterial Skin Infections and Wounds.** Front Pharmacol. 2018 Mar 28;9:281.

Pierschbacher MD, Ruoslahti E. **Cell attachment activity of fibronectin can be duplicated by small synthetic fragments of the molecule.** *Nature* 1984, *309*, 30–33.

Pizzo E, Cafaro V, Di Donato A, Notomista E, **Cryptic Antimicrobial Peptides: Identification Methods and Current Knowledge of their Immunomodulatory Properties**, Curr Pharm Des. 2018;24(10):1054-1066.

Pletzer D, Mansour SC, Hancock REW. **Synergy between conventional antibiotics and anti-biofilm peptides in a murine, sub-cutaneous abscess model caused by recalcitrant ESKAPE pathogens.** PLoS Pathog. 2018 Jun 21;14(6):e1007084.

Presiado I, Erez Y, Huppert D. **Excited-state intermolecular proton transfer of the firefly's chromophore d-luciferin. 2. water-methanol mixtures.** *J. Phys. Chem. A* 2010, *114*, 9471–9479.

Ragland SA, Criss AK. **From bacterial killing to immune modulation: Recent insights into the functions of lysozyme.** PLoS Pathog. 2017 Sep 21;13(9):e1006512.

Rai M, Pandit R, Gaikwad S, Kövics G. (2016). **Antimicrobial peptides as natural bio-preservative to enhance the shelf-life of food.** J. Food Sci. Technol. 53, 3381–3394.

Reffuveille F, de la Fuente-Núñez C, Mansour S, Hancock RE. **A broad-spectrum antibiofilm peptide enhances antibiotic action against bacterial biofilms.** Antimicrob Agents Chemother. 2014 Sep;58(9):5363-71.

Ren H, Xiao F, Zhan K, Kim YP, Xie H, Xia Z, Rao J. **A biocompatible condensation reaction for the labeling of terminal cysteine residues on proteins.** *Angew. Chem. Int. Ed.* 2009, *48*, 9658–9662.

Ridyard KE, Overhage J. **The Potential of Human Peptide LL-37 as an Antimicrobial and Anti-Biofilm Agent.** Antibiotics (Basel). 2021 May 29;10(6):650.

Romanò CL, Scarponi S, Gallazzi E, Romanò D, Drago L. **Antibacterial coating of implants in orthopaedics and trauma: a classification proposal in an evolving panorama.** J Orthop Surg Res. 2015 Oct 1;10:157.

Rosenfeld Y, Shai Y. **Lipopolysaccharide (Endotoxin)-host defense antibacterial peptides interactions: Role in bacterial resistance and prevention of sepsis.** *Biochim. Biophys. Acta Biomembr.* 2006, *1758*, 1513–1522.

Rousseau F, Schymkowitz J, Serrano L. **Protein aggregation and amyloidosis: confusion of the kinds?** Curr Opin Struct Biol. 2006 Feb;16(1):118-26.

Ruoslahti E. **RGD and other recognition sequences for integrins.** *Annu. Rev. Cell Dev. Biol.* 1996, *12*, 697–715.

Santos CP, Sousa CS, Otoni G, Moraes RF, Souza GL, Medeiros AA, Espitia JP, Pires CS, Coimbra SR, Soares FF. **Nisin and other antimicrobial peptides: Production, mechanisms of action, and application in active food packaging.** *Innovative food science & emerging technologies* 48, (2018): 179-194.

Saravanan R, Holdbrook DA, Petrlova J, Singh S, Berglund NA, Choong YK, Kjellström S, Bond PJ, Malmsten M, Schmidtchen A. **Structural basis for endotoxin neutralisation and anti-inflammatory activity of thrombin-derived C-terminal peptides.** *Nat. Commun.* 2018, *9*, 1–14.

Savini F, Bobone S, Roversi D, Mangoni ML, Stella L. **From liposomes to cells: Filling the gap between physicochemical and microbiological studies of the activity and selectivity of host-defense peptides.** Peptide Sci. 2018;110(5):e24041.

Scheenstra MR, van Harten RM, Veldhuizen EJA, Haagsman HP, Coorens M. **Cathelicidins Modulate TLR-Activation and Inflammation.** Front Immunol. 2020 Jun 9;11:1137.

Scheenstra MR, van den Belt M, Tjeerdsma-van Bokhoven JLM, Schneider VAF, Ordonez SR, van Dijk A, Veldhuizen EJA, Haagsman HP. **Cathelicidins PMAP-36, LL-37 and CATH-2 are similar peptides with different modes of action.** Sci Rep. 2019 Mar 18;9(1):4780.

Schneider CA, Rasband WS, Eliceiri KW. (2012) **NIH Image to ImageJ: 25 years of image analysis.** Nat. Methods 9, 671−675.

Selivanova G, Iotsova V, Okan I, Fritsche M, Ström M, Groner B, Grafström RC, Wiman KG. **Restoration of the growth suppression function of mutant p53 by a synthetic peptide derived from the p53 C-terminal domain.** *Nat. Med.* 1997, *3*, 632–638.

Shabir U, Ali S, Magray AR, Ganai BA, Firdous P, Hassan T, Nazir R. **Fish antimicrobial peptides (AMP's) as essential and promising molecular therapeutic agents: A review.** Microb Pathog. 2018;114:50-56.

Shah P, Hsiao FS, Ho YH, Chen CS. **The proteome targets of intracellular targeting antimicrobial peptides.** Proteomics. 2016;16(8):1225-1237.

Shai Y. **Mode of action of membrane active antimicrobial peptides.** Biopolymers. 2002;66(4):236-248.

Shriram V, Khare T, Bhagwat R, Shukla R, Kumar V. **Inhibiting Bacterial Drug Efflux Pumps via Phyto-Therapeutics to Combat Threatening Antimicrobial Resistance.** Front Microbiol. 2018;9:2990. Published 2018 Dec 10.

Siepi M, Oliva R, Masino A, Gaglione R, Arciello A, Russo R, Di Maro A, Zanfardino A, Varcamonti M, Petraccone L, Del Vecchio P, Merola M, Pizzo E, Notomista E, Cafaro V. **Environment-Sensitive Fluorescent Labelling of Peptides by Luciferin Analogues.** International Journal of Molecular Sciences. 2021; 22(24):13312.

Sieprawska-Lupa M, Mydel P, Krawczyk K, Wojcik K, Puklo M, Lupa B, Suder P, Silberring J, Reed M, Pohl J, Shafer W, McAleese F, Foster T, Travis J, Potempa J, 2004. **Degradation of human antimicrobial peptide LL-37 by Staphylococcus aureus derived proteinases.** Antimicrob. Agents Chemother. 48, 4673–4679.

Singh S, Kalle M, Papareddy P, Schmidtchen A, Malmsten M. **Lipopolysaccharide interactions of C-terminal peptides from human thrombin.** Biomacromolecules. 2013 May 13;14(5):1482-92.

Sinha M, Kaushik S, Kaur P, Sharma S, Singh TP. **Antimicrobial lactoferrin peptides: the hidden players in the protective function of a multifunctional protein.** Int J Pept 2013; 2013: 390230.

Steck G, Leuthard P, Bürk RR. **Detection of basic proteins and low molecular weight peptides in polyacrylamide gels by formaldehyde fixation.** Anal Biochem. 1980 Sep 1;107(1):21-4.

Thapa RK, Diep DB, Tønnesen HH. **Topical antimicrobial peptide formulations for wound healing: Current developments and future prospects.** Acta Biomater. 2020 Feb;103:52-67.

The Lancet Infectious Diseases. **Antibiotic research priorities: ready, set, now go**. Lancet Infect Dis. 2017 Apr;17(4):349.

Tooke CL, Hinchliffe P, Bragginton EC, Colenso CK, Hirvonen VHA, Takebayashi Y, Spencer J. **β-Lactamases and β-Lactamase Inhibitors in the 21st Century.** J Mol Biol. 2019 Aug 23;431(18):3472-3500.

Torres MDT, Melo MCR, Crescenzi O, Notomista E, de la Fuente-Nunez C. **Mining for encrypted peptide antibiotics in the human proteome.** Nature Biomedical Engineering. 2021 Nov.

Tsai CW, Lin ZW, Chang WF, Chen YF, Hu WW. **Development of an indolicidin-derived peptide by reducing membrane perturbation to decrease cytotoxicity and maintain gene delivery ability.** Colloids Surf B Biointerfaces. 2018;165:18-27.

van der Plas MJ, Bhongir RK, Kjellström S, Siller H, Kasetty G, Mörgelin M, Schmidtchen A. **Pseudomonas aeruginosa elastase cleaves a C-terminal peptide from human thrombin that inhibits host inflammatory responses.** Nat Commun. 2016 May 16;7:11567.

Vergalli J, Bodrenko IV, Masi M, Moynié L, Acosta-Gutiérrez S, Naismith JH, Davin-Regli A, Ceccarelli M, van den Berg B, Winterhalter M, Pagès JM. **Porins and small-molecule translocation across the outer membrane of Gram-negative bacteria.** Nat Rev Microbiol. 2020 Mar;18(3):164-176.

Vieira J, Da Silva LP, Da Silva JCGE. **Advances in the knowledge of light emission by firefly luciferin and oxyluciferin.** *J. Photochem. Photobiol. B Biol.* 2012, *117*, 33–39.

Vila J, Soriano A, Mensa J. **Molecular basis of microbial adherence to prosthetic materials. Role of biofilms in prosthesis-associated infection.** Enferm Infecc Microbiol Clin. 2008 Jan;26(1):48-54; quiz 55. Spanish.

Wakabayashi H, Fay PJ. **Molecular orientation of Factor VIIIa on the phospholipid membrane surface determined by fluorescence resonance energy transfer.** *Biochem. J.* 2013, *452*, 293–301.

Wiegand I, Hilpert K, Hancock RE. **Agar and broth dilution methods to determine the minimal inhibitory concentration (MIC) of antimicrobial substances.** Nat Protoc. 2008; 3(2):163–75. Epub 2008/02/16.

Wiesner J, Vilcinskas A. **Antimicrobial peptides: The ancient arm of the human immune system.** *Virulence* 2010, *1*, 440–464.

Wilson DN, Hauryliuk V, Atkinson GC, O'Neill AJ. **Target protection as a key antibiotic resistance mechanism.** Nat Rev Microbiol. 2020;18(11):637-648.

Wimley WC. **Describing the mechanism of antimicrobial peptide action with the interfacial activity model.** ACS Chem Biol. 2010;5(10):905-917.

Wozniak RA, Waldor MK. **Integrative and conjugative elements: mosaic mobile genetic elements enabling dynamic lateral gene flow.** Nat Rev Microbiol. 2010;8(8):552-563.

Wu WK, Wong CC, Li ZJ, Zhang L, Ren SX, Cho CH. **Cathelicidins in inflammation and tissue repair: Potential therapeutic applications for gastrointestinal disorders.** 2010. Acta Pharmacol Sin. Sep;31(9):1118-22.

Yasir M, Willcox MDP, Dutta D. **Action of Antimicrobial Peptides against Bacterial Biofilms.** Materials (Basel). 2018 Dec 5;11(12):2468.

Yeaman MR, and Yount NY (2003). **Mechanisms of antimicrobial peptide action and resistance.** Pharmacol. Rev. 55, 27–55.

Yu G, Baeder DY, Regoes RR, Rolff J. **Combination Effects of Antimicrobial Peptides.** Antimicrob Agents Chemother. 2016 Jan 4;60(3):1717-24.

Yu L, Tan M, Ho B, Ding JL, Wohland T. **Determination of critical micelle concentrations and aggregation numbers by fluorescence correlation spectroscopy: Aggregation of a lipopolysaccharide.** Anal. Chim. Acta 2006, 556, 216–225.

Yu Z, Tang J, Khare T, Kumar V. (2020). **The Alarming Antimicrobial Resistance in ESKAPEE Pathogens: Can Essential Oils Come to the rescue?.** Fitoterapia 140, 104433.

Zanfardino A, Pizzo E, Di Maro A, Varcamonti M, D'Alessio G. **The bactericidal action on Escherichia coli of ZF-RNase-3 is triggered by the suicidal action of the bacterium OmpT protease.** FEBS J. 2010 Apr;277(8):1921-8.

Zasloff M. **Antimicrobial peptides of multicellular organisms.** Nature. 2002;415(6870):389-395.

Zeitler B, Herrera Diaz A, Dangel A, Thellmann M, Meyer H, Sattler M, Lindermayr C. **De-novo design of antimicrobial peptides for plant protection.** PLoS One. 2013 Aug 12;8(8):e71687.

Zhang G, Sunkara LT. **Avian antimicrobial host defense peptides: from biology to therapeutic applications.** Pharmaceuticals (Basel). 2014;7(3):220-247. Published 2014 Feb 27.

Zhang M, Wei W, Sun Y, Jiang X, Ying X, Tao R, Ni L. **Pleurocidin congeners demonstrate activity against Streptococcus and low toxicity on gingival fibroblasts.** Arch Oral Biol. 2016 Oct;70:79-87.

Zharkova MS, Orlov DS, Golubeva OY, Chakchir OB, Eliseev IE, Grinchuk TM, Shamova OV. **Application of Antimicrobial Peptides of the Innate Immune System in Combination With Conventional Antibiotics-A Novel Way to Combat Antibiotic Resistance?** Front Cell Infect Microbiol. 2019 Apr 30;9:128.

Zhu C, Tan H, Cheng T, Shen H, Shao J, Guo Y, Shi S, Zhang X. **Human β-defensin 3 inhibits antibiotic-resistant Staphylococcus biofilm formation.** J Surg Res. 2013 Jul;183(1):204-13.

APPENDICES

List of publications

1. Siepi M, Oliva R, Masino A, Gaglione R, Arciello A, Russo R, Di Maro A, Zanfardino A, Varcamonti M, Petraccone L, Del Vecchio P, Merola M, Pizzo E, Notomista E, Cafaro V. **Environment-Sensitive Fluorescent Labelling of Peptides by Luciferin Analogues.** International Journal of Molecular Sciences. 2021; 22(24):13312.

List of communications

1. Masino A, Cafaro V, Gaglione R, Arciello A, Pizzo E, Notomista E.
   Production and biological characterization of human fibrinogen derived peptides. (32nd "A. Castellani" Meeting of PhD students in biochemical sciences (September 13-16, 2021).

2. Cafaro V, Siepi M, Masino A, Bracale A, Bosso A, Arciello A, Bragonzi A, Merola M, Pizzo E, Notomista E.
   In vitro and in vivo efficacy of an antimicrobial and antibiofilm designed peptidomimetic against CF lung pathogens. 17th CONVENTION OF FFC INVESTIGATORS IN CYSTIC FIBROSIS (FFC#18/2018) (november 14-16, 2019).

3. Masino A, Cafaro V, Siepi M, Oliva R, Gaglione R, Arciello A, Zanfardino A, Petraccone L, Del Vecchio P, Di Donato A, Pizzo E, Notomista E.
   Luciferin and aminoluciferin as environment sensitive fluorescent labels for recombinant and synthetic peptides. 9th International Meeting on Antimicrobial Peptides. Utrecht University (The Netherlands), August 28 - 30, 2019.

4. Cafaro V, Siepi M, Masino A, Bracale A, Bosso A, Arciello A, Bragonzi A, Merola M, Pizzo E, Notomista E.

In vitro and in vivo efficacy of an antimicrobial and antibiofilm designed peptidomimetic against CF lung pathogens. 16th CONVENTION OF FFC INVESTIGATORS IN CYSTIC FIBROSIS (FFC#18/2018) (december 10-12, 2018).

Published papers

International Journal of
Molecular Sciences

MDPI

Article

Environment-Sensitive Fluorescent Labelling of Peptides by Luciferin Analogues

Marialuisa Siepi [1,†], Rosario Oliva [2,†], Antonio Masino [1,†], Rosa Gaglione [2], Angela Arciello [2], Rosita Russo [3], Antimo Di Maro [3], Anna Zanfardino [1], Mario Varcamonti [1], Luigi Petraccone [2], Pompea Del Vecchio [2], Marcello Merola [1], Elio Pizzo [1], Eugenio Notomista [1,*,‡] and Valeria Cafaro [1,‡]

[1] Department of Biology, University of Naples Federico II, 80126 Naples, Italy; marialuisa.siepi@unina.it (M.S.); antonio.masino@unina.it (A.M.); anna.zanfardino@unina.it (A.Z.); varcamon@unina.it (M.V.); m.merola@unina.it (M.M.); elipizzo@unina.it (E.P.); vcafaro@unina.it (V.C.)
[2] Department of Chemical Sciences, University of Naples Federico II, 80126 Naples, Italy; rosario.oliva2@unina.it (R.O.); rosa.gaglione@unina.it (R.G.); anarciel@unina.it (A.A.); luigi.petraccone@unina.it (L.P.); pompea.delvecchio@unina.it (P.D.V.)
[3] Department of Environmental, Biological and Pharmaceutical Sciences and Technologies, University of Campania "Luigi Vanvitelli", 81100 Caserta, Italy; rosita.russo@unicampania.it (R.R.); antimo.dimaro@unicampania.it (A.D.M.)
* Correspondence: notomist@unina.it
† Equally contributing authors.
‡ Also these authors contributed equally.

check for updates

Citation: Siepi, M.; Oliva, R.; Masino, A.; Gaglione, R.; Arciello, A.; Russo, R.; Di Maro, A.; Zanfardino, A.; Varcamonti, M.; Petraccone, L.; et al. Environment-Sensitive Fluorescent Labelling of Peptides by Luciferin Analogues. *Int. J. Mol. Sci.* **2021**, *22*, 13312. https://doi.org/10.3390/ijms222413312

Academic Editor: Herbert Schneckenburger

Received: 12 November 2021
Accepted: 7 December 2021
Published: 10 December 2021

Publisher's Note: MDPI stays neutral with regard to jurisdictional claims in published maps and institutional affiliations.

Abstract: Environment-sensitive fluorophores are very valuable tools in the study of molecular and cellular processes. When used to label proteins and peptides, they allow for the monitoring of even small variations in the local microenvironment, thus acting as reporters of conformational variations and binding events. Luciferin and aminoluciferin, well known substrates of firefly luciferase, are environment-sensitive fluorophores with unusual and still-unexploited properties. Both fluorophores show strong solvatochromism. Moreover, luciferin fluorescence is influenced by pH and water abundance. These features allow to detect local variations of pH, solvent polarity and local water concentration, even when they occur simultaneously, by analyzing excitation and emission spectra. Here, we describe the characterization of (amino)luciferin-labeled derivatives of four bioactive peptides: the antimicrobial peptides GKY20 and ApoB$_L$, the antitumor peptide p53pAnt and the integrin-binding peptide RGD. The two probes allowed for the study of the interaction of the peptides with model membranes, SDS micelles, lipopolysaccharide micelles and *Escherichia coli* cells. K_d values and binding stoichiometries for lipopolysaccharide were also determined. Aminoluciferin also proved to be very well-suited to confocal laser scanning microscopy. Overall, the characterization of the labeled peptides demonstrates that luciferin and aminoluciferin are previously neglected environment-sensitive labels with widespread potential applications in the study of proteins and peptides.

Keywords: fluorescent peptide; environment-sensitive fluorophore; peptide labeling; luciferin; membrane-binding peptide; antimicrobial peptide; antitumor peptide; RGD peptide

1. Introduction

Environment-sensitive fluorophores are fluorophores, the excitation spectra, emission spectra and/or quantum yields (QY) of which depend on variables such as pH, solvent polarity, viscosity and even molecular crowding/aggregation state. Several different molecular mechanisms can contribute to modulation of the fluorescence of environment-sensitive fluorophores [1]. Solvatochromic fluorophores, the λ_{max} of which changes with solvent polarity, are often push-pull molecules with an electron-donating and an electron-withdrawing group bound to an aromatic moiety. Solvent polarity strongly affects the intramolecular charge transfer of these molecules, thus modulating their fluorescence [1]. In a less common type of solvatochromic fluorophores, an excited-state intramolecular

proton-transfer event generates tautomeric forms with different absorption and emission spectra [1]. In other cases, conformational changes or variations in the aggregation state strongly influence the fluorescence of the probe [1]. Finally, pH probes have two or more ionizations states with different fluorescence properties [2]. Often, only one of the pH-dependent species is fluorescent.

These fluorophores are very valuable tools in the study of a wide variety of molecular and cellular processes [1,2]. As protein and peptide labels, they find applications in the study of conformational variations of proteins, of protein/protein, protein/ligand and protein/membrane interactions but also in the design of biosensors [1,3,4]. For these reasons, the search for new environment-sensitive fluorescent probes and, in particular, for protein and peptide labels, is a very active research field.

Firefly luciferin (Luc), the substrate of firefly luciferase, is the most popular bioluminescent compound [5]. It is less known that Luc is also an environment-sensitive fluorophore with unusual properties, summarized in Figure 1. Even if Luc is typical push-pull molecule, the hydroxyl group at position 6 of the benzothiazole moiety behaves as a weak acid with a $pK_a \approx 8.7$ (Figure 1A) [6]. Both the phenol and the phenolate forms are strongly fluorescent but with very different excitation and emission wavelengths (Figure 1B) [7]. However, as Luc is a "photoacid" [7–9], it undergoes a light-induced dissociation with a $pK_a < 1$ (Figure 1B). Thus, in the presence of water or other proton acceptors, Luc fluorescence is exclusively the result of the magenta and green pathways shown in Figure 1B. Even in neutral and acidic aqueous media, only the emission of the phenolate at 530 nm is generally observed, regardless of the excitation wavelength. Only in anhydrous organic solvents, e.g., acetonitrile or DMSO, does Luc show the blue fluorescence emitted by the phenol form (blue pathway in Figure 1B) [8,9]. However, very low amounts of water cause the appearance of the green emission. For example, in acetonitrile containing 14% water, the intensity of the blue and green emissions is comparable [8].

Two synthetic Luc analogues (Figure 1B), methoxyluciferin (mLuc) and aminoluciferin (aLuc), bearing non-dissociable groups at position 6 of the benzothiazole moiety show a single emission peak, with emission maxima similar to those of Luc phenol and phenolate forms, respectively [10,11]. mLuc is a very weak fluorophore [10], whereas aLuc is brighter than Luc itself; very interestingly, it is a strongly solvatochromic fluorophore with shifts up to 40 nm in the λ_{max} values [11].

In spite of these intriguing features, there are very few reports of probes exploiting (amino)luciferin fluorescence to detect cell thiols [12–14] or Furin activity [15]. To our knowledge, no example of direct fluorescent labeling of proteins or peptides based on Luc exists. This is even more surprising, considering that a Luc moiety can be incorporated very easily at the N-terminus of proteins and peptides. The final step of biological synthesis of Luc is a spontaneous condensation between D-cysteine and 6-hydroxy-2-cyanobenzothiazole (Figure 1C). This reaction is included among the so-called "click reactions" that are quantitative, irreversible and very fast in physiological conditions (phosphate buffer, pH 7–7.4, 25–37 °C) [16,17].

L-cysteine at the N-terminus of a peptide reacts with 2-cyanobenzothiazole (CBT) similarly to free cysteine, as the carboxyl group is not involved in the reaction (Figure 1C). Moreover, the nature of the substituent at position 6 of CBT also has a limited impact on the reaction. Therefore, peptides with an N-terminal cysteine residue are efficiently labeled trough a Luc-like spacer by using 6-substituted 2-cyanobenzothiazoles carrying any desired molecule (e.g., biotin, metal chelates, fluorophores, etc.) conjugated at position 6 (Figure 1C) [16,17]. In these bioconjugates, the label is usually attached through acylation of the amino group of aLuc or, less commonly, through alkylation of the hydroxyl group of Luc (Figure 1C), thus strongly reducing the fluorescence of (amino)luciferin [10,14,18]. Very interestingly, even if CBT reacts quantitatively and irreversibly with N-terminal cysteines, it generally forms a reversible adduct with the thiol group of internal cysteine residues, which can be removed by adding free cysteine or other

aminothiols [16,17]. Therefore, an N-terminal cysteine can also be selectively labeled in the presence of cysteine residues at other positions on the peptide.

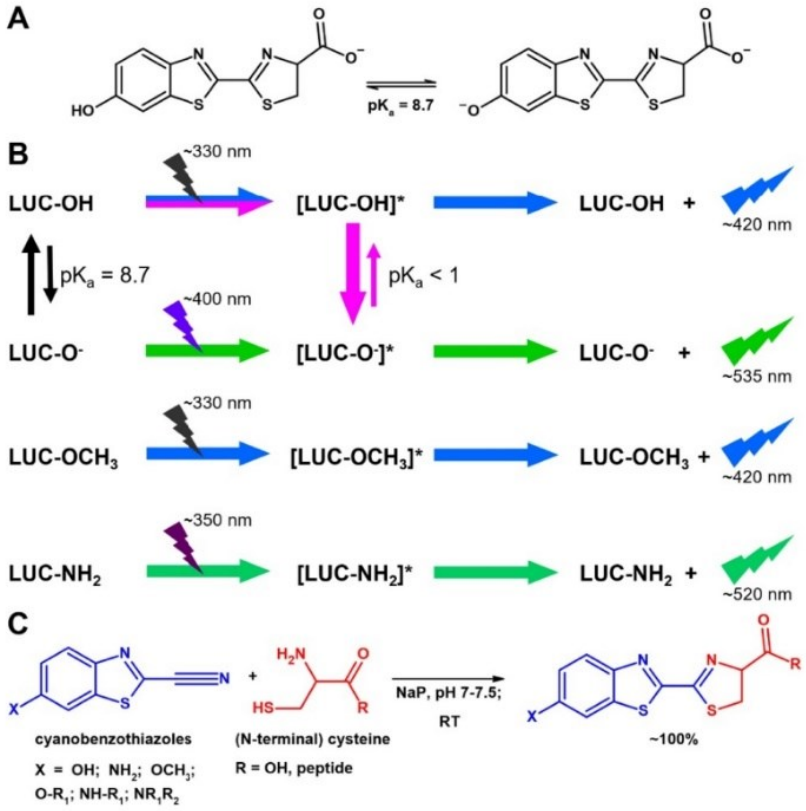

Figure 1. Structure, fluorescence and synthesis of luciferin and its analogues. (**A**) Structure of luciferin in phenol and phenolate forms. (**B**) Fluorescence of luciferin (Luc-OH), luciferin phenolate (Luc-O$^-$), methoxyluciferin (Luc-OCH3) and aminoluciferin (Luc-NH2). Excited states are indicated by an asterisk. (**C**) Condensation reaction between 6-substituted 2-cyanobenzothiazoles and cysteine (free or as N-terminal residue of a peptide). R_1 and R_2 can be a wide variety of alkyl and acyl groups. The nature of R_1 and R_2 has little or no impact on the reaction but can strongly influence fluorescence.

In order to study the possible exploitation of (amino)luciferin as an environment-sensitive fluorescent label for peptides, we synthesized (amino)luciferin conjugates of four peptides of different lengths, compositions and biological properties. Characterization of the fluorescence properties of the labeled peptides demonstrates that Luc and its analogues are previously neglected bright and photostable fluorescent labels suited for in vitro studies like peptide/membrane or peptide/cell interactions and microscopy/imaging studies.

2. Results

2.1. Preparation and Labeling of the Peptides

To evaluate the suitability of Luc and aLuc as environment-sensitive fluorescent labels, we selected four previously described bioactive peptides: GKY20 (20 residues), ApoB$_L$ (37 residues), p53pAnt (37 residues) and RGD (6 residues) (Figure S1, Supplementary Materials). GKY20 [19] and ApoB$_L$ [20] are cryptic cationic antimicrobial peptides (CAMP), peptides unusually rich in cationic and hydrophobic residues, which kill bacteria by dam-

aging structural integrity and functions of bacterial membranes [21–23]. Moreover, CAMPs often show additional pharmacologically relevant biological activities, like antifungal, antitumor and anti-inflammatory activity [23,24]. p53pAnt (also spelled p53p-Ant) is a designed antitumor peptide containing a sequence at the N-terminus that induces apoptosis by interacting with p53, as well as a "cell-penetrating peptide" (CPP) at the C-terminus that derived from the Antennapedia protein homeodomain, which can drive peptides inside eukaryotic cells both by directly crossing the cytoplasmic membrane and by mediating endocytosis [25–27]. RGD is a natural ligand of integrins, cell surface proteins involved in adhesion to the extracellular matrix [28,29]. It is very different from the other three peptides; it is very short, hydrophilic and uncharged. RGD interaction with eukaryotic cell membranes depends on binding to a protein receptor rather than on a direct interaction with membrane lipids, as in the case of CAMPs and CPPs. Immobilized RGD-like peptides are frequently used to promote the adhesion of eukaryotic cells to surfaces, polymers, hydrogels, etc. Moreover, they may find applications in diagnostic and imaging fields [30,31]. Peptides GKY20, $ApoB_L$ and p53pAnt with an additional cysteine residue at the N-terminus—herein named (C)GKY20, (C)$ApoB_L$ and (C)p53pAnt—were prepared using a recently described strategy for the preparation of recombinant toxic peptides in *E. coli* based on the selective cleavage of a carrier/peptide fusion bearing the acid sensitive sequence Asp-Cys [32] (details in Supplementary Materials, Sections S2–S4). Peptide RGD with an additional cysteine residue at the N-terminus—(C)RGD—was obtained by chemical synthesis. The four peptides were labeled with either a Luc or an aLuc moiety at the N-terminus by incubation with a slight molar excess of 6-hydroxy-2-cyanobenzothiazole or 6-amino-2-cyanobenzothiazole, respectively, in aqueous buffer at pH 7.4 at 25 °C (Supplementary Materials, Section S5). As expected, based on the well-known high efficiency of this reaction, Luc-labeled peptides (Luc-GKY20, Luc-$ApoB_L$, Luc-p53pAnt and Luc-RGD) and aLuc-labeled peptides (aLuc-GKY20, aLuc-$ApoB_L$, aLuc-p53pAnt and aLuc-RGD) were obtained with yields close to 100% after very short incubation times (30–60 min). (C)GKY20 was also treated with 6-methoxy-2-cyanobenzothiazole to obtain an mLuc-labeled peptide (mLuc-GKY20) and with PyMPO maleimide, the thiol-reactive version of PyMPO, a widely used photostable solvatochromic fluorophore [33–35], to obtain the peptide PyMPO-(C)GKY20. After purification (Section 4 and Supplementary Materials), the mass of all labeled peptides was confirmed by MALDI-MS (Table S1). SDS-PAGE analysis of labeled GKY20, $ApoB_L$ and p53pAnt shows their bright fluorescence under UV light (365 nm) and their solvatochromic nature appreciable even by the naked eye (Figure S2).

2.2. Stability and Biological Activity of Luc-Labeled Peptides

When choosing the best fluorophore to label a peptide, in addition to excitation and emission wavelengths, other relevant parameters are (photo)stability and molecular features, which might influence the biological activity of the peptide to be labeled (molecular weight, charge, hydrophobicity, etc.).

Although Luc is a fairly stable molecule, in order to evaluate the photostability of Luc-labeled peptides, we monitored the fluorescence of Luc-GKY20, aLuc-GKY20 and mLuc-GKY20 for 60 min, constantly exciting the three labeled peptides at their respective maximum absorption. As comparative control, we used the very photostable fluorophore PyMPO [33] by treating PyMPO-(C)GKY20 in the same conditions. Luc-GKY20 lost only 30% of its initial fluorescence (Figure S3), thus proving to be even more photostable than PyMPO-(C)GKY20, which lost 43% of its initial fluorescence. aLuc-GKY20 and mLuc-GKY20 proved to be slightly less photostable than Luc-GKY20, with a loss of initial fluorescence of about 55% and 60%, respectively. Therefore, Luc can be considered a very stable label, though aLuc is also a suitable tool.

An ideal fluorescent label or probe should not significantly change the properties (size, hydrophobicity, charge, etc.) of the peptide to be labeled in order to minimize the risk of altering its chemical-physical behavior and/or biological activity. Therefore, we compared molecular weight, accessible surface area (ASA), polar ASA, ratio of polar ASA/ASA and number of charged groups (Table S2) of Luc, aLuc and a wide panel of commonly used solvatochromic and non-solvatochromic fluorescent labels that can be attached either at the N-terminus of a peptide (generally through an amide or a sulfonamide bond) or at the side-chain sulfur of a cysteine residue (generally through a thioether bond). Only NBD and some coumarin dyes among fluorescent labels that can be attached at the N-terminus and only bimane among fluorescent labels that can be attached to the side chain of a cysteine residue have an ASA smaller than that of Luc and aLuc. Moreover, several solvatochromic and not-solvatochromic fluorophores are either quite hydrophobic (e.g., pyrene-1-butirrate, Atto 495, most BODIPY labels, BADAN etc.) or very hydrophilic and with several charged groups (e.g., Alexa Fluor™ 405 and Alexa Fluor 488-C5-maleimide), whereas Luc and aLuc have an intermediate ratio of polar ASA/ASA (0.31–0.34) and no (aLuc) or low charge (Luc at neutral pH). Therefore, Luc and aLuc can be confidently considered fluorescent labels with a low impact on the molecular properties of the labeled peptide.

In order to determine the influence of Luc labels on the biological activity of the peptides considered in this study, we compared the antimicrobial activity of labeled GKY20 and $ApoB_L$ with that of the corresponding unlabeled recombinant peptides, (P)GKY20 [36] and (P)$ApoB_L$ [20] (Supplementary Materials, Section S6). The cytotoxic activity of labeled and unlabeled p53pAnt was also investigated (Supplementary Materials, Section S7). The minimum inhibitory concentrations (MIC) of Luc-GKY20 and aLuc-GKY20 were found to be identical to those measured for (P)GKY20 on Gram-negative and Gram-positive strains (Table S3). The MIC values of Luc-$ApoB_L$ and aLuc-$ApoB_L$ were found to be very similar to those measured for (P)$ApoB_L$ (the observed differences, not higher than one dilution, are generally considered not significant in the microdilution assay).

Luc-p53pAnt and (C)p53pAnt showed similar toxicity when assayed on two human cell lines, namely HaCaT noncancerous immortalized keratinocytes and HeLa cervical cancer cells (Figure S4). It is worth noting that labeled and unlabeled p53pAnt showed significantly higher toxicity for HeLa cancer cells than for HaCaT cell, as expected of an anticancer peptide.

Finally, we tested the effect Luc-RGD and unlabeled RGD on HaCaT and HeLa cells. As expected, we did not observe any significant toxic effect.

2.3. Response of the Labeled Peptides to Solvent Polarity Changes

Most solvatochromic fluorophores show an increase in fluorescence emission and a blue shift of the λ_{max} as solvent polarity decreases. Therefore, we measured emission spectra and QY of the labeled peptides in sodium phosphate 10 mM, pH 7.4 (NaP) and in the same buffer containing 50% (*v*:*v*) either isopropanol or methanol.

The emission spectra in NaP of the Luc- and aLuc-labeled peptides showed maximum emission at 539 and 526 nm, respectively (Figure S5 and Table 1). As expected, all the labeled peptides showed a blue shift of the λ_{max} in the presence of the organic solvents (Table 1). The blue shift was less in the case of Luc-labeled peptides (6–7 nm) and greater in the case of aLuc-labeled peptides (9–15 nm). Furthermore, aLuc-labeled peptides showed a considerably greater blue shift in isopropanol than in methanol, thus confirming that aLuc is a probe more sensitive to solvent polarity compared to Luc. mLuc-GKY20 showed blue-shift values very similar to those of aLuc-GKY20, whereas PyMPO-(C)GKY20 showed a 5 nm blue shift only in the presence of isopropanol.

Intriguingly, emission intensities (Figure S5) and QY values (Table 2) showed complex and partially unexpected variation characteristic of each peptide. For example, all the variants of GKY20 showed very large increases in emission intensities and QY values in the presence of the organic solvent (2.5–6 times higher in 50% isopropanol than in water). On the contrary, Luc-p53pAnt and aLuc-p53pAnt showed a 30–35% reduction in QY. Both

labeled variants of $ApoB_L$ and RGD showed little or no variation in emission intensities (Figure S5) and QY (Table 2). These puzzling variations are likely the result of a very well-known phenomenon, i.e., the quenching of fluorophores bound to protein/peptides. Even if several mechanisms can contribute to quenching, the most common is photoinduced electron transfer (PET), a reversible light-triggered transfer of electrons from amino-acid residues to the fluorophore [37]. The most efficient donors are tryptophan and tyrosine, although to a lesser extent, histidine and methionine can also contribute significantly to quenching [38]. Obviously, the redox potential of a fluorophore and therefore its propensity to accept electrons, influences its sensitivity to quenching [37].

Table 1. λ_{max} and blue-shift values of the labeled peptides.

Peptide	λ_{max} (nm) [a]							
	NaP pH 7.4	MeOH 50%	IPA 50%	SDS (25 mM)	POPC +POPG	POPC	LPS (200 μg/mL)	*E. coli* Cells
Luc-GKY20	538	533 (5)	531 (7)	526 (12)	520 (19)	520 (19)	516 (23)	522 (16)
Luc-$ApoB_L$	539	533 (6)	533 (6)	526 (13)	522 (17)	539 (0)	508 (31)	534 (5)
Luc-p53pAnt	539	533 (6)	533 (6)	526 (13)	522 (17)	539 (0)	nd [b]	nd
Luc-RGD	539	533 (6)	533 (6)	533 (6)	539 (0)	539 (0)	nd	nd
aLuc-GKY20	525	515 (10)	510 (15)	506 (19)	499 (26)	499 (26)	503 (22)	509 (16)
aLuc-$ApoB_L$	527	516 (11)	512 (15)	505 (22)	497 (27)	527 (0)	486 (41)	518 (9)
aLuc-p53pAnt	526	516 (10)	515 (11)	504 (22)	499 (25)	526 (0)	nd	nd
aLuc-RGD	526	517 (9)	513 (13)	510 (16)	526 (0)	526 (0)	nd	nd
mLuc-GKY20	439	429 (10)	424 (15)	422 (17)	nd	nd	nd	nd
PyMPO-(C)GKY20	563	563 (0)	558 (5)	556 (7)	535 (28)	541 (22)	nd	nd

[a] Blue-shift values with respect to the λ_{max} in NaP are shown in parenthesis. [b] nd = not determined.

Table 2. Relative quantum yield of the labeled peptides.

Peptide	QY [a] (Variation Relative to NaP pH 7.4)		
	NaP pH 7.4	IPA 50% [b]	NaAc [c] pH 5.0
PyMPO-GKY20	0.080	0.373 (4.66)	nd[d]
mLuc-GKY20	0.008	0.021 (2.63)	nd
Luc-GKY20	0.111	0.639 (5.76)	0.269 (2.42)
aLuc-GKY20	0.202	0.969 (4.80)	nd
Luc-$ApoB_L$	0.365	0.389 (1.07)	0.450 (1.23)
aLuc-$ApoB_L$	0.574	0.757 (1.32)	nd
Luc-p53pAnt	0.261	0.184 (0.70)	0.418 (1.60)
aLuc-p53pAnt	0.432	0.274 (0.63)	nd
Luc-RGD	0.519	0.443 (0.85)	0.510 (0.98)
aLuc-RGD	0.937	1.040 (1.11)	nd

[a] Errors $\leq$ 5% of the reported values. [b] Isopropanol:NaP pH 7.4 (1:1, *v*/*v*). [c] Sodium acetate 20 mM. [d] nd = not determined.

PET is also very sensitive to distance and orientation of the donor/acceptor couple, so the quenching efficiency can be influenced even by minor variations in the conformation of the labeled protein/peptide. In fact, PET-mediated quenching is a powerful tool for detection of conformational variations in proteins and peptides [37].

Very interestingly, the peptides that show the largest variations, namely GKY20 and p53pAnt, contain several residues with strong quenching ability (tryptophan, histidine and two tyrosines in GKY20; two tryptophans, three histidines and a methionine in p53pAnt; Figure S1).

The QY values of the Luc-labeled peptides were also measured in sodium acetate at pH 5.0 to induce the protonation of the histidine residues. Protonation of histidine residue can influence PET quenching both directly, by reducing the donor ability of the imidazole

ring, and indirectly, by inducing conformational changes. As expected, significant increases in QY values were observed only for the three peptides containing histidine residues: GKY20, p53pAnt and $ApoB_L$ (Table 2). To date, it has not been possible to determine the relative contribution of the direct and indirect effect of histidine protonation on quenching.

2.4. Response of Luc-Labeled Peptides to pH

Luc has a phenolic hydroxyl, which behaves as a weak acid, with a pK_a of about 8.7 [6]. As Luc and its phenolate have quite different excitation spectra, with maxima at 330 and 395 nm, respectively, the excitation spectra of the Luc-labeled peptides recorded at pH 7.4 show a characteristic shoulder at 390–400 nm originating from the small amount of phenolate ion present at this pH (Figure S6). It should be noted that the shoulder is also visible in the presence of organic solvents (Figure S5). On the other hand, the shoulder disappears in buffers with pH values below 6, as Luc becomes protonated, whereas the peak at 400 nm prevails at pH values greater than 8.5 (Figure S6). By recording the emission at 539 nm of the Luc-labeled peptides after excitation at 400 nm in buffers with different pH values, we determined the actual pK_a values of the Luc moieties (Table 3). All pK_a values were found to be slightly lower than those of free Luc, with small differences among the peptides, likely due to differences in the net charge and distribution of positively charged residues. In particular, the highest pK_a value was found for Luc-RGD, the only peptide with a negative net charge at pH values close to the pK_a of the Luc moiety (Table 3). The remaining three peptides have a high positive net charge, which could stabilize the phenolate anion, thus lowering the pK_a value. The possibility of selectively exciting the phenolic or phenolate form of Luc not only makes Luc a useful pH probe for the pH range of 7–8 but also allows for monitoring of the formation of peptide/ligand complexes in which the ionization of the Luc moiety is suppressed or altered. The next sections show some applications of this peculiar feature of Luc.

Table 3. pK_a values of the phenolic group in Luc and Luc-labeled peptides.

Peptide	Net Charge of the Peptidyl Moiety [a]	pK_a
Free Luc	not applicable	8.70 [b]
Luc-RGD	−1	8.40 ± 0.03
Luc-GKY20	+4	8.13 ± 0.04
Luc-$ApoB_L$	+6	8.11 ± 0.04
Luc-p53pAnt	+11	7.97 ± 0.03

[a] Theoretical net charge at pH 7.5–9.0 calculated attributing a charge = +1 to each lysine/arginine residue and a charge = −1 to each aspartate/glutamate residue and to the free C-terminus. [b] From reference [6].

2.5. Interaction of Labeled Peptides with Liposomes

Both CAMPs and CPPs are able to interact with biological membranes, and this interaction is essential to their properties. Therefore, in order to verify whether Luc-labeling can be used to investigate peptide/membrane interaction, we studied the behavior of the labeled peptides in the presence of liposomes composed either of pure palmitoyl-oleoyl-phosphatidylcholine (POPC) or of a mixture of POPC and palmitoyl-oleoyl-phosphatidylglycerol (POPG) at a molar ratio of 4:1. As the POPC head group is zwitterionic, liposomes composed only of this lipid are neutral and are usually considered mimetic of eukaryotic cell membranes. On the contrary, POPG-containing liposomes are negatively charged and are considered a simplified model of bacterial cell membranes.

The short, hydrophilic and negatively charged labeled RGD was used as a negative control. As expected, the excitation and emission spectra of Luc-RGD were essentially identical in NaP and in the presence of the two types of liposomes (Figure 2).

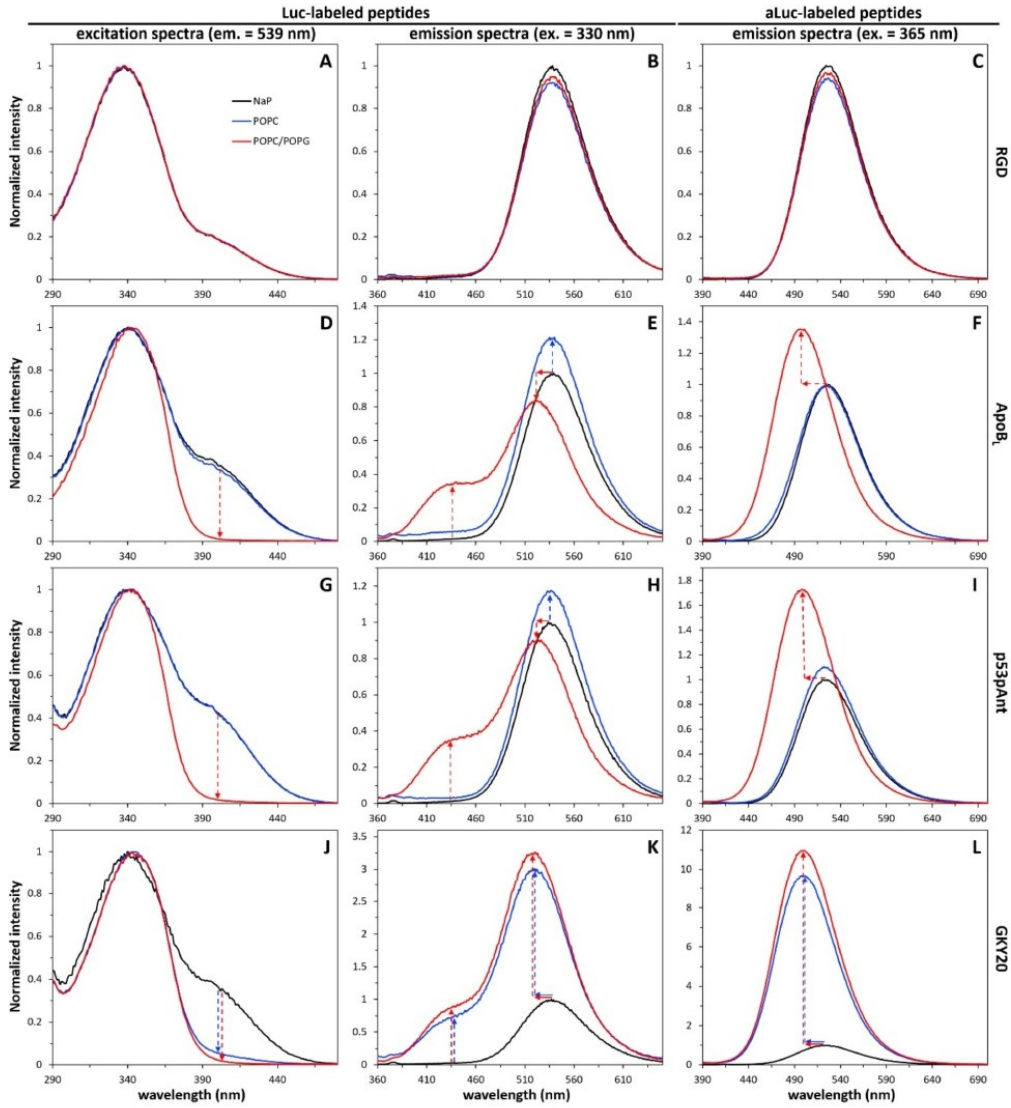

Figure 2. Fluorescence of labeled peptides in the presence of liposomes of POPC or POPC/POPG (5:1). Excitation spectra of luciferin (left), emission spectra of luciferin (center) and emission spectra of aminoluciferin (right) were recorded for peptides RGD (**A–C**), ApoB$_L$ (**D–F**), p53pAnt (**G–I**) and GKY20 (**J–L**). Spectra recorded in the presence of liposomes were normalized to the corresponding spectra in NaP. Arrows highlight the main changes with respect to NaP.

The same result was obtained in the case of the emission spectrum of aLuc-RGD (Figure 2). On the contrary, in the case of Luc-ApoB$_L$, the excitation spectrum in the presence of POPC/POPG liposomes was clearly different from the spectra in NaP and in the presence of POPC liposomes, completely lacking a shoulder at 400 nm (Figure 2). This suggests that in the presence of POPC/POPG liposomes, the deprotonation of the Luc phenolic group is inhibited. Two mechanisms could explain this finding: (i) embedding of the phenolic group of Luc among the lipids would directly prevent deprotonation; or (ii) binding of the Luc probe to the surface of the negatively charged POPC/POPG liposomes could

prevent deprotonation as a consequence of the more acidic local environment. In fact, it is well-known that polyanionic surfaces and polymers determine the formation of acidic local environments by attracting protons from the bulk solution [39,40]. Further information was obtained from analysis of the emission spectra. Once more, the emission spectrum in the presence of POPC/POPG liposomes was very different from the other two spectra, showing the presence of a large shoulder at 425–430 nm (Figure 2). As mentioned above, this blue emission is characteristic of the phenolic form of Luc and can only be observed when Luc is in an environment with very low water content, a condition able to suppress the photoinduced dissociation. Therefore, the presence of a blue shoulder in the emission spectrum of Luc-ApoB$_L$ is a clear indication that the Luc moiety is deeply embedded into the POPC/POPG bilayer. This is further confirmed by the 16–18 nm blue shift (from 539 to about 522 nm) of the peak in the green region (Table 1). The analysis of the emission spectra of aLuc-ApoB$_L$ is simpler but not less informative. This peptide shows a considerable increase in the fluorescence emission and a 27–28 nm blue shift (from 525 to about 497 nm) only in the presence of POPC/POPG liposomes (Figure 2 and Table 1). Given the solvatochromic nature of aLuc, this is an indication that, only in the case of negatively charged liposomes, the probe is embedded in a hydrophobic environment. Therefore, three different and independent phenomena confirm binding and embedding of labeled ApoB$_L$ into the POPC/POPG bilayer: (i) inhibition of the deprotonation of Luc; (ii) inhibition of the photoinduced dissociation of Luc; (iii) the blue shift of Luc and aLuc emission peaks. In this regard, it is worth noting that the interaction of ApoB$_L$ with anionic liposomes of phosphatidylcholine and phosphatidylglycerol has been recently demonstrated by using differential scanning calorimetry [41].

Labeled p53pAnt showed a behavior essentially similar to labeled ApoB$_L$ (Figure 2), whereas GKY20 showed that it can interact with both types of liposomes. Indeed, the emission spectra of Luc and aLuc-GKY20 and the excitation spectra of Luc-GKY20 in the presence of POPC and POPC/POPG liposomes are very similar (Figure 2). All the emission spectra show a large blue shift compared to those recorded in NaP (Table 1). Furthermore, the emission spectra of Luc-GKY20 show a blue shoulder, thus indicating that the (a)Luc moiety is embedded in a less polar environment. The spectra of PyMPO-(C)GKY20 in the presence of liposomes were found to be very similar to those of aLuc-GKY20 (Figure S7), thus demonstrating that the binding to both liposome types is not an artifact due to (a)Luc. These findings agree with previous studies performed using unlabeled GKY20 and the same model membranes [42]. We do not have a straightforward explanation for the observed varying behavior of the two CAMPs. However, very interestingly, further analyses conducted on labeled GKY20 and ApoB$_L$ evidence several additional differences, as described in the next sections.

2.6. Interaction of Labeled CAMPs with SDS and LPS Micelles

In order to further confirm the ability of Luc probes to reveal the interaction of peptides with lipidic structures, we also recorded fluorescence spectra in the presence of 25 mM SDS (Figure 3A–C). At this concentration, well above the critical micelle concentration (CMC) of about 8 mM, SDS forms micelles containing an average of 60 molecules [43]. For this reason, SDS has been frequently used as a membrane mimetic, such as for determination of the NMR structure of membrane-binding peptides. However, it should be remembered that SDS is a strong detergent able to interact unspecifically with peptides. Accordingly, in the presence of SDS, not only labeled GKY20, ApoB$_L$ and p53pAnt but also labeled RGD showed spectral behavior, suggesting interaction with micelles (Figure 3A–C). Nonetheless, the spectra of labeled RGD were not completely superimposable to those of the other three peptides. For example, in the excitation spectra of Luc-RGD in the presence of SDS, a tail at 400–420 nm is still visible, indicating that not all of the peptide is strongly associated to the micelles (Figure 3A–C). In the emission spectrum of Luc-RGD, the blue peak is less evident than in the corresponding spectra of the other three peptides (Figure 3A–C), and the ratio between the area of the peaks in the blue (380–465 nm) and green (466–640 nm) regions was

0.16, whereas the same ratio for Luc-GKY20, Luc-ApoB$_L$ and Luc-p53pAnt was 0.27, 0.36 and 0.33, respectively. It is also evident that the peak in the green region is less blue-shifted than in the case of Luc-GKY20, Luc-ApoB$_L$ and Luc-p53pAnt (Figure 3A–C and Table 1).

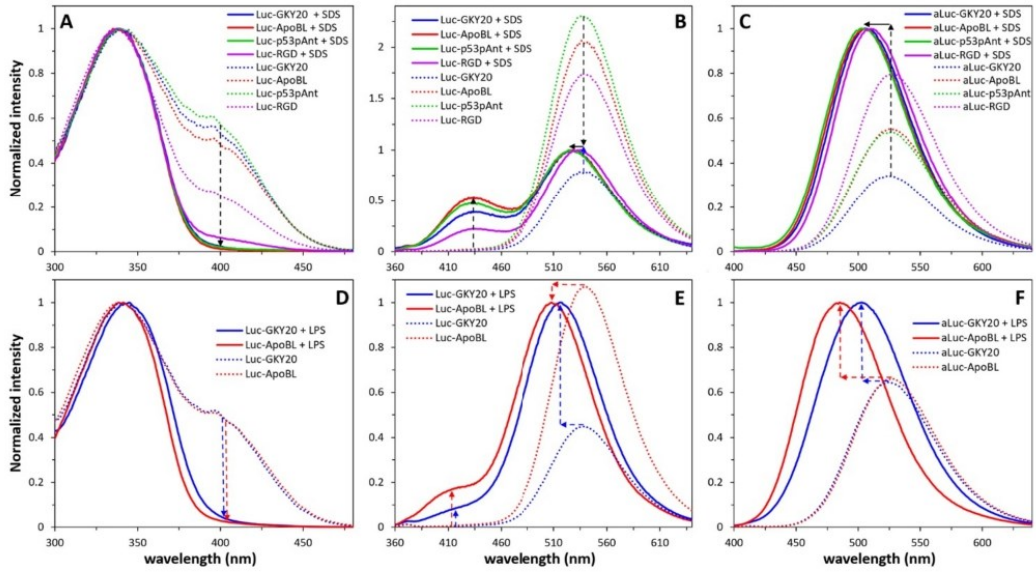

Figure 3. Fluorescence of labeled peptides in the presence of SDS or LPS micelles. (**A**,**D**) Excitation spectra of Luc-labeled peptides (em. = 539; Luc-GKY20 + LPS, em. = 516 nm; Luc-ApoBL + LPS, em. = 508 nm). (**B**,**E**) Emission spectra of Luc-labeled peptides (ex. = 330 nm). (**C**,**F**) Emission spectra of aLuc-labeled peptides (ex. = 363 nm). Solid line, spectra recorded in the presence of SDS or LPS; dotted line, spectra recorded in NaP. In (**B**,**C**,**E**,**F**), spectra recorded in NaP were normalized to the corresponding spectra recorded in the presence of SDS or LPS. Arrows highlight the main changes with respect to NaP.

As in the case of the emission spectra recorded in the presence of liposomes, the spectra of aLuc-labeled peptides recorded in the presence of SDS also showed a significant increase in emission intensity, as well as a blue shift. However, again, the blue shift was smaller in the case of aLuc-RGD (Figure 3A–C and Table 1). These results indicate that the hydrophilic RGD peptide interacts less tightly with the SDS micelles than Luc-GKY20, Luc-ApoB$_L$ and Luc-p53pAnt.

GKY20 and ApoB$_L$ bind to and neutralize lipopolysaccharides (LPS), the main components of Gram-negative bacteria outer membrane, with strong proinflammatory effects in higher eukaryotes [19,20,44]. These very complex molecules have three portions with different compositions: (i) lipid A, a phosphorylated disaccharide bearing 4–6 fatty acid residues; (ii) the core, an oligosaccharide with a variable number of phosphate groups; (iii) the O-antigen, a species and strain-specific polysaccharide [45]. It should be noted that pure LPS, like SDS, does not form regular bilayers but negatively charged micelles [46]. However, the CMC of LPS is usually in the low micromolar range [46]. The ability to bind and neutralize the strong pro-inflammatory and sometimes life-threatening effects of LPS is one of the most pharmacologically relevant properties of CAMPs [45]. Therefore, the study of the CAMP/LPS interaction is of outstanding importance.

Accordingly, we studied the interaction of labeled GKY20 and ApoB$_L$ by using a commercially available LPS from *E. coli* strain 0111:B4. Firstly, we recorded the excitation and the emission spectra of Luc-GKY20 and Luc-ApoB$_L$ in the presence of 200 μg/mL LPS, i.e., a concentration well above the CMC of this LPS (about 1.3–1.6 μM corresponding to 13–16 μg/mL) [46]. As expected, the binding of the two peptides to LPS caused the

disappearance of the shoulder at 400 nm in the excitation spectra (Figure 3D–F). The emission spectra of Luc-GKY20 and Luc-ApoB$_L$ show the expected blue shift of the peak in the green region—even larger than those observed in the presence of SDS and liposomes (Table 1) However, surprisingly, only a very low shoulder was observed in the blue region, especially in the case of Luc-GKY20 (Figure 3D–F). The ratio between the area of the peaks in the blue (365–435 nm) and green (436–640 nm) regions is 0.046, and 0.095 for Luc-GKY20 and Luc-ApoB$_L$, respectively, i.e., even lower than the ratio observed for the Luc-RGD peptide in the presence of SDS. Very interestingly, the peak in the blue region is also blue-shifted (about 20 nm) with respect to the same peak observed in the case of liposomes and SDS. Finally, the emission spectra of aLuc-GKY20 and aLuc-ApoB$_L$ show, as expected, an increase in emission intensity and a large blue shift, particularly in the case of aLuc-ApoB$_L$ (41 nm). These findings suggest that the orientation of the Luc moiety when the peptides are bound to LPS is very different from that adopted when the peptides are bound to liposomes and SDS micelles. The high blue-shift values suggest that the (a)Luc moiety is in a very non-polar environment, while the very weak emission in the blue region indicate that the phenolic OH group of Luc points toward the solvent or a proton acceptor in the LPS (e.g., a basic group in the lipid A of LPS). Possible orientations of the Luc moiety in LPS and SDS or liposomes explaining the observed variations in excitation and emission spectra are schematically drawn in Figure S8.

2.7. Interaction of Labeled CAMPs with Non-Micellar LPS

Next, we recorded the emission spectra of Luc-GKY20, Luc-ApoB$_L$, aLuc-GKY20 and aLuc-ApoB$_L$ at a constant peptide concentration in the presence of increasing concentrations of LPS (Figure 4). All peptides showed a turn-off of the fluorescence associated with a considerable blue shift of λ_{max} values for LPS concentrations up to 10–20 μg/mL, followed by a turn-on phase with smaller changes in λ_{max} values. The biphasic nature of the process is clearly visible by plotting the area beneath the spectra and the λ_{max} values as a function of the LPS concentration (Figure 4B,D,F,H). Only in the case of (a)Luc-ApoB$_L$, a turn-on phase with no shift in λ_{max} values was visible at very low LPS concentrations (0–2 μg/mL).

A similar behavior has been previously described for GKY25, HVF18 and VFR12, three CAMPs derived, like GKY20, from the C-terminus of human thrombin. In particular, GKY25 is a variant of GKY20, with five additional residues at the C-terminus [47]. In that case, the authors, exploiting the intrinsic fluorescence of the single tryptophan residue present in all the thrombin-derived CAMPs, observed a biphasic process with a turn-off phase for LPS concentrations below 10 μg/mL and a turn-on phase at higher concentrations. Therefore, the turn-off/turn-on switch seems to be independent of the nature and position of the fluorophore. As the CMC of *E. coli* LPS is about 16 μg/mL, it can be speculated that the turn-off and turn-on phases might be the result of the binding to free and micellar LPS, respectively. The additional turn-on phase observed at very low LPS concentrations only in the case of (a)Luc-ApoB$_L$ might be due to a conformational change in this peptide induced by the presence of small amounts of LPS. In this regard, it is worth noting that the CD spectra of unlabeled GKY20 and ApoB$_L$ in the presence of LPS are quite different [19,20]. In the case of ApoB$_L$, circular dichroism studies suggest that this peptide adopts a β-sheet conformation upon interaction with LPS [20]. On the other hand, the CD spectrum of GKY20 in the presence of LPS is not similar to any of the CD spectra of model conformations [19]. It could also be hypothesized that LPS might form small aggregates even below the CMC, which could be responsible for the turn-off phase, whereas the first turn-on phase observed at very low LPS concentrations would be due to the association of (a)Luc-ApoB$_L$ with truly monomeric LPS molecules. This aspect would require further investigation, which lies outside the scope of this work.

We also recorded the emission spectra of Luc-GKY20 and Luc-ApoB$_L$ after excitation at 400 nm in order to follow the binding process by monitoring the disappearance of the phenolate form in the solution (Figure 5). As expected for a saturable binding process, we

observed a progressive reduction in the fluorescence, which reached a minimum at about 50 μg/mL LPS for both peptides.

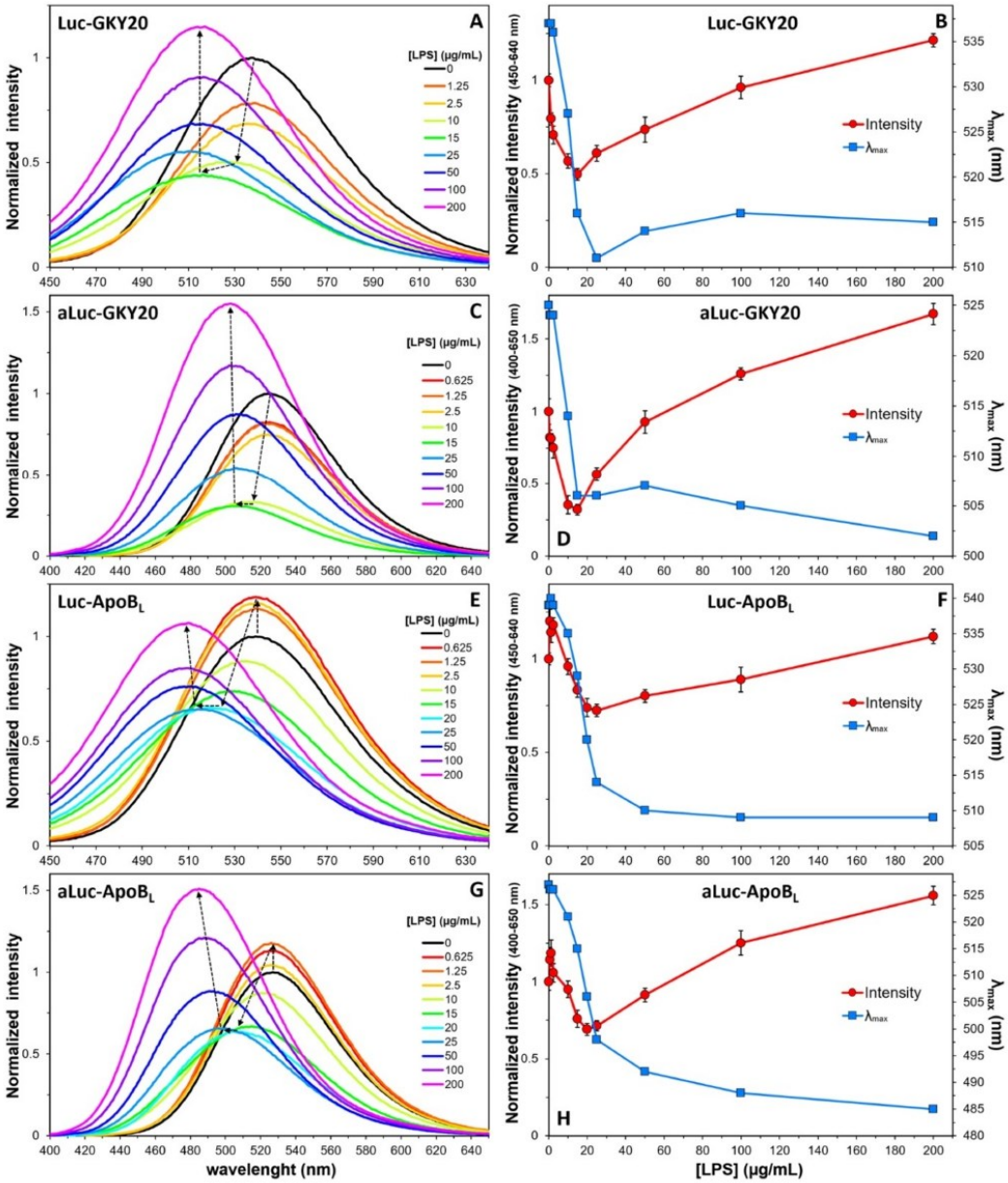

Figure 4. Fluorescence of the labeled peptides in the presence of increasing concentrations of LPS (0–200 μg/mL). (**A**,**C**,**E**,**G**) Emission spectra of the peptides recorded after excitation at 330 nm (Luc-labelled peptides) and 363 nm (aLuc-labelled peptides). Spectra recorded in the presence of LPS were normalized to the corresponding spectra recorded in NaP (black lines). Arrows highlight the main changes with respect to NaP. (**B**,**D**,**F**,**H**) Variation of total fluorescence (in the indicated ranges) and of the λ_{max} values as a function of LPS concentration.

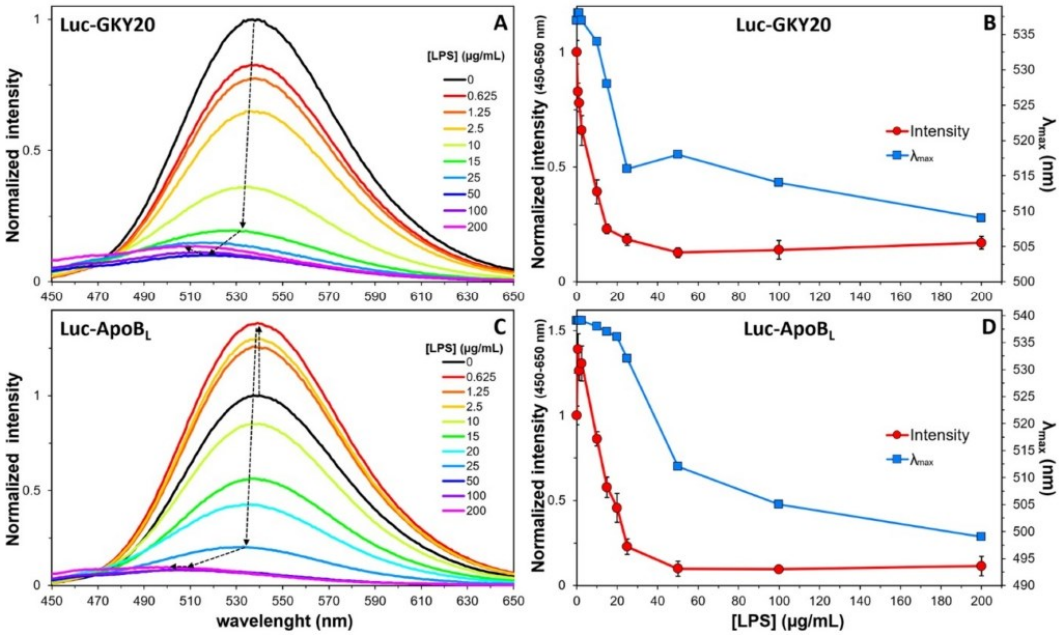

Figure 5. Fluorescence of the Luc-labeled peptides in the presence of increasing concentrations of LPS (0–200 μg/mL). (**A**,**C**) Emission spectra of Luc-labeled peptides recorded after excitation at 400 nm. Spectra recorded in the presence of LPS were normalized to the corresponding spectra recorded in NaP. Arrows highlight the main changes with respect to NaP. (**B**,**D**) Variation of total fluorescence (in the indicated ranges) and of the λ_{max} values as a function of LPS concentration.

2.8. Quantitative Analysis of the Peptide/LPS Interaction

The curves measured at constant peptide concentration and variable LPS concentration could be used to determine K_d values (Supplementary Materials, Section S9). However, as such K_d values would be the result of measurements obtained using concentrations below and above the CMC of LPS, their meaning would be questionable. In order to determine the K_d value of Luc-labeled peptides for micellar LPS, we repeated the experiment at variable Luc-labeled peptide concentration and constant LPS concentration (40 μg/mL corresponding to ~4 μM). The experimental data were fitted to the model described in Section S9, Supplementary Materials. The model allows for the estimation not only the K_d value but also the number of binding sites and hence the stoichiometry of binding. The spectra and the fittings are shown in Figure 6. Luc-GKY20, Luc-$ApoB_L$ and Luc-p53pAnt show K_d values in the range 50–400 nM. As expected, Luc-RGD did not bind to LPS, and the resulting plot of the fluorescence emission as function of the peptide concentration was a straight line (Figure 6). The fact that the anticancer peptide Luc-p53pAnt binds to LPS with affinity comparable to those of the two CAMPs is not surprising, considering that it has an amino-acid composition similar to that of the CAMPs (Figure S1) and that it is the most cationic of the three peptides (Table 3).

On the other hand, the three peptides show very different binding stoichiometries (Figure 6). Only Luc-$ApoB_L$ binds to LPS in a 1:1 ratio. In the case of Luc-GKY20, three molecules of the peptide bind to two molecules of LPS, whereas in the case of Luc-p53pAnt, two molecules of the peptide bind to three molecules of LPS. The higher number of binding sites found for Luc-GKY20 might be due to the fact that this peptide is considerably shorter than the other two. However, Luc-$ApoB_L$ and Luc-p53pAnt have exactly the same length; therefore, the different stoichiometry might be due to a different mode of binding or a different fold adopted by the peptides upon binding.

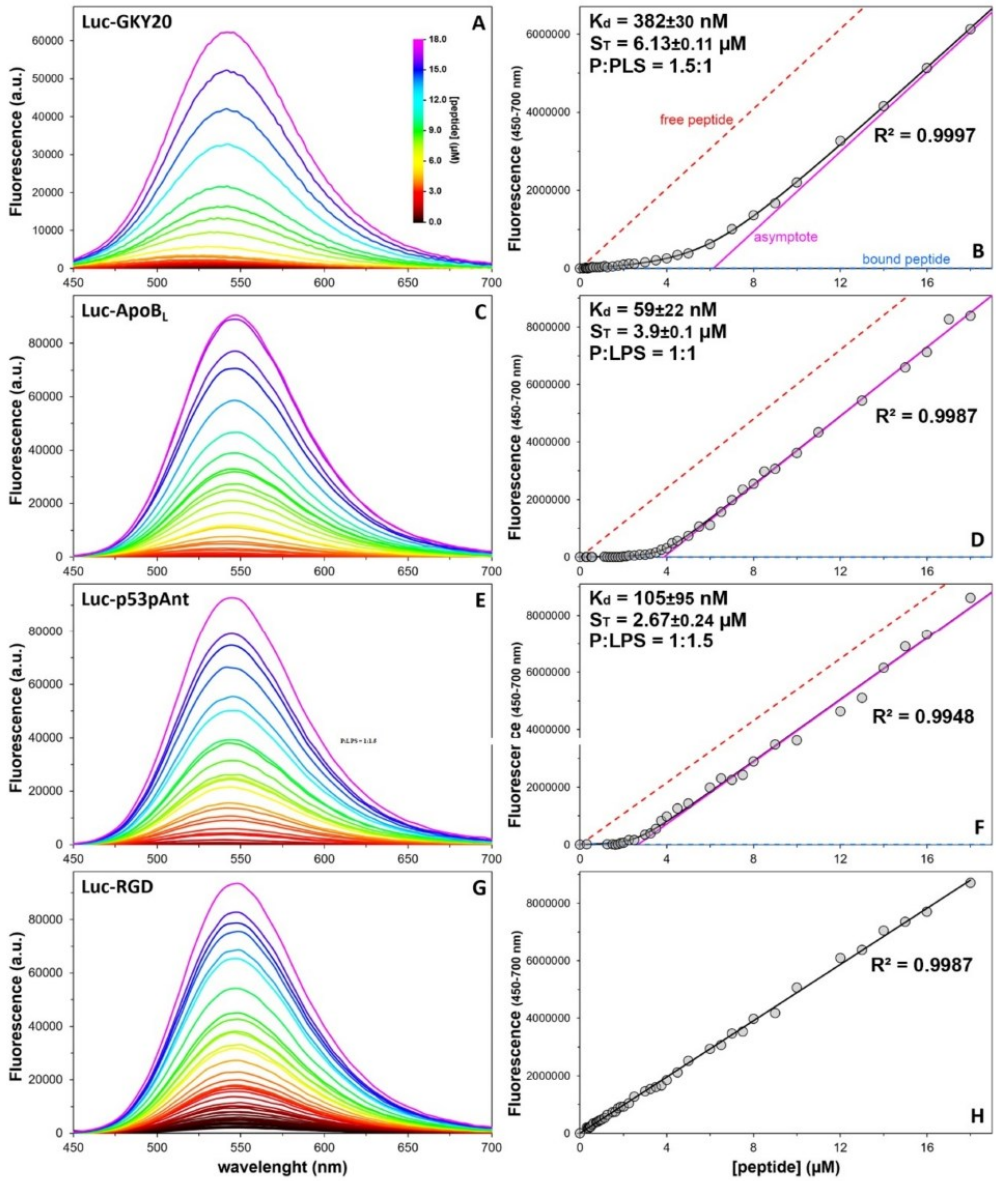

Figure 6. Determination of the K_d values and stoichiometry for the peptide/micellar LPS interaction. (**A**,**C**,**E**,**G**) Emission spectra of Luc-labeled peptides (0–18 µM) in the presence of 40 µg/mL LPS (ex. = 400, 415, 425 and 410 nm, respectively). (**B**,**D**,**F**,**H**) Variation of total fluorescence (450–700 nm) as a function of peptide concentration. The dashed lines are the expected fluorescence of the free and bound peptide, respectively. Black lines, K_d and stoichiometry (S_T) values were obtained using the equation described in Supplementary Materials. The ratio P:LPS was calculated from S_T, assuming that *E. coli* LPS has an average molecular weight of 10 kDa. In (**H**), data were fitted to a straight line.

2.9. Interaction of Labeled CAMPs with E. coli Cells

In order to study the interaction of GKY20 and $ApoB_L$ with whole bacterial cells, we recorded the emission spectra of the labeled peptides in the presence of *E. coli* cells at an

optical density of 0.1 OD_{600} (corresponding to about 0.63 × 10^9 CFU/mL). The emission spectra of Luc-GKY20 and Luc-$ApoB_L$ obtained after excitation at 330 nm show that in both cases, binding to *E. coli* cells causes a moderate decrease in the fluorescence emission (Figure S9A), accompanied by a blue shift of 16 nm in the case of Luc-GKY20 (a value slightly lower than those observed in the case of liposomes and micellar LPS) and of only 5 nm in the case of Luc-$ApoB_L$ (Table 1). In the blue region, the emission of Luc-GKY20 was higher than that of Luc-$ApoB_L$, which is the opposite of what was observed in the case of LPS (Figure S9B). The differences between the spectra of the labeled peptides in the presence of whole bacterial cells and those obtained in the presence of liposomes and purified LPS might be due to the fact that the outer membrane of Gram-negative bacteria is a very complex mixture of LPS, phospholipids and proteins.

The emission spectra of Luc-GKY20 and Luc-$ApoB_L$ obtained after excitation at 400 nm show a strong decrease in fluorescence emission (Figure S9C), likely due to a reduced hydrolysis of the Luc hydroxyl group of the cell-bound peptides.

Finally, *E. coli* cells caused a significant increase in the fluorescence emission of aLuc-GKY20 and a slight decrease in the fluorescence emission of aLuc-$ApoB_L$ (Figure S9D). In the case of aLuc-labeled peptides, we also observed a blue shift lower than that observed in the case of liposomes and micellar LPS (Table 1).

The spectra shown in Figure S9 were recorded after an incubation time of 20 min in the case of labeled GKY20 and of 120 min in the case of labeled $ApoB_L$. The different incubation times were necessary for an unexpected difference in the binding kinetic of the two peptides, as shown in Figure S9E. In the case of Luc-GKY20, the slope of the curve obtained by plotting fluorescence intensity (ex. = 400 nm; em. = 539 nm) as a function of time was about 6.7 times higher than that observed in the case of Luc-$ApoB_L$. Intriguingly, in the case of purified LPS, the binding process was complete within the preparation time of the samples (about 60 s) for both peptides. The reasons for such differences were not further investigated. Nonetheless, these results highlight another useful application of Luc labeling.

We also observed *E. coli* cells treated with the labeled peptides (3 μM) using a fluorescence microscope equipped with a mercury arc lamp (Figures S10 and S11). In the case of GKY20-treated cells, in addition to homogeneously labeled cells, we observed several cells with a heterogeneous labeling pattern (Figures S10K,N and S11E). The same pattern was observed in *E. coli* cells treated with PYMPO-(C)GKY20, indicating that heterogeneous labeling is not an artifact of Luc labeling (Figure S10A–D). For incubation times longer than 30 min, we observed an increased amount of highly fluorescent and large bodies (Figure S11), likely aggregates of cell debris and/or dead cells. This is not surprising, as GKY20 and $ApoB_L$, like many CAMPs, cause cell lysis [19,44].

2.10. Confocal Laser Scanning Microscopy

Confocal Laser Scanning Microscopy (CLSM) allows for the attainment of high resolution tridimensional images of biological samples by stacking several bidimensional images taken at different depths [48]. As in CLSM, fluorophore excitation is obtained through high-power but very narrow laser beams. It is mandatory that the excitation peak of the chosen fluorescent label overlaps the wavelength of one of the available laser lines [48]. Moreover, the fluorescent label should be photostable enough to avoid a quick bleaching of the sample. This is especially important in the case of live-imaging applications. We have already shown that Luc and aLuc are very stable fluorophores. As regards the excitation wavelength, it is interesting to note that the excitation spectra of neutral Luc and its phenolate show an isosbestic point at about 355 nm, a wavelength very close to that of the argon-ion laser (351 nm). Therefore, this laser could be used to simultaneously excite both forms of Luc. A blue diode laser (405 nm) could be used to excite aLuc, the broad excitation peak of which is centered at 360–370 nm but has also a remarkable tail in the violet region. Differently from an argon-ion laser, which is not common, the blue diode laser is present on most CLSM devices used to excite blue fluorophores. In order to evaluate the suitability

of aLuc as label for CLSM, we incubated HaCaT and HeLa cells with aLuc-p53pAnt or aLuc-RGD for 60–150 min; hence, samples were either observed or incubated for 15 additional min with LysoTracker™ Red DND-99, a red probe that is actively taken up by acidic organelles [49], and/or NucRed™ Live 647, a far-red cell-permeant vital stain for nucleic acids [50,51]. Samples were observed without any further wash or treatment in order to minimize artifacts and to mimic the conditions of live imaging.

Non-cell-specific uptake of p53pAnt has been previously demonstrated by Western blotting of cell lysates and immunostaining by an antibody specific to the p53-derived portion of p53pAnt [25,52], whereas confocal microscopy with a rhodamine B-labeled peptide showed that it accumulates both in the cytosol and the nuclei of two prostate cancer cell lines [52]. Our CLSM analysis of HaCaT and HeLa cells treated with aLuc-p53pAnt confirm the previous findings. In the case of HaCaT cells treated with aLuc-p53pAnt, the peptide was localized at the cell periphery, mainly in the form of circular spots, thus suggesting the presence of the peptide in an endosomal compartment (Figure S12). A very small fraction of the cells, however, displayed a very strong signal, partly diffused into the cell and partly associated to the nucleus (Figure S13). The signal was very strong at the nuclear periphery but also present inside the nucleus in the form of one or more patches of different dimensions (Figure S13). As discussed below, colocalization studies with NucRed Live confirm that the peptide binds to nucleic acids. Very interestingly, in the case of HeLa cells, the proportion between the two types of staining pattern was reversed, with the highly stained cells being predominant (Figure S13). Considering that p53pAnt is much more toxic for HeLa cancer cells than for HaCaT cells (Figure S4) and that it has been suggested that p53pAnt induces apoptosis, it can be speculated that highly stained cells are apoptotic or pre-apoptotic cells. It is well known that apoptosis causes relevant alterations of cell membranes, e.g., externalization of phosphatidylserine [53], a negatively charged lipid, which could determine an increased afflux into the cytosol of p53pAnt. Once in the cytosol, p53pAnt could migrate into the nucleus and bind nucleic acids due to its high positive charge.

HaCaT cells treated with aLuc-p53pAnt and LysoTracker Red showed, as expected, numerous red spots (Figures 7 and S15). Very interestingly, we observed partial colocalization between LysoTracker Red and aLuc-p53pAnt (Figures 7E,F and S14A–D). Cells showing a strong aLuc-p53pAnt fluorescence did not show the presence of LysoTracker Red (Figure 7A–D). The same pattern was observed in the case of HeLa cells, except that, again, the frequency of cells showing only the strong fluorescence of aLuc-p53pAnt was higher than in the case of HaCaT cells (Figure S15A–D). Accumulation of LysoTracker Red, requiring acidification of endosomes, is expected only in metabolically active cells; therefore, these findings are in agreement with the hypothesis that cells strongly stained with aLuc-p53pAnt are apoptotic or pre-apoptotic cells.

Unexpectedly, our attempts to perform three-color imaging by staining aLuc-p53pAnt-treated HaCaT cells with LysoTracker Red and NucRed Live for 15 min revealed an alteration of the localization both of LysoTracker Red and of aLuc-p53pAnt (Figure S14E–H). The change was particularly evident in the case of LysoTracker Red, which appeared more homogeneously diffused inside the cell than in the absence of NucRed. On the contrary, the signal of aLuc-p53pAnt appeared less diffused and with more defined spots (Figure S14E). The alteration in the distribution of aLuc-p53pAnt was more pronounced by co-incubating HaCaT cells with NucRed Live and aLuc-p53pAnt for one hour (Figure S14I–L). In that case, in the majority of the cells, aLuc-p53pAnt appeared as numerous large and well-defined spots at the cell periphery. In the case of aLuc-p53pAnt-treated HeLa cells, staining with NucRed Live for 15 min had minor effects on the appearance of the putative apoptotic/pre-apoptotic cells (Figure S15E–H). Interestingly, inside the nuclei of these cells, aLuc-p53pAnt and NucRed Live were essentially colocalized (Figure S15M–O), thus suggesting that aLuc-p53pAnt is bound to nucleic acids. Similarly to what was observed in the case of HaCaT cells, LysoTracker Red was more diffused in the presence of NucRed Live (Figure S15). When HeLa cells were treated with NucRed Live for one hour, we

no longer observed the putative apoptotic/pre-apoptotic cells (Figure S15I–L), and the staining pattern was very similar to that of the HaCaT cells treated for one hour with NucRed Live (Figure S14I–L). Very interestingly, NucRed Live also proved to change the behavior of aLuc-RGD, as described below.

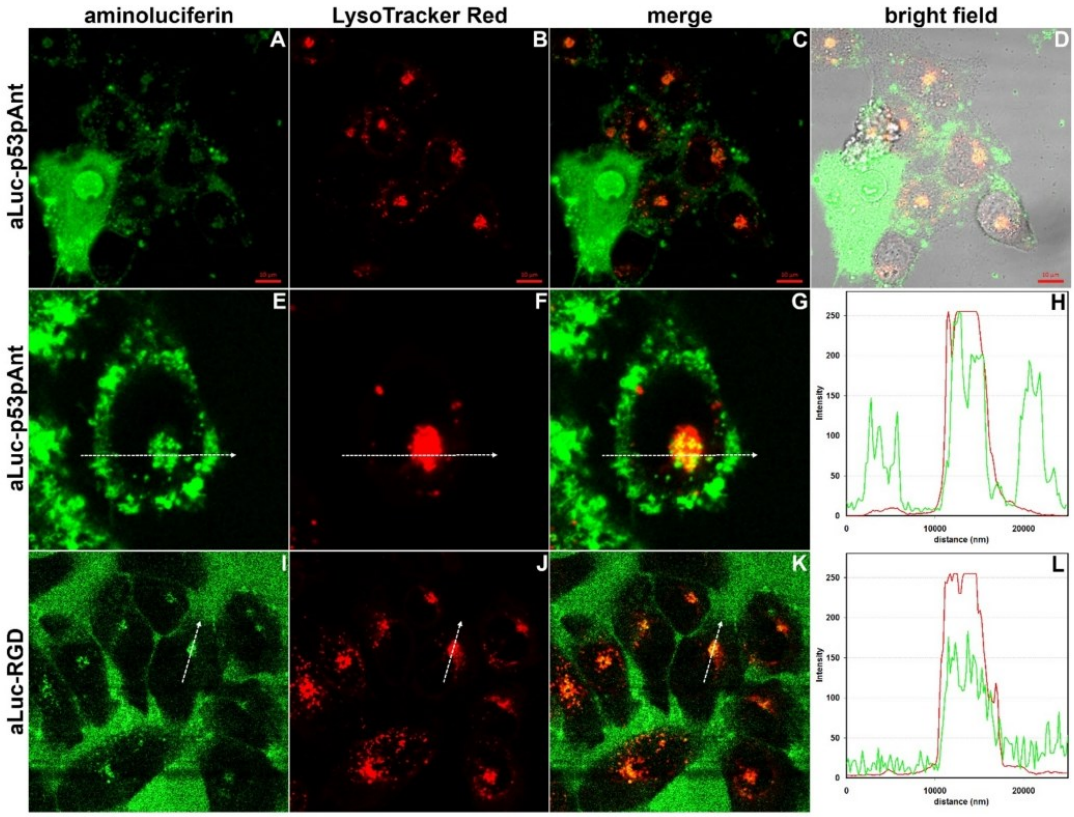

Figure 7. CLSM images of HaCaT cells treated with aLuc-p53pAnt or aLuc-RGD. (**A**–**D**) Cells were incubated with aLuc-p53pAnt for 120 min and with LysoTracker™ Red DND-99 for 15 additional minutes. Bar = 10 µm. (**E**,**F**) Single representative HaCaT cell treated with aLuc-p53pAnt (from Figure S14A–D). White arrow = 25 µm. (**I**–**K**) Cells were incubated with aLuc-RGD for 90 min and with LysoTracker™ Red DND-99 for 15 additional minutes (bright field in Figure S16E). White arrow = 25 µm. (**H**,**L**) Fluorescence intensity across the white arrows in panels (**E**–**G**) and (**I**–**K**), respectively (green curve, aLuc; red curve, LysoTracker Red).

RGD is a known integrin ligand derived from fibronectin; therefore, it is expected to undergo receptor-mediated endocytosis, as demonstrated for other similar peptides [54]. In particular, it has been demonstrated that peptide GRGDNP, which differs by one amino acid (N at position 5) from RGD, is endocytosed in Molt-4 cells (leukaemic T-cell line) [55]. Differently from aLuc-p53pAnt, aLuc-RGD was homogeneously dispersed in the culture medium in the case of both HaCaT and HeLa cells, which appeared as non-fluorescent regions (Figures 7I–L and S16, respectively). Nonetheless, as expected, an intracellular signal was visible and colocalized with LysoTracker Red (Figures 7I–L and S16). In the presence of NucRed Live, aLuc-RGD was no longer visible inside the cells, whereas the signal of LysoTracker Red appeared homogeneously diffused inside the cytosol (Figure S16), as observed in the case of the analysis of aLuc-p53pAnt.

Overall, NucRed Live seems to be able to interfere with endocytosis and intracellular trafficking. NucRed Live is a relatively recent stain, and we did not find other reports regarding its potential biological effects. On the other hand, it has been demonstrated that another far-red, membrane-permeable nuclear stain, DRAQ5™, alters membrane fluidity and inhibits the internalization of bacterial toxins [56]. Reduction in membrane fluidity and/or alteration of membrane potential by NucRed Live might prevent translocation of p53pAnt from the endosomes to cytosol, thus causing accumulation of the peptide in the lumen of endosomes. This, in turn, would prevent its interaction with p53, thus inhibiting the proapoptotic effect of the peptide. The effect on LysoTracker Red could be explained, at least in part, by assuming that NucRed Live is also able to inhibit endosome acidification. We did not further study the effects of NucRed Live, as this is beyond the scope of the current work; nonetheless, the analysis reported herein clearly shows that aLuc is very well suited as a probe for CLSM.

3. Discussion

We have shown that Luc and aLuc are very well suited as environment-sensitive fluorescent labels for peptides. Labeling is fast, quantitative, very specific and can be performed in very mild conditions (RT, buffer phosphate at pH 7–7.5) using commercially available reagents and peptides with an N-terminal cysteine that can be prepared either by chemical synthesis or by several recombinant strategies ([32] and references therein). Luc and aLuc are photostable fluorophores with a large Stoke shift (about 210 and 145 nm, respectively) and a high quantum yield. Moreover, they are small molecules (low molecular weight and low solvent-accessible surface), uncharged (aLuc) or with a low percentage of ionized form at pH 7 (Luc), neither highly polar nor particularly hydrophobic, thus minimizing the impact of labeling on the structure of the peptides and presumably on their properties. Furthermore, N-terminal labeling is very well suited for most peptides, and indeed, it is a very common choice. On the other hand, Luc and aLuc possess complementary properties. Luc has a very uncommon dual emission with a main emission in the green region (~539 nm), commonly observed in aqueous buffers and a blue emission (~450 nm), which can only be observed in an environment with a very low water content. Moreover, both peaks undergo significant blue shifts (20–30 nm) in hydrophobic environments. This behavior makes Luc a very useful probe for the study of the interactions of peptides with membranes, liposomes, micelles of detergents and LPS. The very large difference between the excitation maxima of the neutral and the phenolate form (330 and 400 nm, respectively) makes Luc an intriguing probe for the pH range of 6.5–9.5 (hypothesizing pK_a values in the range 7.5–8.5 for peptide-bound Luc). Moreover, it can be exploited to detect binding events that influence its ionization state, as shown in the case of binding to liposomes, SDS, LPS and *E. coli* cells, and to determine K_d values and stoichiometries. aLuc is not sensitive to pH and shows less pronounced variations in fluorescence emission. However, it is, in turn, a strongly solvatochromic fluorophore, showing blue shifts up to 40 nm. This makes aLuc an alternative probe for the study of the interactions of peptides with their targets. In addition, aLuc is very well suited as a label for CLSM, and it does not require special equipment. It can be efficiently excited by the common 404 nm laser, and emitting at 500–520 nm, it allows for colocalization studies with the many commercially available and widely used orange, red and far-red probes, as was shown by our analysis of the colocalization of p53pAnt and RGD with LysoTracker™ Red DND-99 and NucRed™ Live 647.

It is worth noting that we have only explored a minimal part of the potentialities of Luc and aLuc as fluorescent labels for peptides. For example, when N-terminal labeling is not suitable or when large proteins have to be labeled, a 1,2-aminothiol functionality could be introduced at internal positions, e.g., as N^{ε}-cysteinyl-L-lysine [57], or by modifying a cysteine residue [58]. Furthermore, Luc and aLuc might be bound to internal cysteine or lysine residues via the carboxyl group of luciferins, exploiting conventional chemical strategies to crosslink carboxyl groups to amines and thiols [59]. Even more interestingly,

in the attempt to find new substrates for firefly luciferase, an astonishing number of Luc and, in particular, aLuc derivatives and analogues have been published [60,61]. Many of these compounds are fluorescent and show intriguing properties; for example, many aLuc derivatives show red-shifted λ_{max} values (up to 576 nm) and/or altered solvatochromic behavior (increased or decreased, depending on the nature of the substituents bound to the N6 nitrogen atom) [11,61,62]. Moreover, halogenated luciferins show decreased pK_a values—e.g., 7-F- and 7-Cl-luciferin have pK_a values of 7.1 and 6.7, respectively [63]—thus expanding the useful pH range in applications based on pH-dependent fluorescence. Most of the cited derivatives and analogues were synthetized by reacting the corresponding 2-cyano-benzothiazole with cysteine. Thus, they could be directly generated at the N-terminus of peptides with a terminal cysteine residue. The others might be linked to peptides through the activation of their carboxylate group, which, being essential for the catalytic activity of firefly luciferase, is present in all the analogues.

Therefore, Luc and aLuc can reasonably be regarded as the prototypes of a huge new and variegated family of fluorescent labels for proteins and peptides.

4. Materials and Methods

4.1. Materials and General Methods

Materials and general methods can be found in Section S1 (Supplementary Materials). The sequences of the peptides GKY20, ApoBL, p53pAnt and RGD are shown in Figure S1, and their preparation, purification and labeling are described in Sections S2–S6 (Supplementary Materials).

4.2. Steady-State Fluorescence Spectroscopy in Water/Organic Solvent Mixtures and SDS

Fluorescence spectra were recorded on a Fluoromax-4 fluorometer (Horiba, Edison, NJ, USA) using a 1 cm path length quartz cuvette at a temperature of 25 °C, using a peltier that can ensure an accuracy of ±0.1 °C. All experiments were carried out at a fixed peptide concentration (2 μM) in 10 mM sodium phosphate (NaP), pH 7.4, at 25 °C, unless otherwise stated. The excitation wavelengths were set to 330 nm (Luc-labeled peptides, phenol form), 400 nm (Luc-labeled peptides, phenolate form), 363 nm (aLuc-labeled peptides), 330 nm (mLuc-GKY20) and 408 nm for 1-[2-(maleimido)ethyl]-4-[5-(4-methoxyphenyl)-2-oxazolyl]pyridinium-labeled GKY20 [PyMPO-(C)GKY20]. The excitation spectra were recorded by varying the wavelength of excitation between 200 nm and 500 nm (em. = 539 nm). To evaluate the solvatochromic properties of labeled peptides, fluorescence spectra were recorded in the presence of NaP:methanol (50% *v*:*v*), NaP:isopropanol (50% *v*:*v*) and SDS (25 mM) under the experimental condition described above.

4.3. Steady-State Fluorescence Spectroscopy in the Presence of Liposomes

Liposome preparation is described in Section S8, Supplementary Materials. Fluorescence spectra were recorded on a FluoroMax-4 fluorometer (Horiba, Kyoto, Japan). The emission spectra of Luc-labeled peptides were acquired, upon excitation at 330 nm, in the range 350–650 nm. For the aLuc-labeled peptides, the emission spectra were acquired in the range 380–700 nm, upon excitation at 363 nm. In addition, for Luc-labeled peptides, excitation spectra were also recorded. The excitation spectra were recorded by varying the wavelength of excitation between 275 nm and 480 nm and monitoring the emission at 539 nm. All the spectra were recorded at a lipid-to-peptide ratio of 200 in 10 mM NaP, pH 7.4. The concentration of peptides was in the range of 2.2–3.6 μM.

4.4. Quantum-Yield Determination

Fluorescence quantum yields were determined for all the labeled peptides in 10 mM phosphate buffer, pH 7.4, in a mixture composed of phosphate buffer and isopropanol in the ratio 1:1 (*v*:*v*) and in acetate buffer, pH 5. Determination of the quantum yields was performed by comparing the fluorescence of samples to that of a standard, as previously described [64]. Fluorescein (in 0.1 M NaOH) was used as standard in the case of (a)Luc-

and PyMPO-labeled peptides, whereas coumarin-6 (in pure ethanol) was used in the case of mLuc-labeled GKY20.

4.5. pK_a Determination of Luc-Labeled Peptides

In order to measure pK_a values, phenolate concentration was evaluated by titrating a solution of Luc-labeled peptide (2 µM) as a function of pH (0.2 M sodium acetate, pH 4–6; 0.2 M sodium phosphate, pH 6–7.4; 0.2 M Tris/HCl, pH 7–9; 0.2 M Glycine/NaOH, pH 8–11). The excitation wavelength was set to 400 nm. Excitation spectra were recorded at 539 nm. pK_a values were determined by GraphPad Prism software (version 6, San Diego, CA, USA) by plotting variation of total fluorescence (450–700 nm) as a function of pH values.

4.6. Interaction of Labeled CAMPs with LPS

Binding of CAMPs (2 µM) to LPS (200 µg/mL) from *E. coli* 0111:B4 (MW 10,000) [46] was performed in 10 mM NaP buffer, pH 7.4. Mixtures were equilibrated at 25 °C for 10 min before recording emission (Luc-peptides, ex. = 330; aLuc-peptides, ex. = 363 nm) and excitation spectra (Luc-GKY20, em. = 516 nm; Luc-$ApoB_L$, em. = 508 nm) by means of a FluoroMax-4 fluorimeter. To test the influence of micellar and sub-micellar LPS concentration on CAMP fluorescence (2 µM), emission spectra (Luc-peptides, ex. = 330 or 400 nm; aLuc-peptides, ex. = 363 nm) were also recorded in the presence of increasing concentrations of LPS (0.62 e 200 µg/mL). Variation of total fluorescence (450–700 nm) was reported as a function of LPS concentration. The assays to determine K_d and binding stoichiometry of Luc-peptides toward LPS were carried out in 96-well polystyrene microtiter plates containing 100 µL of peptide/LPS mixtures. Spectra were recorded using a Synergy™ H4 microplate reader (BioTek Instruments Inc., Winooski, VT, USA) in 10 mM NaP buffer, pH 7.4, in the presence of 40 µg/mL (≈4 µM; MW 10,000) LPS and Luc-peptides (0.25–18 µM). Mixtures were incubated 15 min before emission spectra were recorded by excitation between 400 and 425 nm (phenolate form). Variation of total fluorescence (450–700 nm) was reported as a function of peptide concentration, and data were fitted to the model using Graphpad Prism (Supplementary Materials, Section S9).

4.7. Interaction of Labeled CAMPs with E. coli Cells

Bacterial *E. coli* ATCC 25922 strain was cultured in LB medium at 37 °C overnight. Culture was diluted 1:100 in fresh LB medium, and bacteria were grown until 1 OD_{600} optical density. Cells were collected by centrifugation at 8000× *g* for 5 min at 4 °C, washed three times in 10 mM NaP buffer, pH 7.4, and suspended at 1 OD_{600} concentration (10x cell stock solution) in the same buffer. The bacteria mixture was stored on ice until use. Binding of labeled CAMPs to *E. coli* cells was performed in 10 mM NaP buffer, pH 7.4, in the presence of 0.1 OD_{600} bacterial cells and 2 µM peptides. Mixtures were incubated at 25 °C for 20 min [(a)Luc-GKY20] and 120 min [(a)Luc-$ApoB_L$] before recording emission spectra (Luc-peptides, ex. = 330 and 400 nm; aLuc-peptides, ex. = 363 nm).

4.8. Kinetic Analysis

Binding kinetic to LPS and *E. coli* cells was carried out in 10 mM NaP buffer, pH 7.4, in the presence of either 50 µg/mL LPS or 0.1 OD_{600} bacterial cells prepared as described above. Binding reactions were started by adding peptides (2 µM) and manually mixing the samples for 40 s. Binding was monitored, exciting at 400 nm and reading at 539 nm. One reading per minute was performed over 16 min observation time. Samples were not irradiated in the period between two readings in order to minimize peptide photobleaching. Photobleaching of peptides was also verified by control experiments carried out in the absence of LPS and cells.

4.9. Microscopy Analysis of E. coli Cells Treated with the Labeled Peptides

Binding of labeled CAMPs (3 μM) to *E. coli* cells was performed in 10 mM NaP buffer, pH 7.4, in the presence of 0.1 OD_{600} bacterial cells. Fluorescence microscopy images of treated and untreated *E. coli* cells were taken over 50 min incubation at 25 °C. For this purpose, 10 μL of each sample was observed with an Olympus BX51 fluorescence microscope (Olympus, Tokyo, Japan) using DAPI (aLuc-labeled peptides) and FITC (Luc-labeled peptides) filters. Standard acquisition times were 1000 ms. Images were captured using an Olympus DP70 digital camera. The experiments were performed at least three times.

4.10. Interaction of aLuc-p53pAnt and aLuc-RGD with HeLa and HaCaT Cells

Normal human keratinocytes (HaCaT) and human cancer epithelial cells (HeLa cells) were cultured in Dulbecco's Modified Eagle's Medium (DMEM), supplemented with 10% fetal bovine serum (FBS), 2 mM L-glutamine and 1% penicillin–streptomycin in a 5% CO_2 humidified atmosphere at 37°C. HaCaT and HeLa cells were seeded in chambered well plates (500 μL/well; Nunc™ Lab-Tek™ Chambered Coverglass systems, Thermo Fisher Scientific, Waltham, MA, USA) with a density of 4.5×10^4 and 2.5×10^4/well, respectively, and then grown at 37 °C for 48 h. Cells were washed three times with PBS and then incubated with aLuc-peptides (10 μM) for 1 h in medium without FBS, supplemented with 2 mM L-glutamine and 1% penicillin–streptomycin in a 5% CO_2 humidified atmosphere at 37 °C. Lysotracker™ Red DND-99 and NucRed™ Live 647 (Thermo Fisher Scientific, Waltham, MA, USA) were added to the cells at the concentrations recommended by the producer and incubated for 15 min in a 5% CO_2 humidified atmosphere at 37 °C. The samples were then analyzed using a confocal laser scanning microscope (Zeiss LSM 710, Zeiss, Germany) and a 63X objective oil-immersion system. Acquired images were analyzed using the Zen Lite 2.3 software package. In the case of the images shown in Figure 7A–D the intensity of the green channel was increased in order to show both the apoptotic and non-apoptotic cells. Each experiment was performed in triplicate.

Supplementary Materials: The following are available online at https://www.mdpi.com/article/10.3390/ijms222413312/s1.

Author Contributions: E.N., E.P. and V.C.: conceptualization, methodology, supervision, writing—original draft preparation; R.O., M.S., A.M., R.G., A.A., R.R. and A.Z.: investigation, writing—review and editing; A.D.M., P.D.V., L.P., M.V. and M.M.: formal analysis, writing—review and editing. All authors have read and agreed to the published version of the manuscript.

Funding: This research was funded by the Italian Cystic Fibrosis Research Foundation, grant numbers FFC#16/2017 and FFC#18/2018.

Data Availability Statement: The data presented in this study are available in the article or Supplementary Materials. The raw datasets are available from the corresponding authors upon reasonable request.

Conflicts of Interest: The authors declare no conflict of interest. The funders had no role in the design of the study; in the collection, analyses or interpretation of data; in the writing of the manuscript or in the decision to publish the results.

References

1. Klymchenko, A.S. Solvatochromic and Fluorogenic Dyes as Environment-Sensitive Probes: Design and Biological Applications. *Acc. Chem. Res.* **2017**, *50*, 366–375. [CrossRef] [PubMed]
2. Han, J.; Burgess, K. Fluorescent Indicators for Intracellular pH. *Chem. Rev.* **2010**, *110*, 2709–2728. [CrossRef] [PubMed]
3. Loving, G.S.; Sainlos, M.; Imperiali, B. Monitoring protein interactions and dynamics with solvatochromic fluorophores. *Trends Biotechnol.* **2010**, *28*, 73–83. [CrossRef] [PubMed]
4. Donadio, G.; Di Martino, R.; Oliva, R.; Petraccone, L.; Del Vecchio, P.; Di Luccia, B.; Ricca, E.; Isticato, R.; Di Donato, A.; Notomista, E. A new peptide-based fluorescent probe selective for zinc(II) and copper(II). *J. Mater. Chem. B* **2016**, *4*, 6979–6988. [CrossRef]
5. Li, S.; Ruan, Z.; Zhang, H.; Xu, H. Recent achievements of bioluminescence imaging based on firefly luciferin-luciferase system. *Eur. J. Med. Chem.* **2021**, *211*, 113111. [CrossRef]

6. Morton, R.A.; Hopkins, T.A.; Seliger, H.H. Spectroscopic properties of firefly luciferin and related compounds; an approach to product emission. *Biochemistry* **1969**, *8*, 1598–1607. [CrossRef]
7. Ando, Y.; Akiyama, H. PH-dependent fluorescence spectra, lifetimes, and quantum yields of firefly-luciferin aqueous solutions studied by selective-excitation fluorescence spectroscopy. *Jpn. J. Appl. Phys.* **2010**, *49*, 117002. [CrossRef]
8. Presiado, I.; Erez, Y.; Huppert, D. Excited-state intermolecular proton transfer of the firefly's chromophore d-luciferin. 2. water-methanol mixtures. *J. Phys. Chem. A* **2010**, *114*, 9471–9479. [CrossRef]
9. Kuchlyan, J.; Banik, D.; Roy, A.; Kundu, N.; Sarkar, N. Excited-state proton transfer dynamics of fireflys chromophore d -luciferin in DMSO-water binary mixture. *J. Phys. Chem. B* **2014**, *118*, 13946–13953. [CrossRef]
10. Vieira, J.; Da Silva, L.P.; Da Silva, J.C.G.E. Advances in the knowledge of light emission by firefly luciferin and oxyluciferin. *J. Photochem. Photobiol. B Biol.* **2012**, *117*, 33–39. [CrossRef]
11. Kakiuchi, M.; Ito, S.; Yamaji, M.; Viviani, V.R.; Maki, S.; Hirano, T. Spectroscopic Properties of Amine-substituted Analogues of Firefly Luciferin and Oxyluciferin. *Photochem. Photobiol.* **2017**, *93*, 486–494. [CrossRef]
12. Zheng, M.; Huang, H.; Zhou, M.; Wang, Y.; Zhang, Y.; Ye, D.; Chen, H.Y. Cysteine-Mediated Intracellular Building of Luciferin to Enhance Probe Retention and Fluorescence Turn-On. *Chem. A Eur. J.* **2015**, *21*, 10506–10512. [CrossRef]
13. Miao, Q.; Li, Q.; Yuan, Q.; Li, L.; Hai, Z.; Liu, S.; Liang, G. Discriminative Fluorescence Sensing of Biothiols in Vitro and in Living Cells. *Anal. Chem.* **2015**, *87*, 3460–3466. [CrossRef]
14. Zheng, M.; Wang, Y.; Shi, H.; Hu, Y.; Feng, L.; Luo, Z.; Zhou, M.; He, J.; Zhou, Z.; Zhang, Y.; et al. Redox-Mediated Disassembly to Build Activatable Trimodal Probe for Molecular Imaging of Biothiols. *ACS Nano* **2016**, *10*, 10075–10085. [CrossRef]
15. Zhao, X.; Lv, G.; Peng, Y.; Liu, Q.; Li, X.; Wang, S.; Li, K.; Qiu, L.; Lin, J. Targeted Delivery of an Activatable Fluorescent Probe for the Detection of Furin Activity in Living Cells. *ChemBioChem* **2018**, *19*, 1060–1065. [CrossRef]
16. Ren, H.; Xiao, F.; Zhan, K.; Kim, Y.P.; Xie, H.; Xia, Z.; Rao, J. A biocompatible condensation reaction for the labeling of terminal cysteine residues on proteins. *Angew. Chem. Int. Ed.* **2009**, *48*, 9658–9662. [CrossRef]
17. Chen, K.T.; Ieritano, C.; Seimbille, Y. Early-Stage Incorporation Strategy for Regioselective Labeling of Peptides using the 2-Cyanobenzothiazole/1,2-Aminothiol Bioorthogonal Click Reaction. *ChemistryOpen* **2018**, *7*, 256–261. [CrossRef]
18. Shinde, R.; Perkins, J.; Contag, C.H. Luciferin derivatives for enhanced in vitro and in vivo bioluminescence assays. *Biochemistry* **2006**, *45*, 11103–11112. [CrossRef]
19. Kasetty, G.; Papareddy, P.; Kalle, M.; Rydengård, V.; Mörgelin, M.; Albiger, B.; Malmsten, M.; Schmidtchen, A. Structure-activity studies and therapeutic potential of host defense peptides of human thrombin. *Antimicrob. Agents Chemother.* **2011**, *55*, 2880–2890. [CrossRef]
20. Gaglione, R.; Dell'Olmo, E.; Bosso, A.; Chino, M.; Pane, K.; Ascione, F.; Itri, F.; Caserta, S.; Amoresano, A.; Lombardi, A.; et al. Novel human bioactive peptides identified in Apolipoprotein B: Evaluation of their therapeutic potential. *Biochem. Pharmacol.* **2017**, *130*, 34–50. [CrossRef]
21. Wiesner, J.; Vilcinskas, A. Antimicrobial peptides: The ancient arm of the human immune system. *Virulence* **2010**, *1*, 440–464. [CrossRef]
22. Pane, K.; Durante, L.; Crescenzi, O.; Cafaro, V.; Pizzo, E.; Varcamonti, M.; Zanfardino, A.; Izzo, V.; Di Donato, A.; Notomista, E. Antimicrobial potency of cationic antimicrobial peptides can be predicted from their amino acid composition: Application to the detection of "cryptic" antimicrobial peptides. *J. Theor. Biol.* **2017**, *419*, 254–265. [CrossRef]
23. Pizzo, E.; Cafaro, V.; Di Donato, A.; Notomista, E. Cryptic Antimicrobial Peptides: Identification Methods and Current Knowledge of their Immunomodulatory Properties. *Curr. Pharm. Des.* **2018**, *24*, 1054–1066. [CrossRef]
24. Dell'Olmo, E.; Gaglione, R.; Cesaro, A.; Cafaro, V.; Teertstra, W.R.; de Cock, H.; Notomista, E.; Haagsman, H.P.; Veldhuizen, E.J.A.; Arciello, A. Host defence peptides identified in human apolipoprotein B as promising antifungal agents. *Appl. Microbiol. Biotechnol.* **2021**, *105*, 1953–1964. [CrossRef]
25. Selivanova, G.; Iotsova, V.; Okan, I.; Fritsche, M.; Ström, M.; Groner, B.; Grafström, R.C.; Wiman, K.G. Restoration of the growth suppression function of mutant p53 by a synthetic peptide derived from the p53 C-terminal domain. *Nat. Med.* **1997**, *3*, 632–638. [CrossRef]
26. Li, Y.; Mao, Y.; Rosal, R.V.; Dinnen, R.D.; Williams, A.C.; Brandt-Rauf, P.W.; Fine, R.L. Selective induction of apoptosis through the FADD/Caspase-8 pathway by a p53 C-terminal peptide in human pre-malignant and malignant cells. *Int. J. Cancer* **2005**, *115*, 55–64. [CrossRef]
27. Li, Y.; Rosal, R.V.; Brandt-Rauf, P.W.; Fine, R.L. Correlation between hydrophobic properties and efficiency of carrier-mediated membrane transduction and apoptosis of a p53 C-terminal peptide. *Biochem. Biophys. Res. Commun.* **2002**, *298*, 439–449. [CrossRef]
28. Pierschbacher, M.D.; Ruoslahti, E. Cell attachment activity of fibronectin can be duplicated by small synthetic fragments of the molecule. *Nature* **1984**, *309*, 30–33. [CrossRef]
29. Ruoslahti, E. RGD and other recognition sequences for integrins. *Annu. Rev. Cell Dev. Biol.* **1996**, *12*, 697–715. [CrossRef]
30. Knetsch, P.A.; Zhai, C.; Rangger, C.; Blatzer, M.; Haas, H.; Kaeopookum, P.; Haubner, R.; Decristoforo, C. [68Ga]FSC-(RGD)3 a trimeric RGD peptide for imaging αvβ3 integrin expression based on a novel siderophore derived chelating scaffold-synthesis and evaluation. *Nucl. Med. Biol.* **2015**, *42*, 115–122. [CrossRef]
31. Karimi, F.; O'Connor, A.J.; Qiao, G.G.; Heath, D.E. Integrin Clustering Matters: A Review of Biomaterials Functionalized with Multivalent Integrin-Binding Ligands to Improve Cell Adhesion, Migration, Differentiation, Angiogenesis, and Biomedical Device Integration. *Adv. Healthc. Mater.* **2018**, *7*, e1701324. [CrossRef] [PubMed]

32. Pane, K.; Verrillo, M.; Avitabile, A.; Pizzo, E.; Varcamonti, M.; Zanfardino, A.; Di Maro, A.; Rega, C.; Amoresano, A.; Izzo, V.; et al. Chemical Cleavage of an Asp-Cys Sequence Allows Efficient Production of Recombinant Peptides with an N-Terminal Cysteine Residue. *Bioconjug. Chem.* **2018**, *29*, 1373–1383. [CrossRef] [PubMed]
33. Litak, P.T.; Kauffman, J.M. Syntheses of reactive fluorescent stains derived from 5(2)-aryl-2(5)-(4-pyridyl)oxazoles and bifunctionally reactive linkers. *J. Heterocycl. Chem.* **1994**, *31*, 457–479. [CrossRef]
34. Dou, Y.; Goodchild, S.J.; Velde, R.V.; Wu, Y.; Fedida, D. The neutral, hydrophobic isoleucine at position I521 in the extracellular S4 domain of hERG contributes to channel gating equilibrium. *Am. J. Physiol. Cell Physiol.* **2013**, *305*, 468–478. [CrossRef]
35. Wakabayashi, H.; Fay, P.J. Molecular orientation of Factor VIIIa on the phospholipid membrane surface determined by fluorescence resonance energy transfer. *Biochem. J.* **2013**, *452*, 293–301. [CrossRef]
36. Pane, K.; Durante, L.; Pizzo, E.; Varcamonti, M.; Zanfardino, A.; Sgambati, V.; Di Maro, A.; Carpentieri, A.; Izzo, V.; Di Donato, A.; et al. Rational design of a carrier protein for the production of recombinant toxic peptides in Escherichia coli. *PLoS ONE* **2016**, *11*, e0146552. [CrossRef]
37. Doose, S.; Neuweiler, H.; Sauer, M. Fluorescence quenching by photoinduced electron transfer: A reporter for conformational dynamics of macromolecules. *ChemPhysChem* **2009**, *10*, 1389–1398. [CrossRef]
38. Chen, H.; Ahsan, S.S.; Santiago-Berrios, M.B.; Abruña, H.D.; Webb, W.W. Mechanisms of quenching of alexa fluorophores by natural amino acids. *J. Am. Chem. Soc.* **2010**, *132*, 7244–7245. [CrossRef]
39. Goldstein, L.; Levin, Y.; Katchalski, E. A Water-insoluble Polyanionic Derivative of Trypsin. II. Effect of the Polyelectrolyte Carrier on the Kinetic Behavior of the Bound Trypsin. *Biochemistry* **1964**, *3*, 1913–1919. [CrossRef]
40. Maurel, P.; Douzou, P. Catalytic implications of electrostatic potentials: The lytic activity of lysozyme as a model. *J. Mol. Biol.* **1976**, *102*, 253–264. [CrossRef]
41. Gaglione, R.; Smaldone, G.; Cesaro, A.; Rumolo, M.; De Luca, M.; Di Girolamo, R.; Petraccone, L.; Del Vecchio, P.; Oliva, R.; Notomista, E.; et al. Impact of a Single Point Mutation on the Antimicrobial and Fibrillogenic Properties of Cryptides from Human Apolipoprotein B. *Pharmaceuticals* **2021**, *14*, 631. [CrossRef]
42. Oliva, R.; Del Vecchio, P.; Grimaldi, A.; Notomista, E.; Cafaro, V.; Pane, K.; Schuabb, V.; Winter, R.; Petraccone, L. Membrane disintegration by the antimicrobial peptide (P)GKY20: Lipid segregation and domain formation. *Phys. Chem. Chem. Phys.* **2019**, *21*, 3989–3998. [CrossRef]
43. Aniansson, E.A.G.; Wall, S.N.; Almgren, M.; Hoffmann, H.; Kielmann, I.; Ulbricht, W.; Zana, R.; Lang, J.; Tondre, C. Theory of the kinetics of micellar equilibria and quantitative interpretation of chemical relaxation studies of micellar solutions of ionic surfactants. *J. Phys. Chem.* **1976**, *80*, 905–922. [CrossRef]
44. Gaglione, R.; Cesaro, A.; Dell'Olmo, E.; Della Ventura, B.; Casillo, A.; Di Girolamo, R.; Velotta, R.; Notomista, E.; Veldhuizen, E.J.A.; Corsaro, M.M.; et al. Effects of human antimicrobial cryptides identified in apolipoprotein B depend on specific features of bacterial strains. *Sci. Rep.* **2019**, *9*, 6728. [CrossRef]
45. Rosenfeld, Y.; Shai, Y. Lipopolysaccharide (Endotoxin)-host defense antibacterial peptides interactions: Role in bacterial resistance and prevention of sepsis. *Biochim. Biophys. Acta Biomembr.* **2006**, *1758*, 1513–1522. [CrossRef]
46. Yu, L.; Tan, M.; Ho, B.; Ding, J.L.; Wohland, T. Determination of critical micelle concentrations and aggregation numbers by fluorescence correlation spectroscopy: Aggregation of a lipopolysaccharide. *Anal. Chim. Acta* **2006**, *556*, 216–225. [CrossRef]
47. Saravanan, R.; Holdbrook, D.A.; Petrlova, J.; Singh, S.; Berglund, N.A.; Choong, Y.K.; Kjellström, S.; Bond, P.J.; Malmsten, M.; Schmidtchen, A. Structural basis for endotoxin neutralisation and anti-inflammatory activity of thrombin-derived C-terminal peptides. *Nat. Commun.* **2018**, *9*, 2762. [CrossRef]
48. Claxton, N.S.; Fellers, T.J.; Davidson, M.W. Microscopy, Confocal. In *Encyclopedia of Medical Devices and Instrumentation*; Webster, J.G., Ed.; John Wiley & Sons, Inc.: Hoboken, NJ, USA, 2016; pp. 449–477. [CrossRef]
49. Dolman, N.J.; Kilgore, J.A.; Davidson, M.W. A review of reagents for fluorescence microscopy of cellular compartments and structures, part I: BacMam labeling and reagents for vesicular structures. *Curr. Protoc. Cytom.* **2013**, *65*, 1–27. [CrossRef]
50. Nogueira, E.; Cruz, C.F.; Loureiro, A.; Nogueira, P.; Freitas, J.; Moreira, A.; Carmo, A.M.; Gomes, A.C.; Preto, A.; Cavaco-Paulo, A. Assessment of liposome disruption to quantify drug delivery in vitro. *Biochim. Biophys. Acta Biomembr.* **2016**, *1858*, 163–167. [CrossRef]
51. Gargotti, M.; Lopez-Gonzalez, U.; Byrne, H.J.; Casey, A. Comparative studies of cellular viability levels on 2D and 3D in vitro culture matrices. *Cytotechnology* **2018**, *70*, 261–273. [CrossRef]
52. Dinnen, R.D.; Drew, L.; Petrylak, D.P.; Mao, Y.; Cassai, N.; Szmulewicz, J.; Brandt-Rauf, P.; Fine, R.L. Activation of Targeted Necrosis by a p53 Peptide: A Novel Death Pathway That Circumvents Apoptotic Resistance. *J. Biol. Chem.* **2007**, *282*, 26675–26686. [CrossRef]
53. Elmore, S. Apoptosis: A Review of Programmed Cell Death. *Toxicol. Pathol.* **2007**, *35*, 495–516. [CrossRef]
54. Mana, G.; Valdembri, D.; Serini, G. Conformationally active integrin endocytosis and traffic: Why, where, when and how? *Biochem. Soc. Trans.* **2020**, *48*, 83–93. [CrossRef]
55. Buckley, C.D.; Pilling, D.; Henriquez, N.V.; Parsonage, G.; Threlfall, K.; Scheel-Toellner, D.; Simmons, D.L.; Akbar, A.N.; Lord, J.M.; Salmon, M. RGD peptides induce apoptosis by direct caspase-3 activation. *Nature* **1999**, *397*, 534–539. [CrossRef]
56. Webb, J.N.; Koufos, E.; Brown, A.C. Inhibition of Bacterial Toxin Activity by the Nuclear Stain, DRAQ5^{TM}. *J. Membr. Biol.* **2016**, *249*, 503–511. [CrossRef]

57. Nguyen, D.P.; Elliott, T.; Holt, M.; Muir, T.W.; Chin, J.W. Genetically encoded 1,2-aminothiols facilitate rapid and site-specific protein labeling via a bio-orthogonal cyanobenzothiazole condensation. *J. Am. Chem. Soc.* **2011**, *133*, 11418–11421. [CrossRef]
58. Yuan, Y.; Wang, X.; Mei, B.; Zhang, D.; Tang, A.; An, L.; He, X.; Jiang, J.; Liang, G. Labeling thiols on proteins, living cells, and tissues with enhanced emission induced by FRET. *Sci. Rep.* **2013**, *3*, 3523. [CrossRef]
59. Koniev, O.; Wagner, A. Developments and recent advancements in the field of endogenous amino acid selective bond forming reactions for bioconjugation. *Chem. Soc. Rev.* **2015**, *44*, 5495–5551. [CrossRef]
60. Takakura, H. Molecular Design of d-Luciferin-Based Bioluminescence and 1,2-Dioxetane-Based Chemiluminescence Substrates for Altered Output Wavelength and Detecting Various Molecules. *Molecules* **2021**, *26*, 1618. [CrossRef]
61. Sharma, D.K.; Adams, S.T.; Liebmann, K.L.; Miller, S.C. Rapid Access to a Broad Range of 6′-Substituted Firefly Luciferin Analogues Reveals Surprising Emitters and Inhibitors. *Org. Lett.* **2017**, *19*, 5836–5839. [CrossRef]
62. Mofford, D.M.; Reddy, G.R.; Miller, S.C. Aminoluciferins extend firefly luciferase bioluminescence into the near-infrared and can be preferred substrates over d-luciferin. *J. Am. Chem. Soc.* **2014**, *136*, 13277–13282. [CrossRef] [PubMed]
63. Takakura, H.; Kojima, R.; Ozawa, T.; Nagano, T.; Urano, Y. Development of 5′- and 7′-Substituted Luciferin Analogues as Acid-Tolerant Substrates of Firefly Luciferase. *ChemBioChem* **2012**, *13*, 1424–1427. [CrossRef] [PubMed]
64. Fery-Forgues, S.; Lavabre, D. Are Fluorescence Quantum Yields So Tricky to Measure? A Demonstration Using Familiar Stationery Products. *J. Chem. Educ.* **1999**, *76*, 1260. [CrossRef]